

3. SITE 871¹

Shipboard Scientific Party²

HOLE 871A

Date occupied: 23 May 1992
Date departed: 25 May 1992
Time on hole: 12 hr, 15 min
Position: 5°33.432'N, 172°20.658'E
Bottom felt (rig floor, m; drill-pipe measurement): 1265.5
Distance between rig floor and sea level (m): 10.9
Water depth (drill-pipe measurement from sea level, m): 1254.6
Total depth (rig floor, m): 1417.4
Penetration (m): 151.9
Number of cores (including cores with no recovery): 17
Total length of cored section (m): 151.90
Total core recovered (m): 126.05
Core recovery (%): 83
Oldest sediment cored:
Depth (mbsf): 151.9
Age: middle Eocene

HOLE 871B

Date occupied: 25 May 1992
Date departed: 25 May 1992
Time on hole: 12 hr, 15 min
Position: 5°33.432'N, 172°20.658'E
Bottom felt (rig floor, m; drill-pipe measurement): 1264.9
Distance between rig floor and sea level (m): 10.9
Water depth (drill-pipe measurement from sea level, m): 1254.0
Total depth (rig floor, m): 1417.3
Penetration (m): 152.4
Number of cores (including cores with no recovery): 17
Total length of cored section (m): 152.40
Total core recovered (m): 103.94
Core recovery (%): 68.2
Oldest sediment cored:
Depth (mbsf): 152.4
Age: middle Eocene

HOLE 871C

Date occupied: 26 May 1992
Date departed: 31 May 1992

Time on hole: 5 days, 1 hr, 15 min
Position: 5°33.438'N, 172°20.658'E
Bottom felt (rig floor, m; drill-pipe measurement): 1265.5
Distance between rig floor and sea level (m): 10.9
Water depth (drill-pipe measurement from sea level, m): 1254.6
Total depth (rig floor, m): 1735.5
Penetration (m): 500.0
Number of cores (including cores with no recovery): 40
Total length of cored section (m): 376.00
Total core recovered (m): 54.79
Core recovery (%): 14.6
Oldest sediment cored:
Depth (mbsf): 451.6
Nature: mottled red and gray clay with volcanic clasts
Age: early late Paleocene
Measured velocity (km/s): 4.0–4.3
Hard rock:
Depth (mbsf): 451.5
Nature: basalt
Measured velocity (km/s): 4.0–4.7

Basement:

Depth (mbsf): 451.6
Nature: basalt
Measured velocity (km/s): 4.0–4.7

Principal results: Site 871 (proposed Site Har-2) is located at 5°33.43'N, 172°20.66'E, in a water depth of 1255 m in the south central portion of Limalok (Harrie) Guyot, approximately 53.7 km from Mili Atoll in the southern Marshall Islands. This site is the southernmost site of the north-south transect of sites drilled by Leg 144 and on the basis of previous work in this region. Limalok Guyot is considered the youngest of the guyots in the Marshall Island region. The objectives at this location were (1) to recover pelagic sediments for high-resolution stratigraphy; (2) to determine the principal diagenetic processes and the acoustic stratigraphy of thick pelagic carbonate sequences on the top of the guyot; (3) to date the interface between the pelagic cap and the underlying platform, and infer the age and cause of platform drowning; (4) to establish the characteristics of the shallow-water facies and changes with time; and (5) to establish the age of the basement.

Three holes were drilled at Site 871; Hole 871B is located 10 m east of Hole 871A, whereas Hole 871C is located 10 m to the west of Hole 871A. Holes 871A and 871B were cored with the advanced hydraulic piston core (APC) to 139.5 and 133.2 mbsf, respectively, where refusal occurred at the boundary between early Miocene and middle Eocene sediments. These holes were continued by extended core barrel (XCB) coring to 151.9 mbsf achieving a total of 83% recovery (Hole 871A), and 152.4 mbsf achieving a total of 68.2% recovery (Hole 871B). The APC cores are poor candidates for high-resolution stratigraphic studies because the recovered sediments are winnowed and very soupy.

A third hole, Hole 871C, was spudded using the rotary core barrel (RCB). After washing through the pelagic cap, cores were recovered from 133.7 to 500 mbsf total depth (TD). The recovered material includes platform limestones from 133.7 to 422.9 mbsf, clay from 422.9 to 451.5

¹ Premoli Silva, I., Haggerty, J., Rack, F., et al., 1993. *Proc. ODP, Init. Repts.*, 144: College Station, TX (Ocean Drilling Program).

² Shipboard Scientific Party is as given in the list of participants preceding the contents.

mbsf, and altered basalt from 451.5 to 500 mbsf. Recovery in Hole 871C averaged 14.6% with only 3.5% recovery in the sedimentary section.

A free-fall reentry funnel was deployed through the moonpool in preparation for logging Hole 871C. Two attempts were made with the Japanese, lightweight, slim-hole magnetometer to log the basement rocks. Although the drill pipe was kept deep in the hole to avoid running the magnetometer past potential bridges in the limestone section of the hole, a bridge had formed in the deeper section of the hole and a subsequent obstruction of the drill pipe with clay prevented successful logging. A successive series of problems with the clay section resulted in the decision not to log the lowermost portion of the hole, but successful logging was conducted across the entire limestone section. Standard Schlumberger geophysical and geochemical logs were run, as well as two runs with the Formation MicroScanner.

Four lithologic units were identified at Site 871 using a combination of visual core descriptions, augmented by smear slide and thin section data as well as downhole logging data. Age identification of these units was based on calcareous plankton (pelagic cap) and larger benthic foraminifers (platform limestones). The identified lithologic units are, from top to bottom:

Unit I (0–133.7 mbsf) consists of foraminifer nannofossil ooze and foraminifer ooze of Pleistocene to early Miocene age. Sediment composition allowed the subdivision of Unit I in two subunits. Subunit IA (0–26.5 mbsf) is comprised of light gray nannofossil foraminifer ooze of Pleistocene to latest Miocene age; Subunit IB (26.5–133.7 mbsf) is comprised of white homogeneous foraminifer ooze with a medium sand texture, well-sorted and winnowed, of middle to early Miocene age. The transition between the two subunits is marked by a hiatus that spans the late middle to latest Miocene.

Unit II (133.7–422.9 mbsf) consists of a sequence of white to very pale brown platform carbonates of middle Eocene to early late Paleocene age. Unit II is subdivided into six subunits on the basis of fossil content and lithology. The carbonate rock types in Unit II include packstone, grainstone, and wackestone with abundant benthic foraminifers (mostly miliolids with agglutinated foraminifers, *Nummulites*, alveolinids, and *Asterocyclina*), common red and green algae (corallinaceans, squamariaceans, solenoporaes, and udoteaceans) and common molluscan molds of bivalves and gastropods. The porosity of these rocks is estimated at 5%–10% and is predominantly moldic, solution-enlarged interparticle, and/or microvuggy. Porosity is moderately reduced by passively precipitated, pore-lining carbonate cement; however, most of the secondary porosity remains open. The contact between the pelagic cap and the underlying platform limestone is marked by an iron-manganese oxide and phosphatic hardground. Borings in the hardground are infilled with pelagic sediment of late early Oligocene age.

Unit III (422.9–451.5 mbsf) consists of variegated clay of indeterminate age that displays large variations in the texture and content of lithoclasts. Basalt pebbles occur in the lower part of the unit.

Unit IV (451.5–500 mbsf TD) consists of interbedded volcanogenic sandstones with basaltic breccias and flows. Except for a thin basaltic lava flow, the uppermost 6 m of recovered basement consist of a series of volcanogenic breccias. These are followed by a sequence of massive flows, from 1 m to over 7 m thick. All the flow units appear to have a similar mineralogy with only minor variations; they appear to be nepheline-bearing basalt. The basalt typically has high natural remanent magnetization (NRM) intensities (up to 18 A/m) and negative inclinations. Five or more distinct inclination groups are present, values vary from +2° to –32°, and are compatible with the predicted paleosecular variation.

Interstitial water data indicate minimal diagenesis within the foraminifer ooze comprising the pelagic cap (Unit I). The pelagic cap (Unit I) and platform limestone (Unit II) at Site 871 have a calcium carbonate content of 95%–98% with <0.3% organic carbon and no sulfur. The top of the clay section (Unit III) is enriched in organic carbon and total sulfur (up to 12% and 13%, respectively).

The entire carbonate platform succession was successfully logged. The Paleocene/Eocene boundary at 319 mbsf is marked by a uranium concentration and cementation surface at the top of coralline grainstones from Unit II. A similar uranium cementation horizon at 138 mbsf coincides with the phosphatic hardground at the top of Unit II. Between these two major

surfaces, the Eocene platform generally consists of low-resistivity facies containing several smaller uranium anomalies, especially within the upper 80 m of the platform. The underlying rhodolith and coralline grainstone facies contain several dense, high-resistivity, meter-scale beds, that exhibit high uranium concentrations, that may be an expression of the algal nature of the material.

BACKGROUND AND OBJECTIVES

Site 871 (proposed Site Har-2) is located at 5°33.43'N, 172°20.66'E at a water depth of 1255 m, atop the drowned platform of Limalok (Harrie) Guyot in the Ratak Chain of the southern Marshall Islands. Limalok Guyot occupies a position with respect to Mili Atoll that is morphologically analogous to the Wodejebato Guyot–Pikinni Atoll (Sylvania Guyot–Bikini Atoll) situation; namely, both Limalok and Wodejebato guyots share their volcanic pedestal with a sibling that is a living atoll. Both guyots are interpreted to have the classic guyot pattern of (1) pelagic cap, (2) reef rims, and (3) gullied lower slopes consisting of debris flows. The geologic interpretation is based on an extensive collection of dredged limestones, side-scan imagery, and seismic lines.

The reef limestones dredged from Limalok Guyot are of early Eocene age (Schlanger et al., 1987), significantly younger than the Cretaceous reef material recovered from Wodejebato Guyot and several other guyots in the Marshall Islands (Lincoln et al., in press). This contrast with Wodejebato Guyot, where reef growth may have ceased during Late Cretaceous time (Schlanger et al., 1987), suggests that there may be an older reef history at Limalok Guyot that survived through the early Eocene.

According to Lincoln et al. (in press), the past position of Limalok Guyot does not fall within any hotspot target area. The minimum age of Limalok Guyot is based on early Eocene reef and pelagic limestone containing volcanic debris recovered by dredging (Schlanger et al., 1987). If Limalok Guyot erupted 10–30 m.y. before reef building, as did Anwetak and Midway atolls, then the past position for Limalok Guyot would plot well within a 600-km radius of the Tahiti Hotspot target area. The Paleocene Tahiti track lies near Limalok Guyot, the site of early Eocene reef building.

The SeaMARC II side-scan imagery of Limalok Guyot demonstrates a morphologic similarity to Wodejebato Guyot and the classic guyot pattern. In the side-scan images, a high backscatter band along the perimeter of the summit is interpreted as an area where carbonate platform outcrops from beneath the pelagic cap (Schlanger et al., 1987). This band appears to have a scalloped morphology around the perimeter of the summit.

In 1981, the *Kana Keoki* collected analog seismic profiles of Limalok Guyot. These old analog records were used in conjunction with the new 3.5-kHz echo-sounder records and seismic data produced by the 200 in.³ water gun of the *JOIDES Resolution* during this cruise to characterize the seismic structure of Limalok Guyot.

The pelagic cap is an asymmetric mound of sediments containing three prominent reflectors; below the third reflector, the pelagic cap is acoustically transparent, except for a diffuse hummocky reflector at 0.08 s two-way traveltime (TWT) (see Fig. 1, “Underway and Site Geophysics” section, this chapter). The upper surface of the carbonate platform slopes gently to the south and displays both onlapping and toplapping surfaces; the gradient is 1° to 2°. Acoustic basement also slopes to the south but at a slightly higher gradient of 2° to 3°. The platform sediments between the pelagic cap and acoustic basement thicken in the same direction, from 0.2 s TWT in the northern part of the guyot to >0.5 s TWT near the southern edge. Above the acoustic basement, some coherent reflectors appear to prograde to the south, suggesting either outward building of a volcanoclastic wedge or truncation of seaward-dipping lava flows.

Drilling plans for Limalok Guyot included two sites. One single hole (proposed Site Har-1) near the edge of the summit was planned to recover what was interpreted to be thick marginal reef limestones and 50 m of basement; and a second site was dedicated to double APC

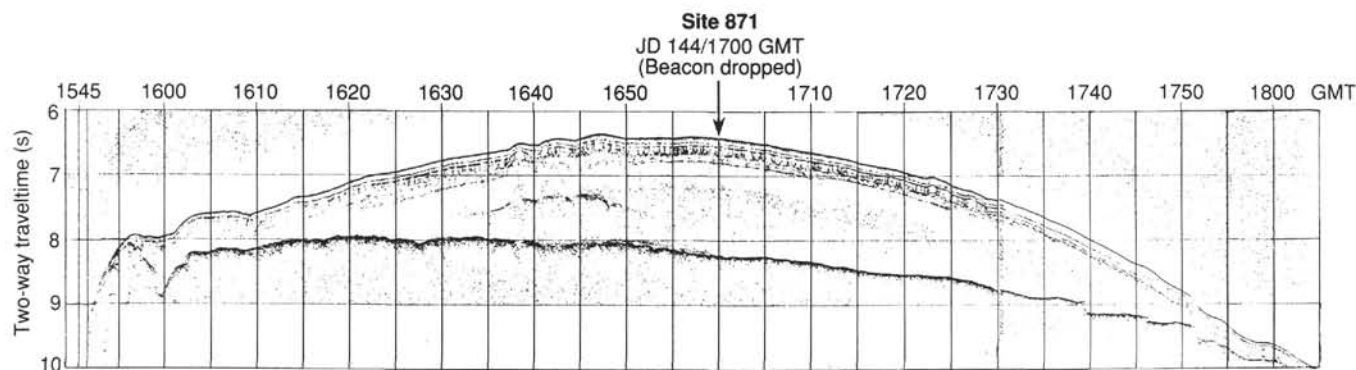


Figure 1. The 3.5-kHz sub-bottom profile across the summit of Limalok Guyot, showing the reflectors within the pelagic cap and the top of the carbonate platform. Note the presence of steps in the southern portion of the profile; these steps may result from faulting and erosion of the guyot.

coring the pelagic cap, with XCB coring across the carbonate platform contact and RCB coring through at least 260 m of platform limestone (Site 871; proposed Site Har-2). At the location of Har-2, in the center of the guyot, the pelagic cap was thicker and the acoustic basement was at a shallower depth than along the rim of the guyot.

Limalok Guyot was the first guyot to be drilled on Leg 144, with another four guyots scheduled for drilling during this leg. Results from Leg 143, also an atoll and guyot drilling leg, indicated that basement objectives on all of the guyots might be deeper than had previously been calculated because the velocity of the platform limestone drilled on Leg 143 was higher than originally estimated. These considerations, and the clear implication of a potential time shortage during Leg 144, resulted in Har-2 (Site 871) being drilled first. The basic objectives planned for the two sites were: (1) to recover the pelagic sediments for high resolution stratigraphy at Har-2, (2) to document the age and duration of the platform at Har-1 and Har-2, and (3) to recover the basement at Har-1, although acoustic basement appeared at a shallower depth at Har-2 than at Har-1. The objectives of both sites were combined at Har-2 because of time constraints.

Drilling at Site 871 (Har-2) will provide the data (1) determine the principal diagenetic processes and the acoustic stratigraphy of thick pelagic carbonate sequences on top of these guyots; (2) to determine if there is a Wodejebato-type Cretaceous reef below the Eocene reef on the guyot; (3) to determine the chronology of platform growth and demise related to sea-level curves and subsidence history; (4) determine the paleolatitude of formation of the edifice; (5) determine the age of the Limalok volcanic edifice; (6) relate the geochemistry of the basalts to the DUPAL/SOPITA anomaly; and (7) to determine the subsidence history of the guyot.

Several problems arose during drilling and logging operations at Site 871. These problems consumed time that would have been used for drilling Har-1; therefore, Har-1 was not drilled. Nevertheless, the majority of the primary objectives for Limalok Guyot were achieved. The only objective not accomplished was the recovery of Limalok reef facies. The reef strata are interpreted to be associated with the guyot rim location of Har-1. These facies were not recovered because Site 871 is located on the central summit of the guyot and is associated with the lagoonal strata of the Limalok carbonate platform.

OPERATIONS

Transit from Majuro to Site 871

The last mooring line in the harbor of Majuro Atoll, Republic of Marshall Islands, was pulled aboard the *JOIDES Resolution* at 1315L on 23 May (L = local time). Two hours were required to steam across Majuro Lagoon and exit into open ocean. After passing outside the lagoon, the magnetometer was streamed and soundings were made with the 3.5- and 12-kHz echo sounders. The ship headed southward past Arno Atoll and around Mili Atoll toward Site 871.

Approach to Site 871

A seismic profile was shot, using a 200-in.³ water gun, along a north-south transect over the Limalok (Harrie) Guyot and through the positions of proposed sites Har-1 and Har-2 so as to assess the basement reflector carefully. The vessel continued beyond the south flank of the guyot before turning to a reciprocal course and steaming back across the sites. A positioning beacon was launched at Har-1 at 0720L on 24 May. The ship continued on a northward track and launched a beacon at Site 871 (Har-2) at 0800L, officially beginning site operations for Leg 144. Total steaming distance, including inside steaming and survey, was only 173 nmi from Majuro.

Site 871 is centrally located on Limalok Guyot. To the northwest are Mili and Vanilli atolls, emergent features on the same volcanic pedestal as Limalok Guyot. The drilling objectives of the site included coring through the pelagic cap and limestone sections and at least 50 m into the underlying volcanic basement.

Hole 871A

In preparation for drilling, all drill-string components were measured and "rabbited" to assure they were unobstructed. Before spudding Hole 871A, two plastic/steel "pigs" were pumped through the drill string to dislodge any loose rust flakes and pipe dope.

Coring began with an advanced hydraulic piston core (APC) of the seafloor interface at 1530L on 24 May. The drill-pipe measurement of seafloor depth is 1265.5 m below the dual elevator stool (DES) or 1254.6 m below sea level. A "backup" positioning beacon was launched at about the same time.

Continuous APC cores were taken in unconsolidated nannofossil foraminifer ooze and foraminifer ooze. The ooze had an extraordinarily high water content and contained only small percentages of nannofossils and/or clay, so that liquefaction occurred when it was disturbed. Core recovery was good (83%; Table 1), but the liquefaction exhibited by the cores and the sandy texture of the sediment led to unstable hole conditions. Magnetic orientation was attempted on Cores 144-871A-3H to -9H, but these efforts were discontinued because of the fluid nature of the cores, and the tendency of the drill string to stick while it was motionless for multishot exposures. The use of "pills" of drilling mud apparently stabilized the hole after a depth of about 100 meters below seafloor (mbsf) was reached. An incomplete stroke of the core barrel was indicated on Core 144-871A-14H at 130 mbsf. The length of stroke could not be estimated because the content of the core liner was fluid. One additional incomplete-stroke APC core was attempted, with similar results, before the coring mode was changed to XCB (extended core barrel).

The contact with the platform limestone was indicated by a change in drilling parameters at 139.5 mbsf. Two XCB cores were taken to a total depth of 151.9 mbsf, with only a few lumps of rubbly limestone

Table 1. Coring summary, Site 871.

Core no.	Date (May 1992)	Time (Z)	Depth (mbsf)	Cored (m)	Recovered (m)	Recovery (%)
135-871A-						
1H	24	0340	0-7.5	7.5	7.49	99.8
2H	24	0415	7.5-17.0	9.5	9.22	97.0
3H	24	0445	17.0-26.5	9.5	8.84	93.0
4H	24	0530	26.5-36.0	9.5	8.19	86.2
5H	24	0610	36.0-45.5	9.5	6.00	63.1
6H	24	0645	45.5-55.0	9.5	8.82	92.8
7H	24	0715	55.0-64.5	9.5	7.64	80.4
8H	24	0755	64.5-74.0	9.5	7.54	79.3
9H	24	0830	74.0-83.5	9.5	7.90	83.1
10H	24	0905	83.5-93.0	9.5	9.15	96.3
11H	24	0950	93.0-102.5	9.5	8.95	94.2
12H	24	1025	102.5-112.0	9.5	8.89	93.6
13H	24	1105	112.0-121.5	9.5	9.33	98.2
14H	24	1150	121.5-130.5	9.0	8.98	99.8
15H	24	1215	130.5-139.5	9.0	8.82	98.0
16X	24	1345	139.5-145.7	6.2	0.03	0.5
17X	24	1440	145.7-151.9	6.2	0.26	4.2
Coring totals				151.9	126.05	83.0
135-871B-						
1H	24	1645	0-6.1	6.1	6.14	100.0
2H	24	1725	6.1-15.6	9.5	9.09	95.7
3H	24	1820	15.6-25.1	9.5	9.60	101.0
4H	24	1855	25.1-34.6	9.5	7.62	80.2
5H	24	1915	34.6-44.1	9.5	8.25	86.8
6H	24	2015	44.1-53.6	9.5	7.25	76.3
7H	24	2040	53.6-63.1	9.5	8.01	84.3
8H	24	2105	63.1-72.6	9.5	0.00	0.0
9H	24	2200	72.6-82.1	9.5	7.83	82.4
10H	24	2225	82.1-91.6	9.5	9.15	96.3
11H	24	2250	91.6-101.1	9.5	9.20	96.8
12H	24	2340	101.1-110.6	9.5	2.85	30.0
13H	25	0010	110.6-120.1	9.5	9.16	96.4
14H	25	0035	120.1-129.6	9.5	9.59	101.0
15H	25	0100	129.6-133.2	3.6	0.00	0.0
16X	25	0220	133.2-142.7	9.5	0.12	1.3
17X	25	0320	142.7-152.4	9.7	0.08	0.8
Coring totals				152.4	103.94	68.2
135-871C-						
1R	25	1630	124.0-133.7	9.7	0.00	0.0
2R	25	1715	133.7-143.3	9.6	0.57	5.9
3R	25	1745	143.3-152.9	9.6	0.24	2.5
4R	25	1835	152.9-162.6	9.7	0.53	5.5
5R	25	1930	162.6-172.3	9.7	0.07	0.7
6R	25	2035	172.3-181.9	9.6	0.51	5.3
7R	25	2135	181.9-191.5	9.6	0.07	0.7
8R	25	2230	191.5-201.2	9.7	0.24	2.5
9R	26	0000	201.2-210.9	9.7	0.44	4.5
10R	26	0105	210.9-220.5	9.6	0.12	1.3
11R	26	0220	220.5-230.1	9.6	0.11	1.1
12R	26	0325	230.1-239.8	9.7	0.09	0.9
13R	26	0430	239.8-249.5	9.7	0.12	1.2
14R	26	0540	249.5-259.2	9.7	0.25	2.6
15R	26	0640	259.2-268.8	9.6	0.24	2.5
16R	26	0745	268.8-278.1	9.3	0.23	2.5
17R	26	0845	278.1-287.5	9.4	0.29	3.1
18R	26	0940	287.5-297.2	9.7	0.00	0.0
19R	26	1050	297.2-306.9	9.7	0.10	1.0
20R	26	1205	306.9-316.5	9.6	0.22	2.3
21R	26	1340	316.5-326.2	9.7	1.38	14.2
22R	26	1500	326.2-335.8	9.6	0.24	2.5
23R	26	1615	335.8-345.4	9.6	0.45	4.7
24R	26	1730	345.4-355.1	9.7	0.04	0.4
25R	26	1840	355.1-364.7	9.6	0.26	2.7
26R	26	1950	364.7-374.3	9.6	0.10	1.0
27R	26	2105	374.3-383.7	9.4	0.07	0.7
28R	26	2210	383.7-393.4	9.7	1.17	12.0
29R	26	2315	393.4-403.1	9.7	0.29	3.0
30R	27	0040	403.1-412.8	9.7	1.31	13.5
31R	27	0210	412.8-422.5	9.7	0.43	4.4
32R	27	0340	422.5-432.2	9.7	6.06	62.5
33R	27	0605	432.2-441.8	9.6	4.54	47.3
34R	27	0915	441.8-451.5	9.7	3.10	31.9
35R	27	1245	451.5-461.1	9.6	5.43	56.5
36R	27	1525	461.1-469.8	8.7	3.05	35.0
37R	27	1740	469.8-471.8	2.0	2.14	107.0
38R	28	2155	471.8-480.4	8.6	7.20	83.7
39R	28	0155	480.4-489.7	9.3	8.29	89.1
40R	28	0645	489.7-500.0	10.3	4.80	46.6
Coring totals				376.0	54.79	14.6

recovered in each (0.5 and 4.2% recovery). The bottom-hole assembly (BHA) was then raised above the seafloor for a second set of APC cores through the pelagic sediment section.

Hole 871B

After the ship had offset 10 m east, Hole 871B was spudded at 0430L on 25 May. The bit was positioned 2 m higher than for Hole 871A to provide a vertical offset of core boundaries. Seafloor depth as measured by the first core was 1264.9 m. Continuous APC cores were taken to refusal at 133.2 mbsf. The temperature-recording shoe was run on Cores 144-871B-3H, -6H, -9H, and -12H, with three of the four attempts recording usable data. Hole conditions were somewhat better than in Hole 871A, although mud flushes were required. The average core recovery of 68.2% was not as good as the recovery from Hole 871A because two core barrels from Hole 871B were recovered empty (Table 1).

At Hole 871B, two XCB cores were attempted across the platform limestone contact at 133.2 mbsf; again, however, only a few pieces were recovered in each core (1.3 and 0.8% recovery). Coring attempts were terminated at 152.4 mbsf, and the drill string was tripped for a standard rotary-core-barrel (RCB) BHA.

Hole 871C

During the round trip, the rig was offset 20 m west of Hole 871B, placing it 10 m west of Hole 871A. Hole 871C was spudded at midnight 25/26 May; the seafloor depth of Hole 871A (1265.5 m) was used because no mud-line core was collected. After washing through the pelagic cap to 133.7 mbsf, continuous RCB cores were recovered to 500 mbsf. Annular velocity was kept below 50 m/min during the drilling to minimize hole erosion in the unstable foraminifer ooze, but sticking tendencies and fill on connections signaled the need for occasional mud pills.

Continuous RCB cores through the sedimentary section of the platform produced low core recovery (3.5%) despite the use of various combinations of drilling parameters. The upper 250 m of the platform limestones were generally friable and drilled at an average penetration rate of over 40 m/hr. The average core recovery rate in this upper portion of the limestone was only 2.8%. The next 40 m of limestone was harder, coring at a somewhat lower rate of penetration (ROP) and a slightly better recovery rate of 5.2%. At 422.9 to 451.5 mbsf clay was penetrated; core recovery jumped to 47.8% whereas ROP fell to an average of 9 m/hr. Altered basalt, encountered at 451.5 mbsf, was cored to 500 mbsf. Core recovery in the basalt was about 63.7% and ROP fell to about 3.5 m/hr.

During the "wiper trip" to prepare the hole for logging, water began to flow from the top of the drill string, indicating a malfunction of the float valve at the bit. The back flow ceased almost immediately and the string was found to be plugged when the circulating pump was started. Various means of unplugging the drill string were tried, including "surging" the string and setting out two stands of pipe. The bit was lowered back toward total depth, where about 13 m of hole fill was found. In the hope that the material plugging the string was confined to the bit or bit sub, the rotary shifting tool (RST) was run to shift the bit so that circulation could be regained (foregoing the planned wiper trip). The RST landed above the depth of the mechanical bit release (MBR), however, and the MBR shifting sleeve could not be engaged. The drill string was pulled until the bit was at about 150 mbsf (just below the limestone/ooze contact). The hole apparently was clean except that an overpull of about 50 K lb occurred through the interval of clay sediments at about 420-440 mbsf. Circulation was again attempted in case the surging action of the trip had dislodged the material plugging the string. When no success was achieved, preparations were made to deploy a free-fall reentry funnel

(FFF) so that logging could be accomplished through an unobstructed drill string after a round trip.

The FFF was dropped through the moonpool at 0145L on 29 May, and the (wet) pipe trip began shortly thereafter. When the bit arrived on deck, the lower BHA was disassembled. As suspected, a piece of basalt core was found to be holding the flapper of the float valve open. The bit subcavity was otherwise clean, but the bores of the outer core barrel and the next two drill collars were found to be plugged by drill cuttings. The outer core barrel also contained three additional pieces of core mixed with the cuttings. After these were cleaned, the same bit and MBR were assembled for a shorter BHA and run back toward the seafloor. A reentry/cleanout bit typically used for logging BHAs was not used in Hole 871C. The development of ledges or bridges in the limestone section and/or clay section was considered likely; these would require additional drilling to clear.

The craters of the three holes of Site 871 were detected easily by the sonar and television systems on the vibration-isolated television (VIT) frame. All the craters were several meters across; Hole 871C was identified as the largest and westernmost one. No sign of the FFF or its floating reflectors was present on either sonar or VIT, but a cautious reentry stab was made into the center of the 10-m-wide crater after about 45 min of positioning. After the stab, the VIT was lowered to the very lip of the crater. We could see that an indistinct sonar echo slightly to one side, tentatively identified as the submerged FFF, became better centralized as the drill string was lowered further. Several stands of pipe were run "without weight indication" and reentry was confirmed.

The bit was run into Hole 871C to 437 mbsf without encountering any obstruction. The top drive was picked up in anticipation of a need to ream through the clay section. Little resistance was met as the bit passed the clay, but drag increased considerably at 469 mbsf, as the basalt section was entered. Circulation and rotation were initiated, and it was necessary to "work" the pipe to reduce the considerable torque attributed to clay attached to the bit and BHA. The hole was cleaned to total depth and a 30-bbl sweep of super-viscous prehydrated gel mud was circulated through the hole.

The RST again was deployed to shift the MBR sleeve and release the terminal restrictions of the drill string. The sleeve proved exceptionally difficult to shift and required vigorous action with the coring line to produce an indication of shifting. After the RST was recovered, there was still no indication of separation of the MBR. The second RST was run to downshift the MBR sleeve and block the side ports. Several "taps" on the RST with the wire-line sinker bars were required before the lower MBR and bit were dislodged.

The sinker bars and top drive were rigged down and the end of the drill string was pulled to 437 mbsf for the first log attempt, leaving the pipe deep in the hole to avoid running the tool past limestone ledges in an open hole. The logging sheaves were rigged and the lightweight Japanese magnetometer tool used for logging basalts at the bottom of the hole, was run down the pipe. The magnetometer exited the pipe without difficulty but came to a stop about 9 m into the open hole. Repeated attempts to work the tool past the bridge were unsuccessful, so it was retrieved to the surface. Two "knobby" drilling joints were added to the drill string and pump circulation was used to advance the string an additional 19 m into the basalt section of the hole, to 456 mbsf. The magnetometer again was run down the pipe, only to be stopped by an obstruction just inside the end of the drill string (probably clay). Pump circulation and lowering the tool several times failed to move it past the clay, and it was necessary to abandon the effort and proceed with the Schlumberger logs.

A "pig" was pumped through the drill string in an effort to clear any clay adhering to the inside of the drill string before the string was raised to 149 mbsf. The new logging depth was just a few meters below the limestone/ooze contact. Raising the pipe one stand with the hoisting system as the logging tools passed would permit logging the lowermost soft ooze, and subsequently lowering the pipe back below the contact would protect against bridging at the hard/soft interface. The second

logging attempt, the geophysical tool string, was assembled in preparation for lowering, but 2.5 hr of trouble shooting were required before proper operation was achieved. Upon reaching the bottom of the drill string, the obstruction was again encountered, but the much heavier Schlumberger tool eventually worked past the sticky spot. No further difficulties were experienced on later runs. The tool string was lowered to 425 mbsf, just above the potentially troublesome clay interval, and a successful log was recorded across the entire limestone section.

The geophysical tool was followed by the Formation MicroScanner (FMS) tool, with two runs recorded across the platform limestone, and then by the geochemical combination log for the same interval. A summary of the well logs recorded from Hole 871C are given in Table 2.

Table 2. Well-log data recorded from Hole 871C.

Log type	Depth (mbsf)
Resistivity	117-425
Bulk density	117-415
Sonic velocity	118-408
Gamma ray/U-Th-K	117-396
Aluminum	119-424
Geochemistry	119-424
Caliper	132-415
Formation MicroScanner	125-422
L-DGO temperature	0-425

Note: Log data assumes that the seafloor is at 1255 m, with all logs correlated and depths shifted to the gamma-ray log from the resistivity tool string.

After the logging equipment was rigged down, the pipe trip out of the hole began. When the end of the drill string was pulled clear of the seafloor, the two positioning beacons used for Site 871 were released acoustically and the ship was maneuvered until the beacons were recovered. The pipe trip continued uninterrupted as the vessel moved slowly toward Site Har-1, where a third beacon was placed on the initial survey. After the drill string was recovered and the thrusters were raised, the ship's speed was increased. Additional time beyond the calculated time estimate for Site 871 was expended because of problems encountered while preparing Hole 871C for logging and during logging operations; therefore, insufficient time remained to accomplish the objectives at Har-1. The decision was made to proceed to proposed Site Pel-3 on Lo-En Guyot. The positioning beacon was recalled and recovered before *JOIDES Resolution* departed the area.

After retrieval of the third beacon, an expendable sonobuoy was deployed to obtain wide-angle reflection and refraction data so as to estimate the acoustic velocity structure of the guyot summit. This short seismic experiment was shot over the southwest edge of Limalok Guyot. The seismic gear was retrieved and the transit to Pel-3 began at approximately 0700L on 31 May.

UNDERWAY AND SITE GEOPHYSICS

Limalok (formerly Harrie) Guyot, located in the southernmost portion of the Ratak Chain in the Marshall Islands (between 5°30' and 5°45'N, and 172°10' and 172°30'E) was the first edifice drilled during Leg 144 (Fig. 2). Nakanishi et al. (1992) show that crust of M22 age (~155 Ma) underlies this portion of the Marshall Islands. As shown by the contour map in Figure 3, the edifice narrows slightly from 27 km in the north to 15 km in the south. The length of the summit is approximately 25 km. A volcanic ridge extends from the north-northwest flank of Limalok, attaching the guyot to the volcanic pedestals underlying Mili and Knox atolls.

Site Survey—Kana Keoki Cruise 1981

Site survey information consisted of data collected during a 1981 *Kana Keoki* cruise. These data included side-scan sonar images,

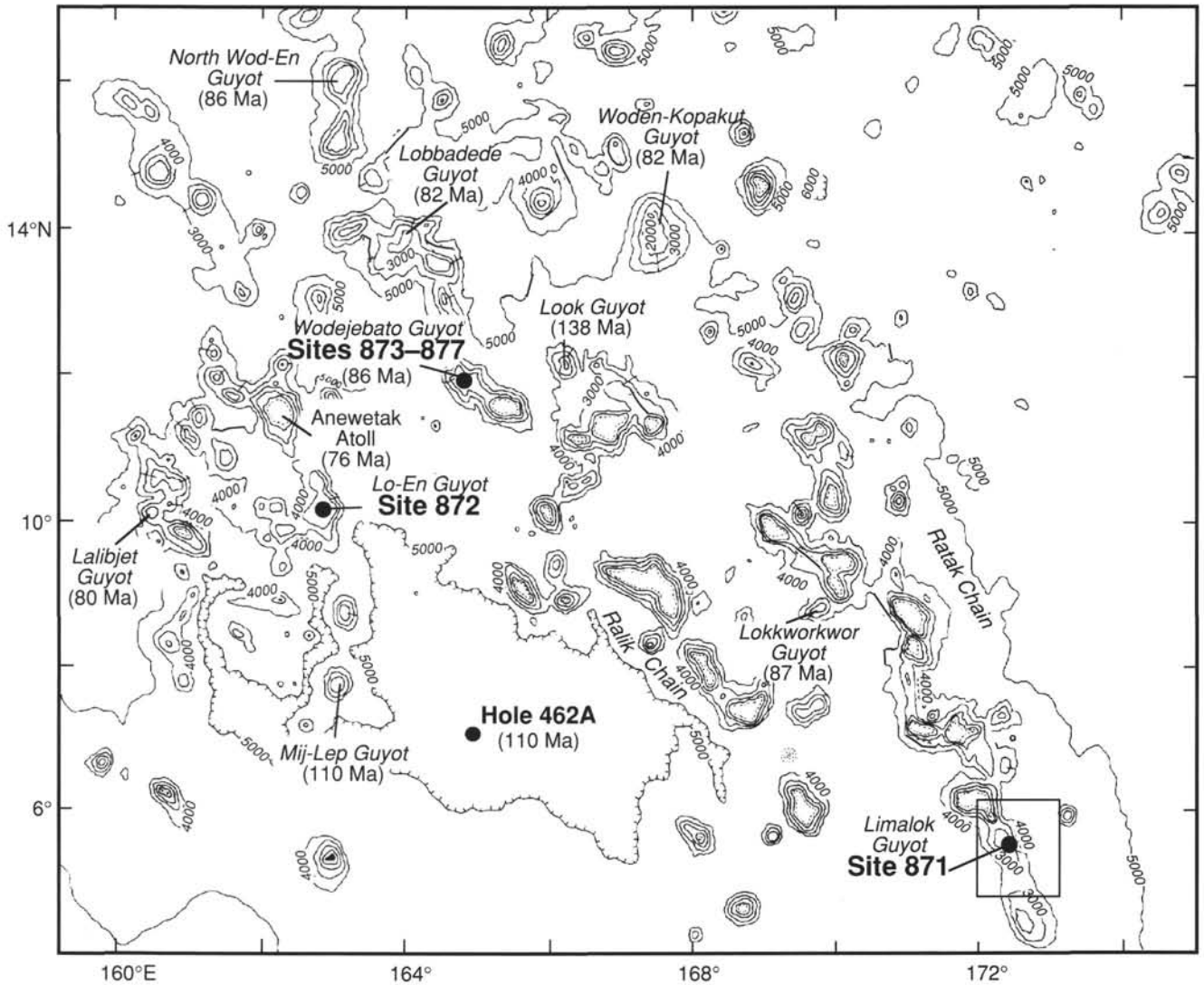


Figure 2. Bathymetry around the Marshall Islands. Contour interval is 1000 m, and the ages shown in parentheses are radiometric dates of basalts collected over a number of different surveys. Radiometric ages from Davis et al. (1989) and Pringle (1992). Figure revised from Hein et al. (1990). The locations of Limalok Guyot and Site 871 are indicated, as well as the location of Hole 462A drilled during Deep Sea Drilling Project Leg 61.

single-channel analog seismic records, gravity measurements, and dredge samples. Limestones dredged from the flanks of this guyot indicate the presence of an Eocene carbonate platform underlying the pelagic cap (Schlanger et al., 1987). In the side-scan images (Fig. 4), a high backscatter (dark) band along the perimeter of the summit marks areas where the carbonate platform crops out from overlying pelagic sediments. The scalloped appearance of this band around the perimeter of the summit suggests some form of erosion is affecting the carbonate platform. Broad terraces, approximately 1–3 km wide, separate the high backscatter band from the flanks of the guyot. The terraces are most prominent along the east, south, and west flanks. Channels, shown as dark lineations oriented perpendicular to the summit of the guyot, are present on all the flanks. From the seismic records, Schlanger et al. (1987) estimated a maximum pelagic cap thickness of 0.15 s (~120 m assuming a velocity of 1.6 km/s) and a minimum carbonate cap thickness of 0.25 s (~250 m assuming a velocity of 2.0 km/s). Volcanic basement at this point reaches a minimum depth of ~1700 m (assuming the velocities listed above). Schlanger et al. (1987) also proposed the following geologic history for Limalok Guyot on the basis of dredge hauls and geophysical data:

1. The volcanic edifice formed in an off-ridge setting and grew upward into the photic zone, allowing reef growth to start by middle early Eocene time. From the absence of any Cretaceous or Paleocene faunal elements in the dredge hauls, they proposed that the edifice had formed by early Eocene time.
2. The volcanic foundation subsided with the thermally rejuvenated plate, and the early Eocene carbonate platform developed and thickened.
3. An emergent period resulting from a rapid fall in sea level caused erosion of the carbonate platform in latest early Eocene time.
4. Continued subsidence coupled with a rapid rise in relative sea level in earliest middle Eocene time drowned the reef on Limalok Guyot.

Site Survey—Leg 144

The existing seismic coverage across Limalok Guyot was minimal and existed only as analog records; therefore we allotted time for a complete north-south transect over the summit before selecting a site so that we could acquire a better understanding of the guyot's subsurface structure (e.g., position and lateral extent of reflectors) and unit thicknesses (e.g., the depth to volcanic basement). Both echo sounder

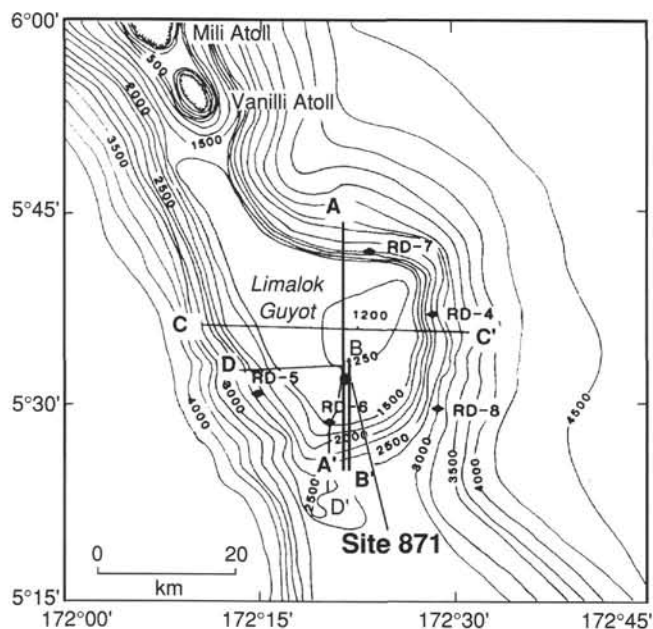


Figure 3. Contoured bathymetry of Limalok Guyot. Contour interval is 250 m. Profiles A-A' and B-B' were collected during Leg 144; Profiles C-C' and D-D' come from the 1981 *Kana Keoki* cruise (Schlanger et al., 1987). RD = rock dredge locations (same cruise).

(3.5 and 12 kHz) and seismic data were acquired during the transect. The seismic gear was deployed on Julian Day (JD) 144 at ~1515Z on a ship's heading of 180°. A 200-in³ water-gun source was used for the seismic data at a towing speed of 6 kt. The ship maintained this southerly course until the entire summit had been crossed, then it turned to a heading of 000° at 1905Z. A suitable site for drilling was located around 2047Z; the ship turned, and the beacon was dropped at 2057Z. The digital seismic data collected during this survey were processed by applying a band-pass filter (25–100 Hz), deconvolution, and automatic gain control (AGC). Figure 1 shows the 3.5-kHz profile, and Figures 5 and 6 show the seismic profiles collected during this cruise.

As shown in the 3.5-kHz record (Fig. 1), the pelagic sediments reach a maximum thickness of 0.18 s near the center of the summit and thin toward the perimeter. The top of the pelagic cap undulates across the length of the summit, probably in response to regional slumping or subsurface faulting of the underlying platform. Unfortunately, seismic lines across the summit are too widely spaced and the side-scan images are too poor in quality to trace the areal extent of the slumping. Along the northern summit edge, the pelagic sediments accumulate behind a topographic high, possibly a reef buildup. Three distinct reflectors exist within the pelagic cap (Fig. 1). The first reflector lies 7.5 m beneath the seafloor (mbsf, assuming a sediment velocity of 1550 m/s). The second reflector defines a packet of sediments 7.5 m thick, the top of which lies at 10.5 mbsf, whereas the third reflector lies 30 mbsf. Beneath these reflectors the pelagic cap is acoustically transparent, except for a diffuse, hummocky reflector at ~65 mbsf near the center of the summit.

The top of the carbonate platform (underlying the pelagic sediments) slopes gently to the south at a gradient of 1° to 2° (Fig. 5). Relief across this surface ranges between 5 to 7 m with the exception of steps which may exceed 15 m of relief. The carbonate platform thickens to the south, increasing from ~0.2 s over the northern half of the guyot to greater than 0.5 s near the southern edge. Concomitant with this thickening is a deepening of acoustic basement. Along the southern flank, faults offset reflectors in the upper portion of the carbonate platform but the depth to which these faults extend is unclear. The scalloped appearance of the high backscatter band in the

side-scan images marking the edge of the carbonate platform along with the terraces formed between this band and the guyot flank may represent faulting and downslope displacement of platform blocks. The acoustic basement reflectors appear to prograde to the south, suggesting either outward building of a volcanoclastic wedge or truncation of flankward-dipping lava flows (Fig. 6).

During the departure from Limalok Guyot, the seismic gear was deployed to record a sonobuoy dropped at the edge of the summit. The signal from the sonobuoy was weak and discernable for only about 30 min. Although this particular refraction experiment failed, testing of the equipment resulted in one configuration change. The height of the receiver antenna was increased by mounting it on the port-side crane, we hope that this change would improve the duration over which the sonobuoy signal could be received.

LITHOSTRATIGRAPHY

Drilling results obtained in all three holes on Limalok Guyot are summarized in a single lithostratigraphic framework (Fig. 7 and Table 3). Lithologic units are identified by such characteristics as color, carbonate and clay content, fossil and particle constituents, lithification, sedimentary structures, and log characteristics. The four major lithologies identified at this site are (1) nannofossil foraminifer ooze (Unit I: 0–133.7 mbsf), (2) skeletal limestone (Unit II: 133.7–422.9 mbsf), (3) variegated, mottled clay containing volcanoclastic debris and basalt rubble (Unit III: 422.9–451.6 mbsf), and (4) basalt (Unit IV: 451.6–500.0 mbsf). Lithologic units and subunits are described below.

Unit I

Intervals: Hole 871A, Cores 144-871A-1H to -15H; Hole 871B, Cores 144-871B-1H to -14H

Depth: Hole 871A, 0–139.5 mbsf; Hole 871B, 0–129.6 mbsf

Age: Pleistocene to early Miocene

Unit I is comprised of yellowish to pinkish gray (5Y 8/1 to 5YR 8/1), homogeneous nannofossil foraminifer ooze and white (10YR 8/2), homogeneous foraminifer ooze. The carbonate content of the sediment of Unit I is near 100%. Unit I is divided into two units based on a decrease in the abundance of nannofossils and a change in the texture (grain size and sorting) and color of the sediments.

Subunit IA

Intervals: Hole 871A, Core 144-871A-1H to Section 144-871A-3H-CC, 24 cm; Hole 871B, Core 144-871B-1H to Section 144-871B-3H-CC, 32 cm

Depth: Hole 871A, 0–26.5 mbsf; Hole 871B, 0–25.1 mbsf

Age: Pleistocene to Pliocene

Subunit IA is mainly a light gray (5Y 6/2) nannofossil foraminifer ooze. Locally intercalated with this light gray and pinkish gray (5YR 8/1) ooze are bands of light brownish gray (2.5Y 6/2) nannofossil foraminifer ooze (e.g., Section 144-871A-2H-2). Such bands are several centimeters to tens of centimeters thick and have a diffuse boundary with the surrounding light gray ooze. Subunit IA is composed of planktonic and benthic foraminifers and nannofossils. Radiolarians, sponge spicules, and diatoms occur in trace abundances. Sediment in the lighter brownish gray layers includes a few black specks that may be iron-manganese micronodules, although X-ray diffraction analyses indicate only the presence of calcite (e.g., Samples 144-871B-3H-1, 80 cm, and -3H-3, 100 cm). Some of the foraminifers in Section 144-871A-2H-2 are stained orange by iron hydroxide.

Subunit IB

Intervals: Cores 144-871A-4H to -15H; Cores 144-871B-4H to -14H

Depth: Hole 871A, 26.5–139.5 mbsf; Hole 871B, 25.1–139.6 mbsf

Age: middle to early Miocene

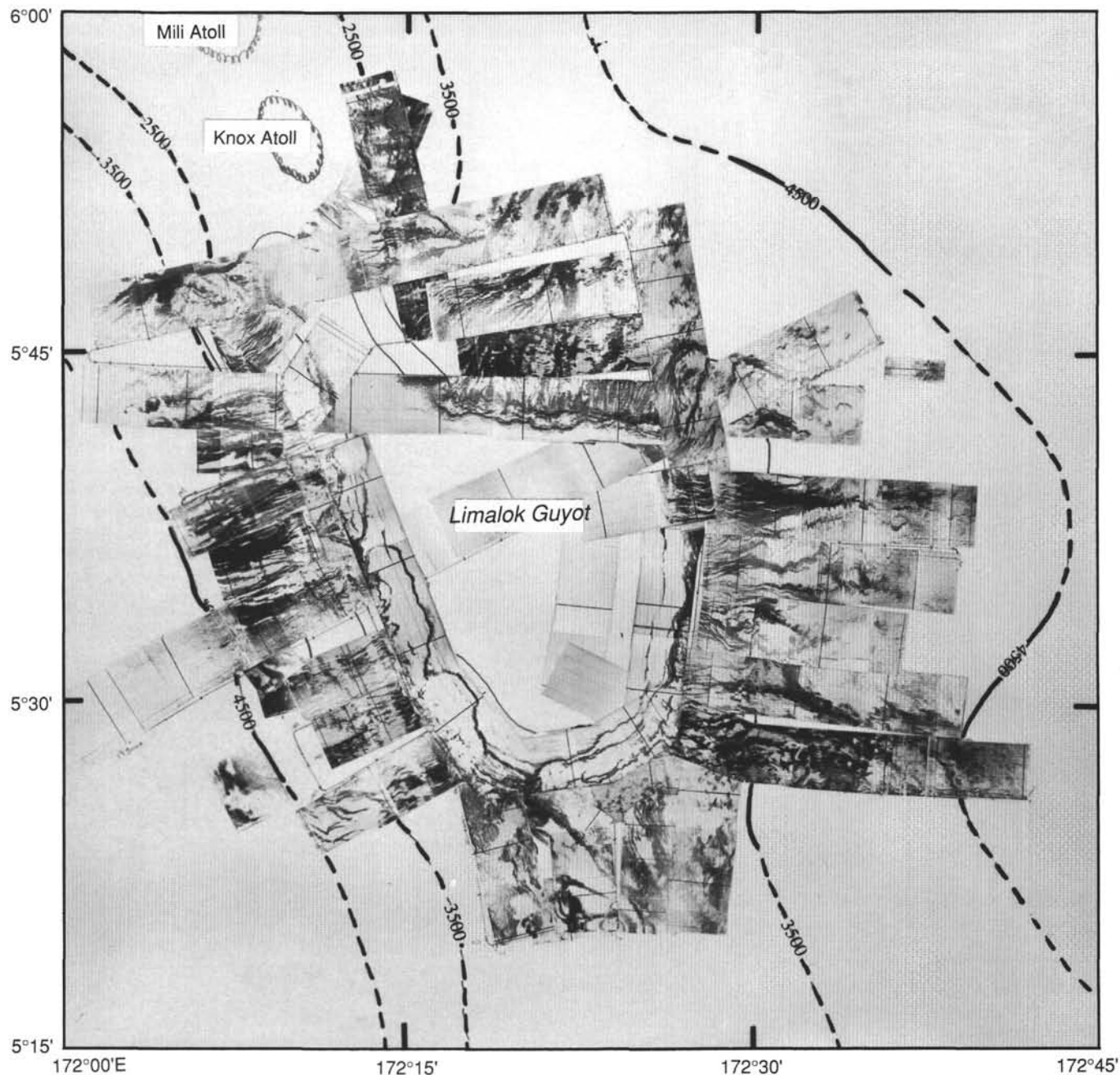


Figure 4. Side-scan images over Limalok Guyot. In this image, dark tones represent high backscatter features and light gray to white tones represent low backscatter features. Figure revised from Schlanger et al. (1987). Knox Atoll = Vanilli Atoll of Figure 3.

Subunit IB is comprised of a white (10YR 8/2), homogeneous foraminifer ooze with medium sand texture that is well-sorted and winnowed. Subunit IB is dominated by pelagic foraminifers (95%) that are less fragmented than those in Subunit IA. Nannofossils are a very minor component (<5%) throughout most of Subunit IB, although they do reach abundances of up to 30% at the top of Subunit IB. The homogenous texture of this subunit may be, in part, the result of extreme drilling disturbance of a poorly packed, water-saturated sandy deposit. Sections 144-871A-14H-1, 14H-4, 14H-5, 14H-6, and 14H-CC contain several lumps (<2 cm thick) of slightly consolidated foraminifer sand. A sediment smear slide made from such lumps shows minor evidence of foraminifer breakage and the presence of

irregular, small carbonate crystals, which may reflect the initial consolidation of the ooze.

Unit II

Intervals: Sections 144-871A-15H-CC to Core 144-871A-17X; Cores 144-871B-16X to -17X; Sections 144-871C-2R-1 to -32R-1, 40 cm
 Depth: Hole 871A, 139.3–151.9 mbsf; Hole 871B, 133.2–152.4 mbsf; Hole 871C, 133.7–422.9 mbsf
 Age: middle Eocene to early late Paleocene

Unit II is comprised of a sequence of white to very pale brown (10YR 8/1 to 10YR 7/3) platform carbonates, 289.2 m thick. The

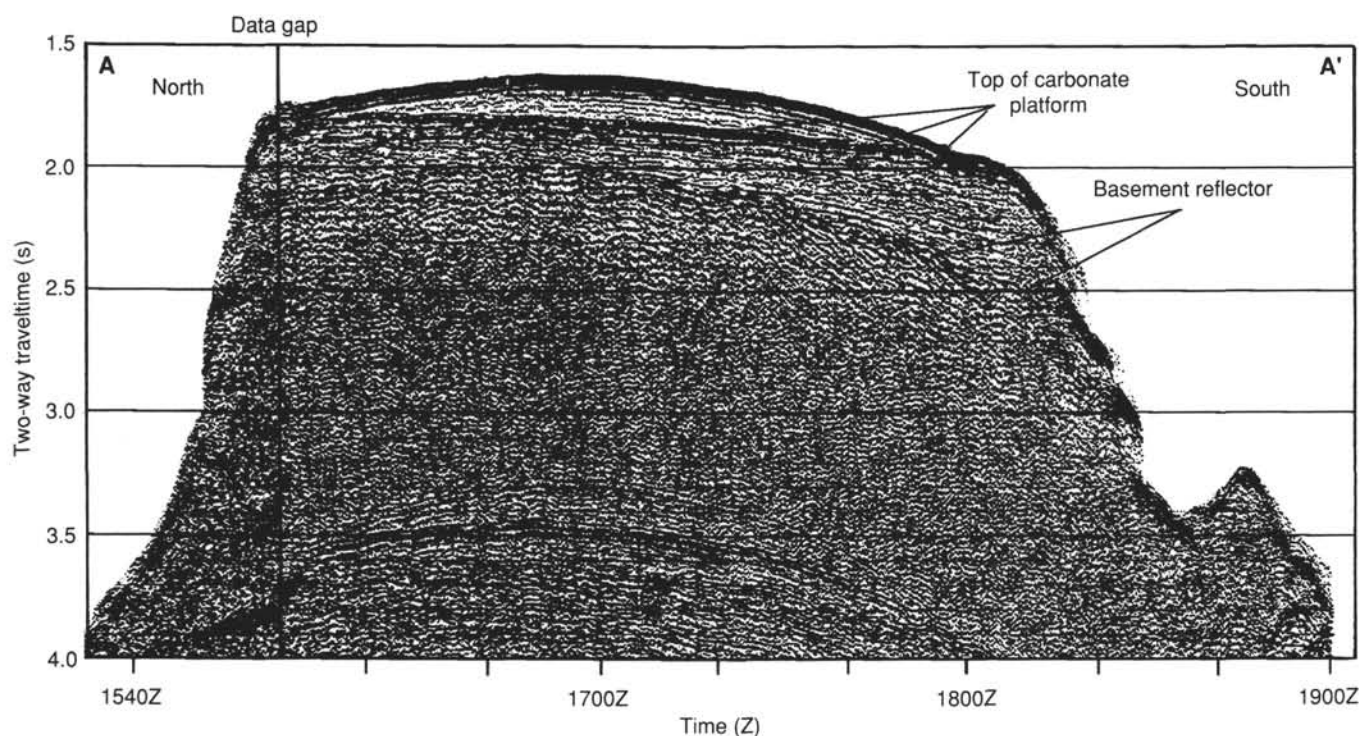


Figure 5. Single-channel seismic Profile A–A' across Limalok Guyot. Acoustic basement deepens to the south with a concomitant thickening of platform sediments. Profile A–A' location is shown in Figure 2; the location of Site 871 is near 1710Z.

maximum recovery within this unit was 14%; the unit average was 3.5% (see “Operations” section, this chapter). Limestones in Unit II include packstone, grainstone, and wackestone with abundant benthic foraminifers (mostly miliolids with agglutinated foraminifers, *Nummulites*, alveolinids, and *Asterocyclina*), common algae (e.g., red algae: corallinaceans, squamariaceans, and solenoporaceans; green algae: udoteaceans), and common molluscan molds (bivalves and gastropods) (Table 4). The porosity of these rocks is estimated at 5%–10%, and is predominantly moldic, solution-enlarged interparticle, and/or microvuggy. Porosity is moderately reduced by passively precipitated, pore-lining carbonate cement (i.e., crusts or drusy fabric); however, most of the secondary porosity remains open.

The top of Unit II is marked by a black, laminated, iron-manganese oxide and phosphatic crust (Fig. 8) that can be clearly discerned in density, resistivity, and total gamma geophysical logs (see “Downhole Measurements and Seismic Stratigraphy” section, this chapter). Borings in the crust are filled by planktonic foraminifers and nannofossils of early late Oligocene age as well as clasts of phosphate and miliolid-wackestone (see “Biostratigraphy” section, this chapter). Six subunits were recognized in Unit II on the basis of depositional texture and variations in skeletal constituents.

Subunit IIA

Interval: Sections 144-871C-2R-1 to -4R-1, 33 cm
Depth: 133.7–153.2 mbsf
Age: middle Eocene

Subunit IIA is comprised of 29.5 m of burrowed, very pale brown (10YR 7/3), benthic-foraminifer packstone and wackestone. Petrographic analyses indicate that benthic foraminifers are abundant and include miliolids, “rotaliids,” and *Nummulites*. Other components include peloids, intraclasts, echinoid fragments, a few smooth-shelled ostracodes, coral fragments, small gastropods, red algal fragments, and oncoids. A distinctive interval of white (10YR 8/2) chalky packstone with very pale brown (10YR 7/3) burrow mottles occurs in

Interval 144-871C-2R-1, 27–68 cm (Fig. 9). Last of all, a manganese-encrusted drilling pebble occurs at 152.9 mbsf (top of Section 144-871C-4R-1). Although this pebble may be the product of downhole contamination, it is interesting to note that an enrichment in uranium, similar to that recorded at the top of Core 144-871C-2R, is recorded in the geophysical logs (e.g., total gamma) at this depth (see “Downhole Measurements and Seismic Stratigraphy” section, this chapter).

Subunit IIB

Intervals: Sections 144-871C-4R-1, 33 cm, to -6R-1
Depth: 153.2–181.9 mbsf
Age: middle Eocene

Subunit IIB is comprised of 28.7 m of skeletal grainstone. Benthic foraminifers are abundant and include miliolids and other smaller foraminifers. Fragments of ostracodes and echinoids are moderately abundant as are bivalves, gastropods, intraclasts, and peloids. Red and green algae are scarce. Miliolid packstone and wackestone may be interbedded. Porosity is ~3%–10% and commonly is moldic. Some moldic porosity is lined with calcite cement.

The top of Subunit IIB is marked by a very coarse, miliolid-intraclast sand with keystone vugs (Fig. 10). Intraclasts are fragments of peloid-foraminifer packstone. The keystone vugs are filled with two generations of calcite cement separated by geopetal internal sediment (Fig. 11). The first generation of cement is a cloudy, thick, isopachous crust (PE_5C = passively precipitated equant [coarsely crystalline; $5 = 0.25$ – 1.0 mm] crust; Folk, 1965). The second generation of cement is a clear equant spar (PE or B_5C = passively precipitated equant or bladed equant crust) with acute crystal terminations. The presence of keystone vugs is important, because such vugs form in aerated environments and thus may be interpreted as evidence of deposition in an intertidal environment. The base of Subunit IIB is a cross-laminated fine skeletal sand with wavy, white (10YR 8/2) and pale brown (10YR 6/3) bandings (Fig. 12). Such a lithology is characteristic of high-energy environments.

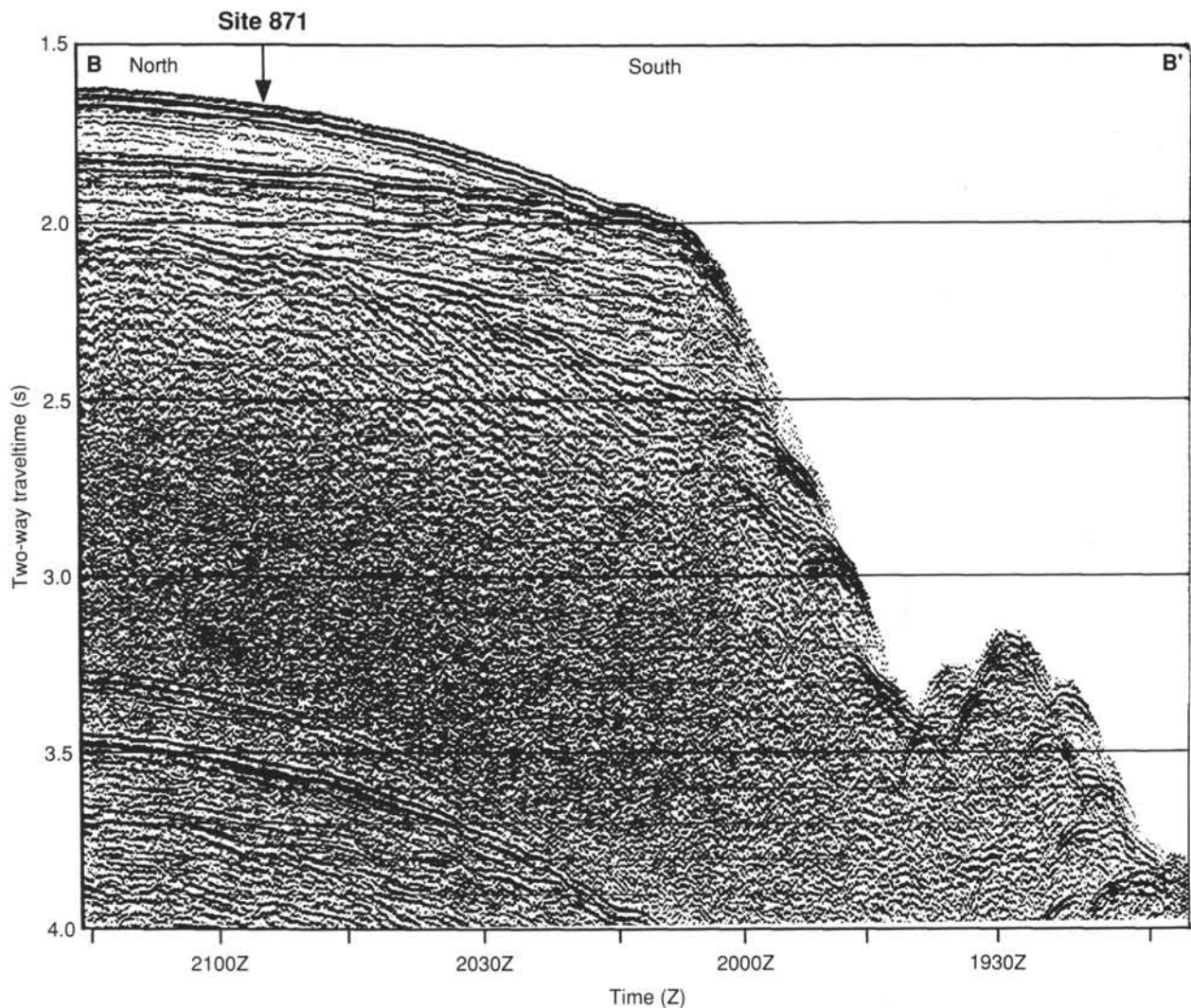


Figure 6. Single-channel seismic Profile B-B' collected during beacon drop over Limalok Guyot. Profile B-B' location is shown in Figure 2; the location of Site 871 is at 2057Z.

Subunit IIC

Intervals: Sections 144-871C-7R-1 to -21R-1, 16 cm
 Depth: 181.9–316.7 mbsf
 Age: middle to early Eocene

Subunit IIC is comprised of 134.8 m of very pale brown (10YR 7/3) benthic foraminifer packstone and wackestone that have moderately abundant miliolid and agglutinated foraminifers. Abundant large alveolinid foraminifers first appear in Interval 144-871C-19R-1, 0–17 cm, and continue through Section 144-871C-20R-1 (Fig. 13). A coral head was recovered near the base of Subunit IIC (Interval 144-871C-20R-1, 0–9 cm; Fig. 10). Several wackestones in Subunit IIC have a poorly diversified microfauna that consists primarily of “discorbids” and agglutinated foraminifers, as well as rare thin-shelled bivalves and small low-spined gastropods (e.g., Intervals 144-871C-9R-1, 9–12 cm, and -10R-1, 10–13 cm). A dense lime mudstone with conchoidal fracture and tubular pores occurs at 201.3 mbsf (Interval 144-871C-9R-1, 4–30 cm; Fig. 14). A thick (up to 40 m) interval of chalky limestones begins at 249.5 mbsf (Section 144-871C-14R-1, 0 cm). Core 144-871C-10R also contains chalky limestones. Moldic and solution-enlarged interparticle porosity (5%–

7%) is developed from dissolution of mollusks and benthic foraminifers; commonly such porosity is reduced by calcite cement.

Subunit IID

Interval: Sections 144-871C-21R-1, 16 cm, to -26R-1
 Depth: 316.7–374.3 mbsf
 Age: late Paleocene

Subunit IID is comprised of 57.6 m of foraminifer and coralline packstones, coralline rudstone, and algal-coralline grainstones. Some wackestones are present (Cores 144-871C-21R, -23R, -24R, -25R, and -26R), but only the wackestone in Core 144-871C-24R is considered stratigraphically robust.

The placement of the boundary between Subunits IIC and IID within Section 144-871C-21R-1, 16 cm, is based on a change in depositional texture from packstone-dominated in Subunit IIC to grainstone-dominated in Subunit IID. The placement of this lithostratigraphic boundary is consistent with the resistivity and total gamma geophysical logs (see “Downhole Measurements and Seismic Stratigraphy” section, this chapter) and a biostratigraphically determined boundary between early Eocene and late Paleocene carbonates. The

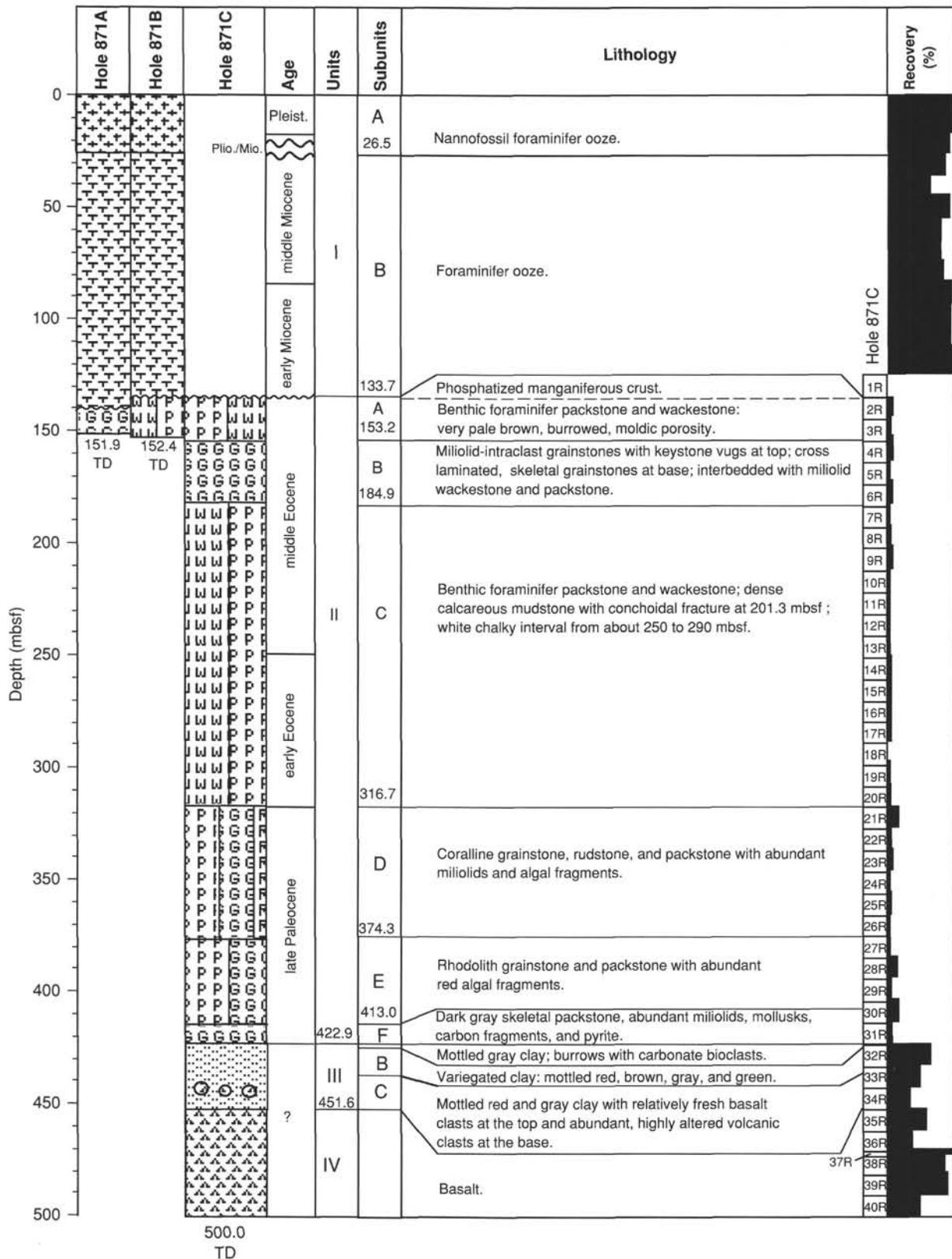


Figure 7. Lithostratigraphic summary of Site 871. TD = total depth.

Table 3. Summary of lithostratigraphic units, Site 871.

Unit	Subunit	Depth (mbsf)	Age	Lithology
Pelagic carbonates:				
I	IA	0.0–26.5	Pleistocene–Pliocene/Miocene	Nannofossil foraminifer ooze
I	IB	26.5–133.7	middle Miocene–early Miocene	Foraminifer ooze
Platform carbonates:				
II	IIA	133.7–153.2	middle Eocene	Benthic foraminifer packstone/wackestone
II	IIB	153.2–181.9	middle Eocene	Miliolid-intraclast grainstone
II	IIC	181.9–316.7	middle Eocene–early Eocene	Benthic foraminifer packstone/wackestone
II	IID	316.7–374.3	late-early Paleocene	Coralline grain/rudstone/packstone
II	IIE	374.3–413.0	late Paleocene	Rhodolith grain/packstone
II	IIF	413.0–422.9	late Paleocene	Dark gray skeletal packstone
Variagated clays and volcanoclastic debris:				
III	IIIA	422.9–423.8	Indeterminate	Mottled gray clay
III	IIIB	423.8–435.9	Indeterminate	Variagated clay
III	IIIC	435.9–451.6	Indeterminate	Mottled red and gray clay
Basalt (see “Igneous Petrology” section, this chapter)				

lithologic boundary between Subunit IIC and IID could alternatively be placed between Cores 144-871C-19R and -20R on the basis of a change from benthic foraminifer-dominated limestones to coralline- and algae-dominated limestones (Fig. 15). Careful examination of the recovered cores (2.3% and 14.2% recovery) does not indicate any breaks in deposition within the interval from 307 to 326 mbsf. Thus, either boundary position is consistent with the lithostratigraphy of Hole 871C; the lower position emphasizes more depositional texture and log character.

Subunit IID is distinguished from the overlying units by its coarser grain size, different skeletal constituents, and abundant carbonate cements. The dominant skeletal allochems in this subunit are corals (Fig. 16; small branching *Porites* and some spherical or digitate *Pocillopora?*), algae (small branching forms, fragments of algal crusts, and fragments of green algae), mollusks, and foraminifers (Fig. 17; miliolids, *Nummulites*, alveolinids, and *Asterocyclina*). Porosity ranges from 2% to 10% and is commonly moldic after mollusks (bivalves and gastropods) and corals; some of the molds have been enlarged by solution; others have been reduced by carbonate cementation. Cements are pore-lining equant and bladed calcite.

Subunit IIE

Interval: Sections 144-871C-27R-1 to -31R-1, 21 cm
Depth: 374.3–413.0 mbsf
Age: late Paleocene

Subunit IIE is comprised of 38.7 m of rhodolith grainstone and packstone. The most characteristic features of Subunit IIE are the dominance of algal limestones, especially rhodoliths, and the decrease in the abundance of lime mud. The nuclei of the rhodoliths consist of skeletal sands or algal remains (Fig. 18). Coralline and squamariacean red algae were identified within single rhodoliths in Section 144-871C-28R-1. Other skeletal constituents include foraminifers (*Asterocyclina*, miliolids, and small *Nummulites*), corals, mollusks, and peloids. Porosity varies from 2% to 5%. Intergranular and moldic pores are rimmed by calcite cements (Fig. 19).

Subunit IIF

Interval: Sections 144-871C-31R-1, 21 cm, to -32R-1, 40 cm
Depth: 413.0–422.9 mbsf
Age: early late Paleocene

Subunit IIF is comprised of a dark gray (2.5YR 4/0) skeletal packstone, 9.9 m thick. Subunit IIF differs from the overlying, light gray limestones mainly in color. The contact between Subunits IIF and IIE was not recovered. The uppermost 6 cm of recovery from Subunit IIF is yellowish orange molluscan-miliolid packstone with limonite staining of the matrix and foraminifers; other foraminifers

are dark gray. The change in color indicates that the top of Subunit IIF may have been oxidized. The contact between Subunit IIF and Unit III is relatively sharp (Section 144-871C-32R-1, 40 cm).

The skeletal packstone in Subunit IIF is poorly sorted. The subunit is coarse grained at its base and becomes finer grained toward the top. Abundant components include thick-shelled bivalve fragments, gastropods, miliolids and larger foraminifers (*Asterocyclina* and *Nummulites*), red algal debris (corallinaceans, solenoporaceans, squamariaceans, rhodoliths), green algae (udotaceans), and echinoderms. Small fragments of corals are rare. In addition, sand-size angular fragments of coal (<1%) are dispersed in Subunit IIF. Pyrite and iron monosulfide replaces some of the foraminifer tests, rims some of the molluscan shell fragments, and forms small “framboidal” aggregates within sparry calcite cement. Gastropod and bivalve shells at the base of Subunit IIF have well-preserved skeletal architecture. The exquisitely preserved prismatic bundles observed in bivalve shells from this interval are indicative of the retention of the aragonite mineralogy. Intraskelatal voids are rimmed by bladed sparry calcite, with some cavities infilled by internal sediment, resulting in the development of geopetal fabric.

Unit III

Interval: Sections 144-871C-32R-1, 40 cm, to -35R-1, 5 cm
Depth: 422.9–451.6 mbsf
Age: indeterminate

Unit III is a variegated clay that displays large variations in the texture, color, and content of lithoclasts. These variations form the basis for delineating the subunits of Unit III.

Subunit IIIA

Interval: Sections 144-871C-32R-1, 40 cm, to -32R-2, 128 cm
Depth: 422.9–423.8 mbsf
Age: indeterminate

Subunit IIIA consists of homogeneous gray clay with patches of a dark-gray, fine-grained, sand-size sediment up to 1 cm thick. Patches are comprised of fragmented shells of mollusks, foraminifers, and unidentified organisms. Some of these shelly patches are distinctly elongate or tubular. Nannofossils with calcite overgrowths and carbonate debris were noted in smear slides. Small gastropods occur in the clay. The deepest sandy patch occurs 44 cm from the top of the unit in Section 144-871C-32R-1. The occurrence of sand-filled patches of marine skeletal grains within the clay is thought to reflect burrowing. In Section 144-871C-32R-1, 93 cm, the clays gradually become light gray (5Y 6/2) and enclose yellowish, limonitic patches. The lower boundary of Subunit IIIA is placed at a distinct change from light-gray clay into olive-gray mottled clay which then grades into brick-red mottled clay over the interval from 93 to 128 cm in Section 144-871C-32R-1.

Table 4. Skeletal and nonskeletal constituents recognized in thin sections from Unit II (platform carbonates), Site 871.

Constituents	Subunit					
	IIA	IIB	IIC	IID	IIE	IIF
Red algae	R			C-F	Ab	Ab
Corallinaceans					Yes	Yes
Squamariaceans					Yes	Yes
Solenoporaceans						Yes
Green algae		R		C-F		R
Udoteaceans		Yes		Yes		
Benthic foraminifers	Ab	Ab	C-F	Ab	Ab	Ab
<i>Asterocyclina</i>				Yes	Yes	Yes
Miliolids	Yes	Yes	Yes	Yes	Yes	Yes
<i>Nummulites</i>	Yes			Yes	Yes	Yes
<i>Alveolina</i>			Yes			
Agglutinated foraminifers			Yes			
"Rotaliids" or "Discorbids"	Yes					
Echinoderm fragments	R	C-F	R	C-F	R	C-F
Corals	R			C-F		C-F
Coral fragments			R			
Bivalves		C-F	R			C-F
Gastropods			C-F	C-F		
Brachiopods		R	R			
Ostracodes			R	R		
Ostracode fragments		C-F				
Worm tubes			R			
Oncoids	R					
Peloids	C-F	C-F	C-F			
Intraclasts	C-F	C-F				C-F
Lithoclasts		C-F		C-F		

Notes: Ab = abundant, C = common, F = few, R = rare, and Yes = present, but abundance was not estimated.

Subunit IIB

Interval: Sections 144-871C-32R-1, 128 cm, to -33R-3, 70 cm
Depth: 423.8–435.9 mbsf
Age: indeterminate

Subunit IIB is comprised of mottled, variegated clays. Alternating clay horizons are observed as mottled dark red (10YR 3/3), pale red (10R 6/3), olive brown (2.5 yr 4/4), greenish gray (10G 7/2), and olive-green layers. Red and pale-brown mottled intervals are more lithified than intervals with lighter shades of mottling and may represent concentration of iron oxides. A few pebbles of highly altered basalt, smaller than 1 cm in size, are intercalated within the clay in Section 144-871C-32R-4.

Subunit IIC

Interval: Sections 144-871C-33R-3, 70 cm, to -35R-1, 5 cm
Depth: 435.9–451.6 mbsf
Age: indeterminate

Subunit IIC is a heterogeneous unit comprised of clay, basalt clasts, and sandy intervals. The top 54 cm of this subunit is comprised of dark to medium-gray clays that enclose at least four clasts of well-preserved basalt. Two clasts of basalt occur in Interval 144-871C-34R-1, 134–144 cm. Some of the basalt clasts have weathered rims and are greenish colored. From Sections 144-871C-33R-3, 124 cm, to -34R-1, 134 cm, the clay becomes a rusty colored mixture of argillaceous sand and clayey intervals. Several less altered pieces of probable volcanoclastics can be recognized within this interval. The remainder of the sediment is a mixture of clay with sandy argillaceous zones. Overall, the number of altered basalt clasts increases toward the base of this subunit.

Subunit IIC is underlain by a medium dark-gray basalt, which forms Unit IV. Refer to "Igneous Petrology" section (this chapter) for a discussion of the basalts that comprise Unit IV.

Preliminary Interpretation of Depositional History

Given the low recovery in the platform carbonate sequence at Site 871 (average 3.5%), a reconstruction of depositional history is specu-

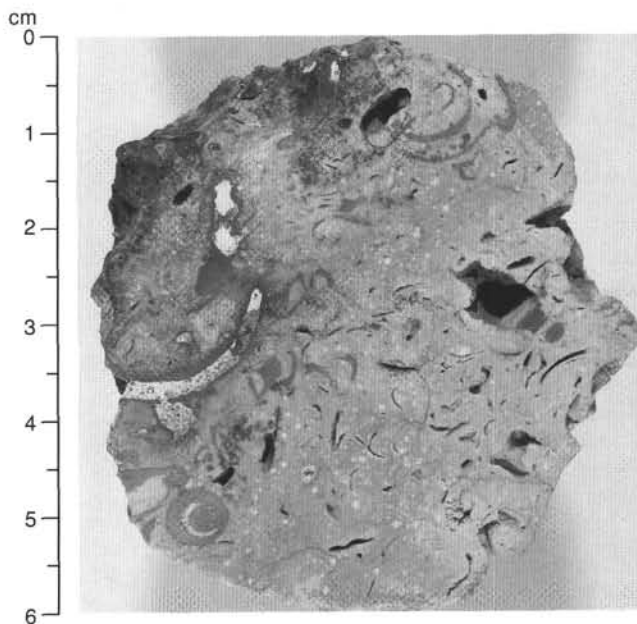


Figure 8. Close-up core photograph of iron-manganese hardground (Interval 144-871C-2R-1, 0–6 cm).

lative. Nevertheless, an overview of the depositional history recovered at Site 871 (Limalok Guyot; formally Harrie Guyot) can be inferred (Fig. 20).

The basalt deposits of Unit IV document the waning phase of volcanic activity. The uppermost part of several of the multiple flow units exhibit alteration, which may result from subaerial weathering or hydrothermal alteration (see "Igneous Petrology" section, this chapter).

The variegated clay and volcanic breccia of Unit III represents a combination of (1) erosion and slumping of volcanoclastic sediments (Subunit IIC), (2) weathering (Subunit IIB), and (3) final submergence of the volcano (Subunit IIIA). The variegated clays of Subunits IIC and IIB may represent a soil horizon developed under tropical weathering conditions. Intercalated, highly altered volcanoclastic intervals and an admixture of clasts of well-preserved basalt with weathering rims suggest some displacement of the soil on the slope of the volcanic island. The sediment of Subunit IIIA is characterized by its more homogeneous texture and light-gray color, which becomes increasingly darker toward the top of the unit. The color transition reflects an increase in organic content (see "Organic Geochemistry" section, this chapter). The organic-rich clay was burrowed 44 cm below the upper contact at 422.9 mbsf. Burrows are filled by predominantly fine sand-size biogenic particles: foraminifers, gastropods, and other molluscan shell debris, as well as nanofossils. The constituents of the burrow fills are similar to those of the overlying limestone. Thus, we interpret these burrow fills as basal transgressive marine deposits.

The platform carbonate sequence (Unit II) at Site 871 records the development and demise of a 289.2-m-thick Paleocene to Eocene carbonate platform or atoll.

Subunit IIF documents the submergence of the volcanic island and concomitant initiation of carbonate sedimentation in the Paleocene at this site. The composition of limestones from Subunit IIF indicates a turbulent, shallow-marine depositional environment. Their packstone texture and coarse sand size are consistent with this interpretation. The depositional environment was probably well oxygenated, as indicated by the diverse biota and good sorting. The presence of pyrite within this limestone, as well as the preservation of carbon fragments, suggests sulfate reduction in the early diagenetic marine environment.

The grainstone and packstone facies of Subunit IIE include a normal marine biota that indicates deposition in shallow waters on an

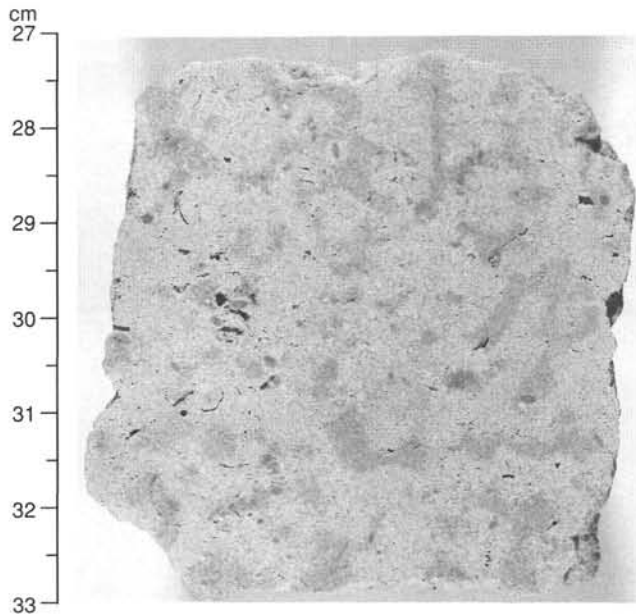


Figure 9. Close-up core photograph of a distinctive interval of white (10YR 8/2) chalky packstone with very pale brown (10YR 7/3) burrow mottles (Interval 144-871C-2R-1, 27–33 cm).

open, but narrow, shelf or steep ramp. Lithostratigraphic evidence from Subunit IID is consistent with a back-reef depositional environment. Both algal-dominated facies (grainstones and a boundstone interval) and foraminifer grainstones to packstones possess a fully marine fauna. Our interpretation of a back-reef depositional environment for this subunit is based on the presence of corals and red algae—the best evidence of reef proximity.

The small-sized, low-spired gastropods (Fig. 21) and overall poor diversity of fauna and flora in the local foraminifer wackestone intervals of Subunit IID suggest restricted conditions with probable environmental fluctuations (e.g., salinity, temperature), possibly a restricted lagoon. The local occurrence of echinoids suggests incursions of normal-salinity marine waters. In thin section, the echinoid material appears abraded and micritized; it could have been carried by storms and then mixed into the sediment by bioturbation. The wackestones may represent periods of increasing restriction, possibly accompanied by shoaling when carbonate production outpaced relative sea-level rise. The wackestone intervals are usually underlain by sediments deposited in normal marine waters. However, it must be stressed that such interpretations are preliminary and that much future work is needed to constrain the dynamic environmental variations encoded in the sediments of Subunit IID.

Lithofacies of Subunit IIC are consistent with a protected, shallow, lagoon depositional environment. Subunit IIC consists mostly of burrowed skeletal foraminifer packstones and wackestones containing *Alveolina* (in the lowermost part only) and miliolids which is consistent with deposition in a protected, shallow lagoon. Fragments of reef organisms (i.e., corals, red algae), which are to be expected from the erosion of a nearby reef, are scarce, except within the transition to Subunit IID. Four wackestone intervals in Subunit IIC that include thin-shelled bivalves, small gastropods, miliolids, and “discorbid” are observed. Foraminifers may indicate periods of restricted conditions.

Subunit IIB marks a return to more turbulent conditions with the prevalence of foraminifer grainstones, although miliolid packstones and wackestones, recovered as rounded cobbles, may be locally interbedded. Fine-grained foraminifer grainstones at the base of Subunit IIB display low-angle cross laminations; the top of this subunit consists of coarse sands exhibiting keystone vugs. These vugs typically form

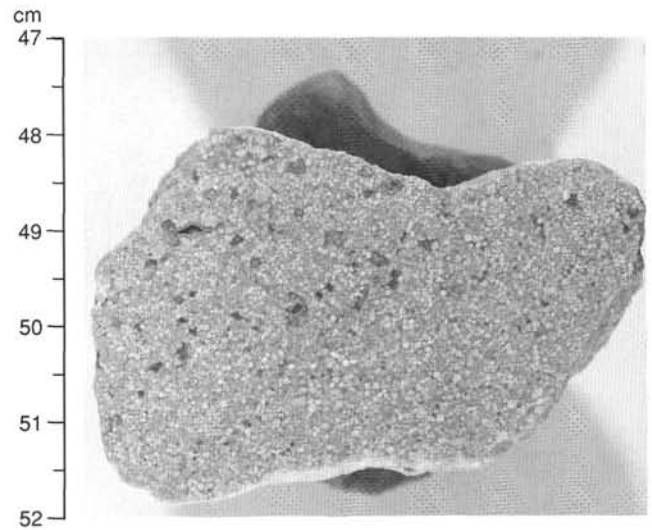


Figure 10. Close-up core photograph of keystone vugs from a miliolid-rich grainstone (Interval 144-871C-4R-1, 48–52 cm).

immediately within the wave swash zone, by the trapping of air bubbles from intergranular pores as a sand body is flooded during the tidal cycle (Dunham, 1970). These grainstones may be interpreted as beach or sand bar deposits. Keystone vugs are rimmed by marine cements of isopachous fibrous calcite.

Subunit IIA consists of foraminifer packstone and wackestone that is interpreted to have been deposited in a protected, shallow lagoon. The upper surface of Subunit IIA is a bored iron-manganese-coated surface. Oligocene planktonic foraminifers fill the borings. The iron-manganese oxide and phosphatic crust suggests the formation of a mineralized submarine hardground at the top of the platform carbonates.

The geologic history of platform carbonates at Site 871 is poorly constrained because of the overall poor recovery of carbonate rocks and probable lack of recovery of critical intervals. However, the Paleocene-Eocene carbonate sequence displays a general shallowing-upward trend, with changes in depositional environment from an open subtidal to a shallow lagoonal depositional setting. The initial development of the narrow Paleocene carbonate platform or steep ramp is characterized by algal-dominated facies with rhodoliths. This association has been noted in Cenozoic atolls (e.g., Site 831; Collot, Greene, et al., 1992), and even Late Cretaceous isolated carbonate platforms (Camoïn et al., 1988). The Paleocene history of this carbonate platform ends with the deposition of coral grainstones and packstones that represent the last record of any reef-related sediments. The Eocene history of this carbonate platform is clearly dominated by shallow lagoonal deposits with no sedimentological evidence of adjacent reef development, although the presence of a lagoon requires some kind of barrier.

The carbonate platform at Limalok Guyot subsided into the pelagic realm by the early Oligocene, as indicated by the planktonic foraminifers and nannofossils that infill borings in the marine hardground. However, the accumulation of pelagic sediments did not begin until the early Miocene. The pelagic cap at Limalok Guyot consists of well-sorted, winnowed foraminifer sand overlain by nannofossil foraminifer ooze. A hiatus broadly coincides with the lithologic change from sand to ooze at the base of Core 144-871A-3H.

Preliminary Interpretation of Postdepositional History

The recognition of products of postdepositional alteration in the carbonate sequence is made especially difficult by the low core recovery. The most pervasive diagenetic features are leached intervals where porosity commonly is moldic, solution-enlarged interparticle,

and microvuggy (Fig. 17). The wholesale leaching of calcitic components, mainly Mg-calcite benthic foraminifers, is especially remarkable. Secondary porosity is moderately reduced locally by the precipitation of pore-lining calcite cements. Local chalky limestones may be the product of meteoric phreatic diagenesis, but definitive statements cannot be made at this time. Another unusual diagenetic feature is the complete neomorphic replacement of several coral fragments by clear, coarse spar with traces of the original skeleton (Interval 144-871C-21R-1, 89–96 cm; Fig. 18).

In the small percentage of the section recovered, unequivocal evidence of subaerial exposure, (e.g., caliche or karst development) was not observed. Sedimentological evidence of exposure above the intertidal zone is likewise lacking. However, it must be stressed that the lack of evidence of platform emergence does not necessarily mean that the platform was never emergent.

BIOSTRATIGRAPHY

Introduction

Three holes were drilled at Site 871. Holes 871A and 871B were drilled to core the Neogene pelagic cap of Limalok Guyot using the APC. Hole 871C was rotary drilled to core the platform carbonate sequence and underlying basaltic basement. Sediments spanning the upper Paleocene through Pleistocene were recovered. Age dating and paleoenvironmental interpretations for the Neogene pelagic cap (Lithologic Unit I) are based on calcareous microplankton fossils. Biostratigraphic control and paleoecologic interpretations for the platform carbonates (Lithologic Unit II) are provided principally by benthic foraminifers, with additional data provided by planktonic foraminifers, calcareous nannofossils, palynomorphs, and diatoms. Palynology of the underlying claystone unit (Lithologic Unit III) provides information about the associated islands.

Neogene Pelagic Cap

Calcareous Nannofossils

The pelagic sequence from Hole 871A was sampled and examined in detail for nannofossils to establish the biostratigraphy. The pelagic sequence from Hole 871B was not sampled extensively. The nannofossil biostratigraphy for this duplicate hole through the pelagic cap, based on core-catcher samples only, is presented in Figure 22 and discussed only when results from this hole differ significantly from those of Hole 871A. In general, the foraminifer oozes of the pelagic cap at Site 871 contain moderate to well-preserved nannofossil assemblages of Neogene age.

The nannofossil biostratigraphy indicates that the Pleistocene in the pelagic cap of Limalok Guyot is relatively complete, with all of the zones of Gartner (1977) preserved in the sequence (Fig. 22). The *Emiliana huxleyi* Acme Zone extends from the top of Core 144-871A-1H through Sample 144-871A-1H-1, 82–83 cm (0–0.83 mbsf). The presence of *Pontosphaera indoceanica* in the uppermost sample (Sample 144-871A-1H-1, 20–21 cm) suggests that only the lower part of the *E. huxleyi* Acme Zone was recovered in this hole. The interval from Samples 144-871A-1H-1, 143–144 cm, through -1H-3, 140–141 cm (1.43–4.41 mbsf), also contains *E. huxleyi*, but it is dominated by the small *Gephyrocapsids*, indicating the *E. huxleyi* Zone of late Pleistocene age.

The middle Pleistocene *Gephyrocapsa oceanica* Zone is represented in only one sample (Sample 144-871A-1H-4, 20–21 cm; 4.71 mbsf). The thinness of this zone, which spans approximately 200 k.y. according to Berggren, Kent, and Van Couvering (1985), suggests a reduced rate of sediment accumulation during this part of the middle Pleistocene. The underlying *Pseudoemiliana lacunosa* Zone is somewhat thicker (5.3–8.3 mbsf), including the interval from Samples 144-871A-1H-4, 80–81 cm, through -2H-1, 80–81 cm. The small *Gephyrocapsa* Zone of early to middle Pleistocene age spans the

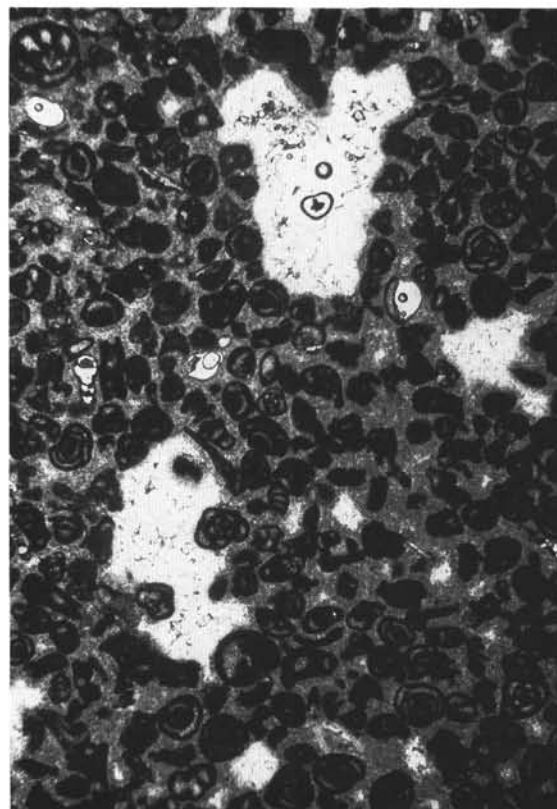


Figure 11. Thin-section photomicrograph of keystone vugs from a miliolid-rich grainstone (Interval 144-871C-4R-1, 48–52 cm). Maximum dimension = 1 cm.

interval from Samples 144-871A-2H-2, 25–26 cm, through -2H-3, 80–81 cm (9.25–11.3 mbsf).

The interval from Samples 144-871A-2H-3, 135–136 cm, through -2H-6, 80–81 cm (13.35–14.8 mbsf), is included within the *Helicospaera sellii* Zone of early Pleistocene age. The interval from Samples 144-871A-2H-6, 135–136 cm, through -3H-1, 80–81 cm (15.35–17.8 mbsf), is characterized by the presence of *Calcidiscus macintyreii* in the absence of discoasters, indicating the *C. macintyreii* Zone of latest Pliocene to earliest Pleistocene age. However, based on the work of Rio et al. (1990), the occurrence of rare *Gephyrocapsa oceanica* indicates that this interval is earliest Pleistocene in age.

The Pliocene is contained entirely within the upper three sections of Core 144-871A-3H. Only three of the ten Pliocene subzones are present within the sequence at Site 871. The upper three sections of Core 144-871A-3H contain two of the subzones of the upper Pliocene *Discoaster brouweri* Zone (CN12): CN12d and CN12a. Subzone CN12d, characterized by the presence of *Discoaster brouweri* in the absence of *Discoaster pentaradiatus*, occurs from Samples 144-871A-3H-1, 135–136 cm, through -3H-2, 50–51 cm (18.35–19.01 mbsf). The last appearance datum (LAD) of *Discoaster asymmetricus*, dated as 2.20 Ma by Berggren, Kent, and Van Couvering (1985), in Sample 144-871A-3H-2, 50–51 cm (19.0 mbsf), provides additional time-stratigraphic control within this interval. Subzone CN12d is separated from the underlying *Discoaster tamalis* Subzone (CN12a) by a disconformity with a minimum hiatus of 200 k.y., based on the chronology of Berggren, Kent, and Van Couvering (1985). Upper Pliocene Subzone CN12a is characterized by the occurrence of *D. tamalis* in the absence of *Reticulofenestra pseudoumbilica*. This subzone is contained within the interval from Samples 144-871A-3H-2, 80–81 cm, through -3H-3, 135–136 cm (19.3–21.36 mbsf).

The remainder of Core 144-871A-3H (Sections 144-871A-3H-4 through -3H-CC; 21.5–26.5 mbsf) contains nannofossil assemblages

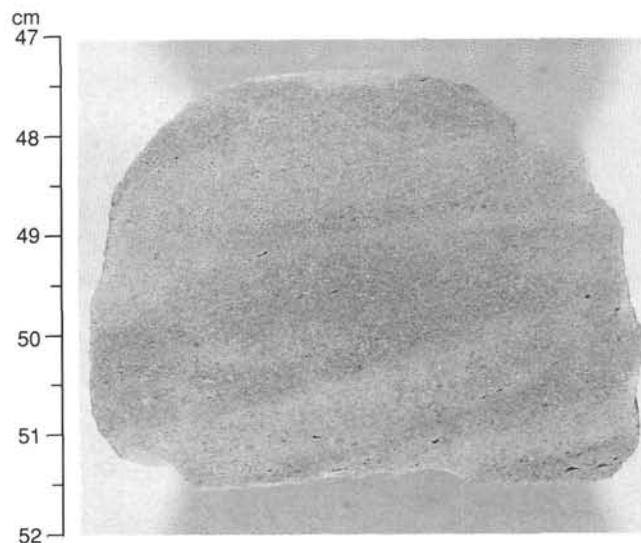


Figure 12. Close-up core photograph of the base of Subunit IIB (Interval 144-871C-6R-1, 47–52 cm), which is a cross-laminated fine skeletal sand with wavy, white (10YR 8/2) and pale brown (10YR 6/3) bandings.

which include *Reticulofenestra pseudumbilica*, *Sphenolithus abies*, *S. neobies*, *S. verensis*, *Amaurolithus primus*, and *A. amplificus* without *Discoaster berggrenii*, *Discoaster quinqueramus*, or any *Ceratolithus* spp. This association of taxa indicates the *Triquetrorhabdulus rugosus* Subzone of the *Amaurolithus tricorniculatus* Zone (CN10a) of earliest Pliocene to latest Miocene age. Although this subzone straddles the Miocene/Pliocene boundary, planktonic foraminifers (see below) suggest that the entire subzone is latest Miocene in age at this site. It is interesting, from a paleoecologic standpoint, that the nominate taxon for this subzone (*T. rugosus*) is absent from the Site 871 assemblages. Nannofossil assemblages within Section 144-871A-3H-6 contain significant reworked taxa, including *Dictyococcites bisectus* and *Cyclicargolithus abisectus*. The presence of *D. bisectus* and *C. abisectus* indicate reworking from the upper Oligocene.

Given the record from Hole 871A, it would appear that the uppermost Miocene (CN10a) is separated from the upper Pliocene (CN12a) by a significant disconformity with a minimum hiatus of 1.5 m.y. (based on the Berggren, Kent, and Van Couvering [1985] time scale). This apparent disconformity is marked in the core by a color change (from 10YR 8/2 above to 10YR 8/1–5YR 8/1 below; see visual core description) between Sections 144-871A-3H-3 and -3H-4. However, a sample from Section 144-871B-3H-CC (25.1 mbsf) contains an assemblage that includes both *Pseudoemiliania lacunosa* and *Reticulofenestra pseudumbilica*, indicating the upper part of the *Reticulofenestra pseudumbilica* Zone (CN11) of late Pliocene age. Thus, it is evident that the apparent disconformity between the upper Miocene and upper Pliocene in Core 144-871A-3H, marked by a significant paleontologic and lithologic break, is (at least in part) an artifact of incomplete core recovery. It is more likely that the hiatus at this disconformity is approximately 0.9 m.y.

The interval from Cores 144-871A-4H through -15H (base of the pelagic cap) contains a thick (113 m) sequence of lower to middle Miocene foraminifer ooze. This sequence disconformably underlies the latest Miocene through Pleistocene sequence with a hiatus of at least 6.0 m.y., based on the geochronology of Berggren, Kent, and Van Couvering (1985).

Core 144-871A-4H through Sample 144-871A-6H-4, 25–26 cm (26.5–49.25 mbsf), contain *Discoaster exilis*, *Discoaster braarudii*, *Discoaster kugleri*, and *Reticulofenestra pseudumbilica*, indicating the *Discoaster kugleri* Subzone of the *Discoaster exilis* Zone (CN5b) of middle Miocene age. Preservation within this interval is generally

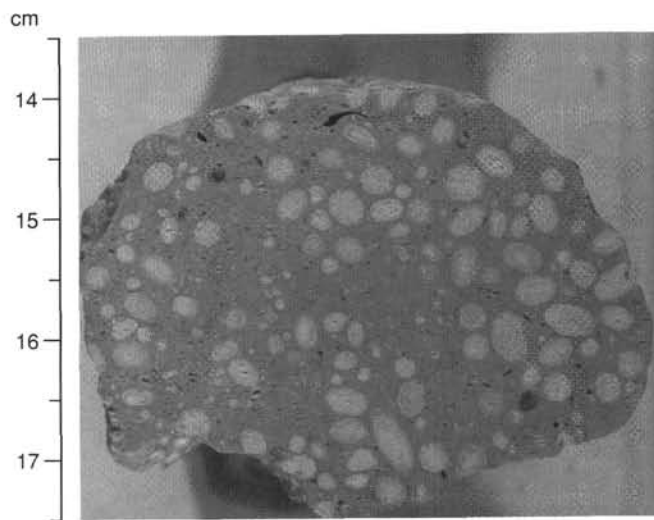


Figure 13. Close-up photograph of alveonid-rich packstone from Subunit IIC (Interval 144-871C-20R-1, 13.5–17.5 cm).

good, although nannofossils comprise a volumetrically small component of these foraminifer oozes.

The interval from Sample 144-871A-6H-6, 50–51 cm, through Core 144-871A-8H (53.5–74.0 mbsf) contains nannofossil assemblages with *Sphenolithus heteromorphus*, *Reticulofenestra pseudumbilica*, and *Discoaster exilis*, indicating the *Sphenolithus heteromorphus* Zone (CN4) of middle Miocene age. The presence of the distinctive *Discoaster musicus* in the samples from Section 144-871A-6H-6 suggest the upper portion of CN4 for this part of the unit. Cores 144-871A-9H through -11H (74.0–102.5 mbsf) contain *Sphenolithus heteromorphus* and *Discoaster exilis* without *R. pseudumbilica*. *Helicospaera ampliaperta*, the index fossil for the *H. ampliaperta* Zone (CN3) was not observed in this sequence, although it is often very rare or absent in deep oceanic sections because of its paleoecologic preference for areas near continental margins. In the absence of *H. ampliaperta* and the secondary marker *R. pseudumbilica*, it is difficult to separate Zone CN3 from Zone CN4. As a result, this interval is assigned to the combined Zone CN3/4 of early Miocene age (Fig. 22).

The interval from Samples 144-871A-12H-1, 50–51 cm, through -13H-1, 50–51 cm (103.0–112.5 mbsf), contains *Sphenolithus belemnus*, *Discoaster druggii*, and *Discoaster adamantus*, indicating the *Sphenolithus belemnus* Zone (CN2) of early Miocene age. The designation of the lower boundary of this zone, the first appearance datum (FAD) of *S. belemnus*, is difficult in this section because of the gradualistic nature of its evolution from *Sphenolithus delphix*. We have used the first occurrence of specimens with a narrow proximal column (of approximately the same width as the lateral cycle of elements) as the FAD of *S. belemnus*. The underlying sequence from Sample 144-871A-13H-3, 50–51 cm, through Core 144-871A-15H (115.5–139.5 mbsf), is assigned to the *Discoaster druggii* Subzone of the *Triquetrorhabdulus carinatus* Zone (CN1c) of early Miocene age based on the occurrence of *D. druggii* and *T. carinatus* and in the absence of *S. belemnus* (as defined above). The foraminifer oozes of this zone apparently lie directly upon the platform carbonates of the drowned ancient “Limalok Atoll.”

Planktonic Foraminifers

The pelagic foraminifer oozes capping Limalok Guyot contain very abundant and generally very well-preserved planktonic foraminifers of early Miocene to Pleistocene age. All core catcher samples from Holes 871A and 871B were examined. Additional samples were taken from Hole 871A, the more completely recovered section, so as

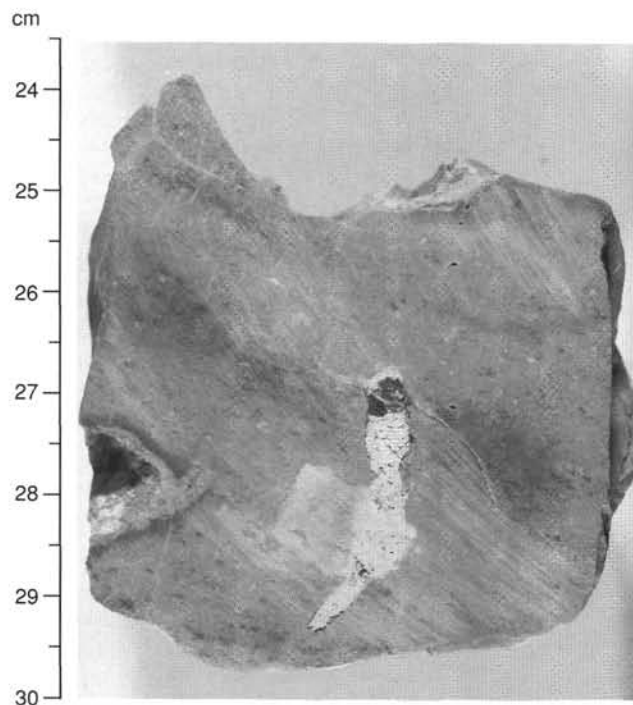


Figure 14. Photograph of dense lime mudstone with conchoidal fracture and tubular pores that occurs within Subunit IIC at 201.3 mbsf (Interval 144-871C-9R-1, 23–30 cm).

to position the zonal boundaries. The foraminifer biostratigraphies of Holes 871A and 871B are shown in Figure 22. The following discussion focuses on the sequence in Hole 871A, which accords well with core-catcher samples from Hole 871B.

The Pleistocene (Zone N22) extends through Cores 144-871A-1H and -2H and is characterized by the occurrence of *Truncorotalia truncatulinoides*, *Sphaeroidinella dehiscens*, *Pulleniatina obliquiculata*, and *Globorotalia tumida*. The nannofossil biostratigraphy provides an accurate subdivision of the Pleistocene at this site and shows it to be relatively complete (Fig. 22; see discussion above). However, the sequence below the Pleistocene, in Core 144-871A-3H, is incomplete. The Pliocene/Pleistocene boundary is placed according to both nannofossils and planktonic foraminifers near the top of Core 144-871A-3H. Sample 144-871A-3H-1, 60–62 cm, contains abundant *Globigerinoides fistulosus*, and common *Globigerinoides obliquus extremus* characteristic of the Pliocene, in addition to specimens transitional from *Truncorotalia tosaensis* to *T. truncatulinoides*. Sample 144-871A-3H-3, 60–62 cm, contains *Sphaeroidinella dehiscens* but lacks *T. tosaensis* and is assigned to Zone N19/N20. The Miocene/Pliocene boundary is placed between Samples 144-871A-3H-4, 60–62 cm, and -3H-5, 60–62 cm, the latter containing *Sphaeroidinella paenedehiscens* and *S. seminulina* but lacking *Sphaeroidinella*. Sample 144-871A-3H-5, 60–62 cm, lacks *Globorotalia tumida* but contains *G. plesiolumida* and is assigned to Subzone N17b.

A very mixed assemblage was obtained from samples taken from near the bottom of Core 144-871A-3H and high in Core 144-871A-4H (Samples 144-871A-3H-6, 60–62 cm, -3H-CC, -4H-1, 126–128 cm, and -4H-2, 126–128 cm). These contain typically upper Miocene forms such as *Globorotalia menardii*, *G. limbata*, and *Neogloboquadrina acostaensis* mixed with middle Miocene indicators such as the *Globorotalia fohsi* group, lower Miocene forms such as *Globigerinoides bisphericus* and *Praeorbulina* spp., and also typically Oligocene forms such as the “*Globigerina*” *ciperoensis* group, *Para-globorotalia opima opima* and *Catapsydrax* spp. In addition, extensive downhole contamination occurs in Samples 144-871A-4H-1, 126–128 cm, and -4H-2, 126–128 cm, from Pliocene-Pleistocene horizons. The samples from

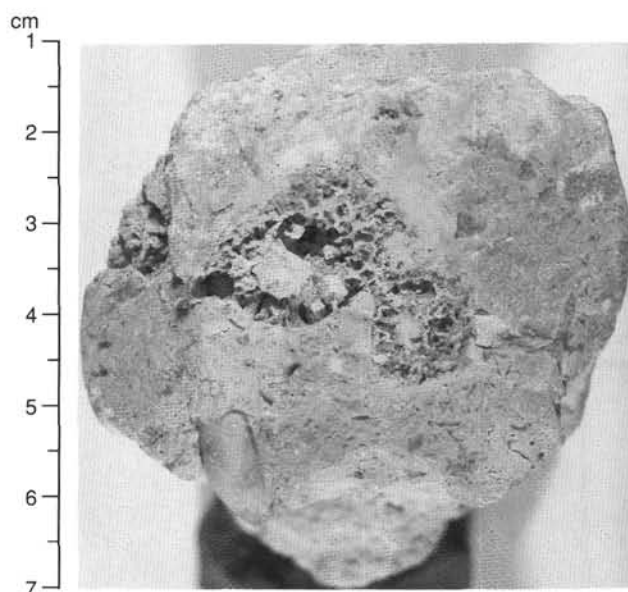


Figure 15. Close-up core photograph of the coralline grainstone that occurs at the bottom of Subunit IID (top of Interval 144-871C-20R-1, 1–7 cm).

this interval exhibit very uneven preservation, with many specimens being broken and having signs of dissolution, especially in the fine fraction. This disturbed and unzoned interval corresponds to a stratigraphic jump from Subzone N17b (upper Miocene) to Zone N12 (middle Miocene) and indicates extensive reworking by bottom currents as well as dissolution. No species diagnostic of the missing interval between Zone N12 and Subzone N17b are recorded.

Excepting minor downhole contamination, Sample 144-871A-4H-3, 124–126 cm, yields an apparently undisturbed fauna from middle Miocene Zone N12, including *Globoquadrina dehiscens*, *Dentoglobigerina altispira globosa*, *Paragloborotalia siakensis*, *Globorotalia praemenardii*, and the advanced forms of the *Globorotalia fohsi* lineage: *G. fohsi fohsi*, *G. fohsi lobata*, and *G. fohsi robusta*. A similar assemblage was obtained in several samples through Cores 144-871A-4H and -5H. Thus, Zone N12, which according to the time scale of Berggren, Kent, and Van Couvering (1985) has a duration of 1.6 m.y., is particularly thick (approximately 20 m) at this site, even though the N12/N13 zonal boundary was not recovered. A less advanced stage of the *G. fohsi* lineage is found in Sample 144-871A-6H-3, 60–62 cm, which includes *G. peripheroacuta*, *G. fohsi fohsi*, and rare occurrences of *G. fohsi lobata*. This assemblage is considered to be representative of the N11/N12 boundary. Samples 144-871A-6H-4, 60–62 cm, and -6H-5, 60–62 cm, contain *G. fohsi fohsi* and *G. peripheroacuta* but no *G. fohsi lobata* and are assigned to Zone N11. Samples 144-871A-6H-6, 60–62 cm, and -6H-CC yield *Globorotalia archeomenardii* and considerably less advanced representatives of the *G. fohsi* lineage, characteristic of Zone N10, namely, *G. peripheroacuta* and *G. peripheroronda*. The interval between Sections 144-871A-6H-5 and -6H-6, corresponding to a jump in the *G. fohsi* morphoserries, probably represents a short hiatus. Nannofossil Subzone CN5a is missing from the record at this level (see above).

The early to middle Miocene can be subdivided according to the evolution of the *Praeorbulina-Orbulina* lineage, members of which are in some samples infrequent and in others moderately well represented. Samples 144-871A-7H-3, 59–61 cm, and -7H-CC contain *Orbulina suturalis*, *Praeorbulina glomerosa glomerosa*, and *Praeorbulina glomerosa circularis* in addition to *Globorotalia archeomenardii*, *G. fohsi peripheroronda*, *Paragloborotalia siakensis*, *Dentoglobigerina altispira*, and *Globoquadrina* spp., belonging to Zone N9. Sample 144-871A-8H-3, 59–63 cm, lacks *Orbulina* but contains *Globigerinoides bisphericus*, *Praeorbulina sicana*, and *P. transitoria*

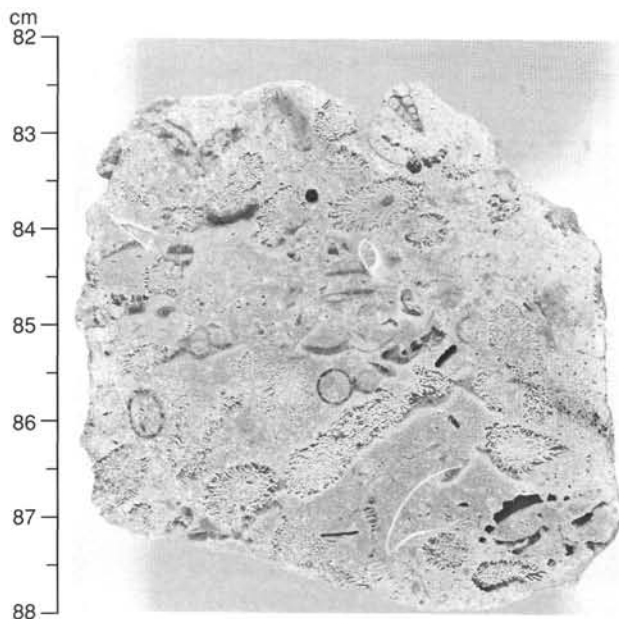


Figure 16. Close-up core photograph of coralline grainstone from Subunit IID (Interval 144-871C-21R-1, 82–88 cm).

and is thus assigned to Zone N8, lower middle Miocene. A similar assemblage was obtained down to Sample 144-871A-9H-3, 59–61 cm.

Sample 144-871A-9H-CC contains *Globorotalia peripheroronda*, *Dentoglobigerina* spp., *Globoquadrina* spp., and *Globigerinatella insueta*, but it lacks *Praeorbulina* and *Globigerinoides bisphericus*; thus, it is assigned to lower Miocene Zone N7. Sample 144-871A-11H-3, 60–62 cm, contains *Globigerinatella insueta* and *Catapsydrax dissimilis*, the co-occurrence of which is definitive of Zone N6. The first occurrence of *Globigerinatella insueta* is placed between this sample and sample 144-871A-11H-CC, the latter sample accordingly being placed in Zone N5 by the absence of this marker species. However, because of the general scarcity of *G. insueta* in these sediments, this assignment must be regarded with some caution.

Samples 144-871A-12H-CC through -15H-CC contain rare to moderately common *Paragloborotalia kugleri* and members of the “*Globigerina*” *ciperoensis* group in association with typically Miocene elements such as *Globoquadrina dehiscens* and diverse and abundant *Globigerinoides* spp. (*G. immaturus*, *G. quadrilobatus*, *G. primordius*). This interval is consequently assigned to the lowermost Miocene Subzone N4b. Samples from Sections 144-871A-16H-CC and 144-871A-17H-CC are platform limestones that are barren of planktonic foraminifers.

Palynomorphs

Core-catcher samples from Cores 144-871A-1H through -15H and -17X, representing the total thickness of the pelagic cap in Hole 871A, were processed for palynology by means of hydrochloric acid digestion and sieving at 20 μ m. All samples were found to be barren of spores, pollen, and organic-walled dinoflagellates.

The organic component throughout the foraminifer oozes of the pelagic cap in Hole 871A is very lean in all samples. The 20- μ m-sieved fraction is dominated mainly by the organic? remains of microforaminifers; however, in foraminifer oozes near the base of the pelagic cap (Sample 144-871A-17X-CC), the organic residue is relatively rich and dominated by light to medium brown woody fragments and membranous (but perhaps not cuticular) plant tissues. These woody, nonvascular tissues are delicate and well preserved. Perhaps they were derived from vegetated islands nearby. Similar tissues were also sporadically recorded higher in the hole but were

seen only in low quantities. Robust angular flakes of partially degraded woody (terrigenous) tissues dominate the >20- μ m fraction in Sample 144-871A-15H-CC. These flakes are medium to dark brown and vary from granular to fibrous; sometimes they appear to be resinous. Similar flakes occur in other samples from the pelagic cap, but they are never as abundant as in Sample 144-871A-15H-CC.

The absence of spores, pollen, and dinoflagellates and the low abundance of organic residue in the pelagic cap deposits can be explained by the winnowing of sediments, as indicated, for example, by the very high ratio of foraminifer tests to nannofossils. The rather well-preserved nature of the woody tissues, at least in some samples, suggest little or no oxidation of the recovered organic fraction.

Siliceous Microfossils and Their Diagenetic Products

Siliceous microfossils, although extremely scarce and poorly preserved, occur in the nannofossil foraminifer and foraminifer oozes of the Neogene pelagic cap. The occurrence of siliceous microfossils is strongly dependent on sediment accumulation rates and silica diagenesis (see “Sedimentation Rates” section, this chapter). Very rare specimens of the dissolution-susceptible skeletons of diatoms and silicoflagellates are preserved in Sections 144-871A-1H-1 and -1H-2 and Section 144-871B-1H-1. The species encountered are characteristic of low latitudes, such as *Azpeitia nodulifer*, *Nitzschia marina*, and other species of the genus *Nitzschia*. These species are unfortunately of little stratigraphic value.

The inverse correlation between the abundance of siliceous microfossils and authigenic silicates, such as phillipsite and clinoptilolite, suggests that the latter were probably precipitated from the silica derived from the dissolution of diatoms and radiolarians. Silica diagenesis has resulted in the total dissolution of all biosiliceous particles below Section 144-871A-1H-2.

The occurrence of radiolarians fragments and occasionally complete but poorly preserved specimens in the middle and lower Miocene cores suggests that higher biosiliceous productivity occurred during the deposition of this sediment.

Platform Carbonates

Calcareous Nannofossils

Numerous samples of platform carbonate were examined for nannofossils, but most were totally barren. Three significant occurrences of nannofossils were discovered in the Hole 871C sequence: at the top and base of the platform carbonate sequence (Fig. 23).

Small quantities of pelagic chalk filling cracks near the top of the platform carbonate sequence (Sample 144-871C-2R-1, 0–2 cm) contain abundant, well-preserved nannofossils. The species in this sample include *Dictyococcites bisectus*, *Dictyococcites scrippsae*, *Zygrhalthus bijugatus*, *Sphenolithus predistentus*, and *Sphenolithus distentus*. This association of species indicates the *Sphenolithus distentus* Zone (CP18) of early Oligocene age. This zone spans the interval from 30.2 to 34.2 Ma according to Berggren, Kent, and Flynn (1985). The specimens of *S. distentus* are characterized by a relatively high angle between the elements of the proximal column and the apical spine, with no hint of the X-shaped extinction figure typical of *Sphenolithus ciperoensis*. This indicates that these specimens are early forms of *S. distentus*, suggesting that this sample is from the lower portion of Zone CP18.

Sample 144-871-15H-CC, 10–13 cm, consists of a manganese crust containing a small quantity of pelagic limestone with intermixed (reworked?) shallow-water debris. Thin section observations revealed a diverse, abundant calcareous nannofossil assemblage that included *Reticulofenestra dictyoda*, *Sphenolithus furcatolithoides*, *Chiasmolithus grandis*, *Chiasmolithus solitus* and *Camplyosphaera dela* but not *Reticulofenestra umbilica*. This assemblage indicates Zone CP13 of middle Eocene age. A questionable specimen of *Nannotetrina* sp. was also observed. The assemblage includes several pentoliths including *Braarudosphaera discula* and *Pemna basquensis*.

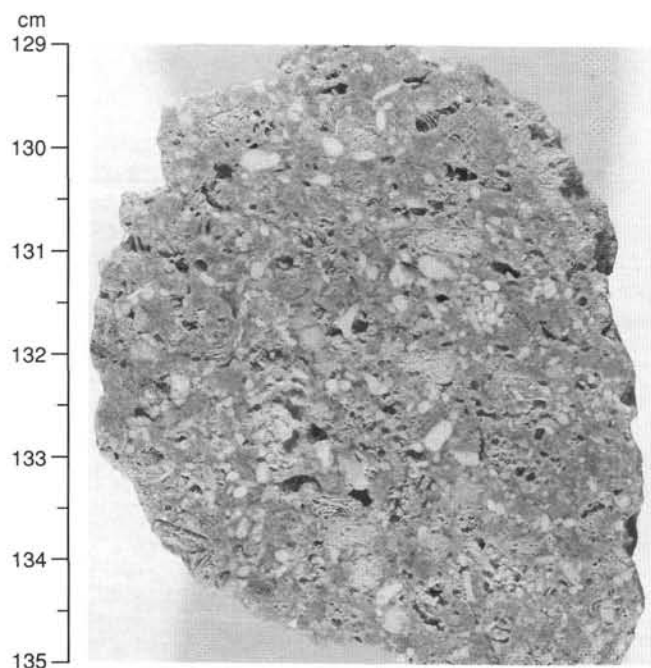


Figure 17. Close-up core photograph of benthic foraminifer packstone that occurs in Subunit IID (Interval 144-871C-21R-1, 129–135 cm).

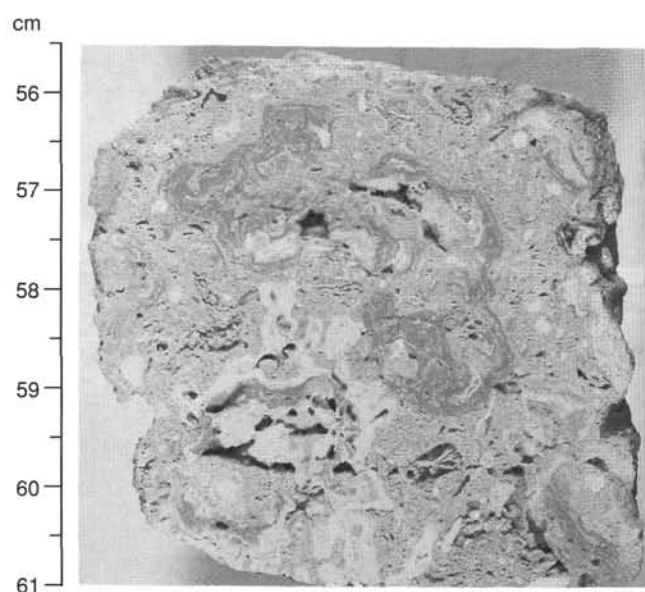


Figure 18. Close-up core photograph of the rhodolith grainstone that is the most characteristic feature of Subunit IIE (Interval 144-871C-28R-1, 56–61 cm).

The platform carbonate sequence is underlain by black fossiliferous packstone and varicolored, charcoal-bearing claystones. Dark gray to black calcareous claystones (Lithologic Subunit IIF) intercalated between the packstones and the varicolored claystones, contain rare, well-preserved calcareous nannofossils. Examination of Sample 144-871C-31R-1, 47–48 cm, revealed an assemblage including *Ericsonia cava*, *E. robusta*, *E. subpertusa*, *Neochiastozygus perfectus*, *Prinsius bisulcus*, *Sphenolithus primus*, *Thoracosphaera saxea*, *T. heimii*, and *Toweius eminens*. None of the zonal index fossils generally associated with these species were observed in this extremely sparse assemblage. The co-occurrence of these species is most con-

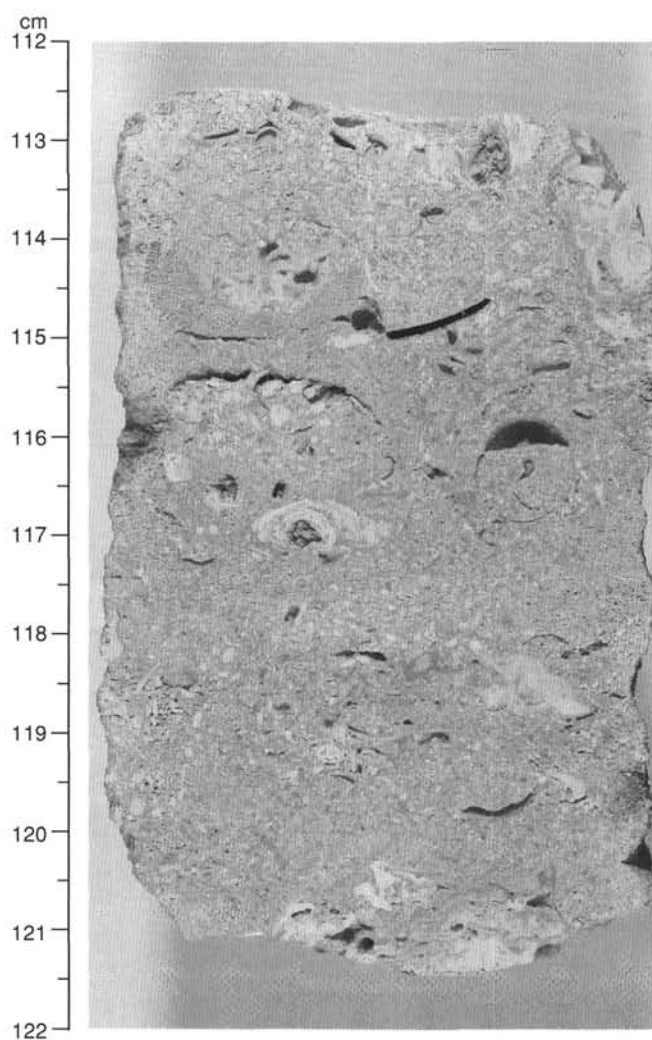


Figure 19. Close-up core photograph of the common development of porosity (2%–5%) in the limestones of Subunit IIE (Interval 144-871C-30R-1, 112–122 cm). Intergranular and moldic pores commonly are rimmed by calcite cements.

sistent with a zonal assignment of CP5 (late Paleocene), although the apparent absence of the fasciculiths and helioliths make this assignment uncertain. The sparse, depauperate nature of this assemblage and the relatively high abundance of thoracosphaerids indicate that this sample was deposited under abnormal marine conditions. Very rare nannofossils have been observed in the varicolored claystone (samples within interval 144-871C-32R-1, 10–90 cm). Sedimentologic examinations suggest that these specimens have been worked downward into the top of the varicolored claystone by bioturbation.

Planktonic Foraminifers

Small quantities of pelagic chalk filling cracks in the platform carbonate (Sample 144-871C-2R-1, 0–2 cm) contain abundant, well-preserved planktonic foraminifers that include *Globoquadrina tripartita*, *G. sellii*, *G. rohri*, “*Globigerina*” *ampliapertura*, *Turborotalia pseudoampliapertura*, and *T. increbescens* associated with catapsydracids and globorotaloids. This assemblage indicates Zone P20 of early late Oligocene age. This is in agreement with the calcareous nannofossil age.

Section 144-871C-8R-1, within the upper part of the platform carbonate sequence, yielded a single specimen of the planktonic

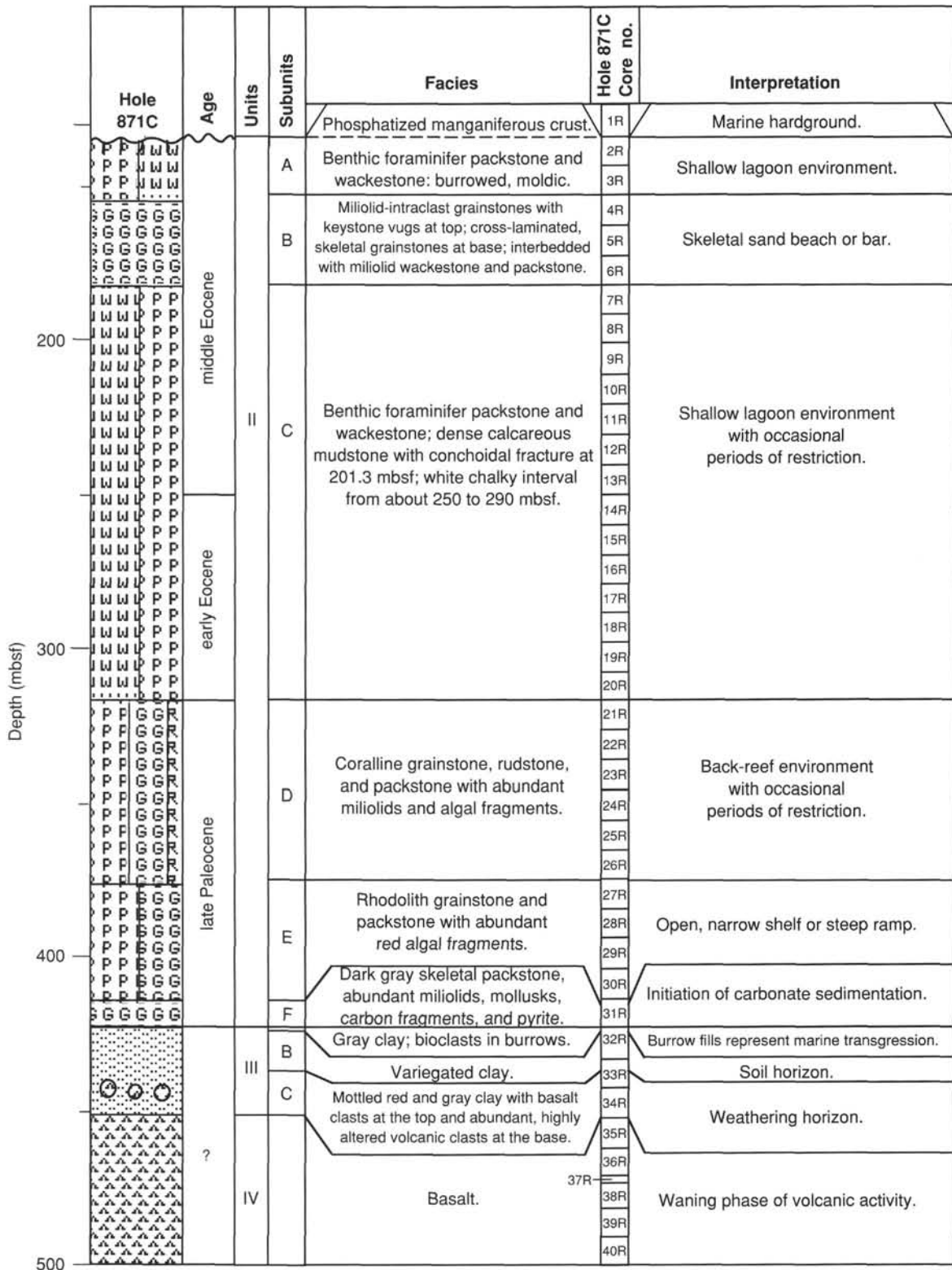


Figure 20. Summary of preliminary interpretations of depositional history at Site 871.

foraminifer *Subbotina praeturritilina*. This species first appears in the middle Eocene and persists into the Oligocene. Its occurrence in the shallow-water carbonate sequence, in combination with its co-occurring larger foraminifers, provides an important age constraint for the sequence. In addition, its presence provides corroborative evidence of a more open-marine influence within the sequence.

Benthic Foraminifers

The 289.2-m-thick sequence of platform carbonates (Lithologic Unit II) recovered in Hole 871C (Core 144-871C-2R to Sample 144-871C-32R-1, 65 cm) yielded poor to rich, moderately diversified faunas of large and small benthic foraminifers associated with fre-



Figure 21. Thin-section microphotograph of a typical wackestone interval within Subunit IID (Interval 144-871C-23R-1, 22–26 cm). Note the presence of very small microfauna (miliolids, "rotaliids," and smooth-shelled ostracodes) and small-sized, low-spined gastropods. Maximum dimension = 3 mm.

quently common mollusks and molluscan fragments, calcareous algae, echinoid fragments, and less frequently corals.

The identification of the microfauna and associated forms from the platform carbonates in Hole 871C was based on thin section and acetate peel examination, and on isolated specimens recovered as cuttings (debris of limestones collected on a sieve as each section of the core was split). The larger foraminifers were the only age-diagnostic forms. Based on their occurrence, the platform carbonate sequence recovered in Hole 871C spans the interval from middle Eocene to late Paleocene. Because the distribution of shallow-water organisms, including the larger foraminifers, varies from layer to layer according to facies changes and evolution of the platform itself, no routine biostratigraphic scheme could be applied to the recovered succession. Biostratigraphically diagnostic foraminifers occur in specific intervals, however, providing tie-points for dating the sequence. These tie-points are as follows:

1. Sample 144-871C-2R-1, 51–54 cm, yielded *Nummulites* sp. cf. *N. gizehensis*, *Nummulites* sp. cf. *N. britannicus*, and *Nummulites* sp. cf. *N. laevigatus*. The first two species also occur in Sample 144-871C-2R-1, 58–62 cm, but their preservation is poor as a result of burrows piercing the shells. *Coskinolina* sp. cf. *C. elongata* co-occurs with these *Nummulites*.

2. Sample 144-871C-4R-1, 14–19 cm, yielded *Nummulites* sp. cf. *N. britannicus*.

3. Cuttings of Core 144-871C-9R-1 yielded *Nummulites* sp. cf. *N. escheri*. According to Schaub (1981), the large *Nummulites* identified here would indicate an early middle Eocene age. This attribution is corroborated by the occurrence of the planktonic foraminifer *Subbotina praeturritilina* (see above) and of *Coskinolina elongata*, which

are known to appear in the middle Eocene and extend into the middle Eocene, respectively.

4. Samples 144-871C-19R-1, 4–10 cm, to -20R-1, 14–17 cm, are characterized by abundant large flosculinized *Alveolina*. The species identified in this interval are *Alveolina subpyrenaica* and *Alveolina canavarii* associated with *Alveolina minuta* in Sample 144-871C-19R-1, 4–10 cm. This association is indicative of the *Alveolina oblonga* Zone of middle early Eocene age (Hottinger, 1960; White, 1992). Sample 144-871C-20R-1, 113–118 cm, yielded few representatives of the *Alveolina rotundata* group associated with more abundant *Alveolina subpyrenaica*. They are indicative of the *Alveolina trempina*-*A. corbarica* Zones of early Eocene age, slightly older than the previous zone.

5. Interval 144-871C-21R-1, 56–64 cm, to Section 144-871A-32R-1, 45 cm, yielded a monotonous larger foraminifer assemblages composed of common *Asterocyclina*, representatives of the *Nummulites globulus* group, few *Discocyclina barkeri*, and rare *Alveolina*. Core 144-871C-21R yielded only poorly cut specimens belonging to the subgenus *Glomalveolina*. Their abundance suggests that this interval may be dated as late Paleocene. One broken specimen attributable to the *Alveolina globosa* group in Sample 144-871C-25R-1, 18–28 cm, seems also to indicate a late Paleocene age. No precise zonal attribution could be made because of the lack of appropriate material.

The late Paleocene age derived from the larger benthic foraminifers is in agreement with an early late Paleocene age inferred from the calcareous nannofossils recorded in the lowermost portion of the carbonate sequence (Samples 144-871C-31R-1, 47–48 cm, and -32R-1, 10–90 cm).

Faunal Assemblages

Hole 871C

The distribution of benthic foraminifers in Hole 871C allow us to distinguish some discrete assemblages characterized by the association of different benthic foraminifer taxa with either calcareous algae or megafossils (Fig. 23).

Uppermost Assemblage I (Interval 144-871C-2R-1, 1–6 cm, to -4R-1, 14–19 cm; 133.7–153.0 mbsf) is characterized by large, pillared *Nummulites* associated with common to very abundant miliolids. Small benthic (agglutinated and calcitic) foraminifers are generally rare except in the lower part, where small calcitic foraminifers (not identified yet) become an important component of the microfauna. Minor components scattered throughout include melobesian algae and echinoid and molluscan fragments.

Assemblage II (Interval 144-871C-4R-1, 48–52 cm, to -17R-1, 4–7 cm; 153.4–278.1 mbsf) is typically characterized by representatives of the genera *Praerhapydionina* throughout and *Pseudochrysalidina* in the upper part. Miliolids vary in abundance from absent to very abundant and seem to be in competition with the small calcitic foraminifers, including biserial forms and rotaliids. Agglutinated foraminifers are more diversified in this interval and include rare to common representative of Verneuilinidae, Valvulinidae, and rarely Textulariidae. Rare sessile benthic foraminifers occur in the upper part of the interval. Calcareous algae are rare overall except in Sample 144-871C-11R-1, 5–15 cm, which contains common *Melobesiae*. Megafossil fragments are diversified and occasionally very abundant. The more consistent constituents of the macrofauna are echinoids followed, in decreasing order, by ostracodes and poorly preserved mollusks. A whole echinoid specimen is present in Interval 144-871C-9R-1, 0–5 cm. Corals are rare and poorly preserved. Microbial activity was detected in some layers. This interval yielded the only planktonic foraminifer (*Subbotina praeturritilina*) identified with certainty in the entire carbonate sequence (see above).

Assemblage III (Interval 144-871C-19R-1, 4–10 cm, to -20R-1, 13–17 cm; 297.2–307.0 mbsf) is characterized by the absolute domi-

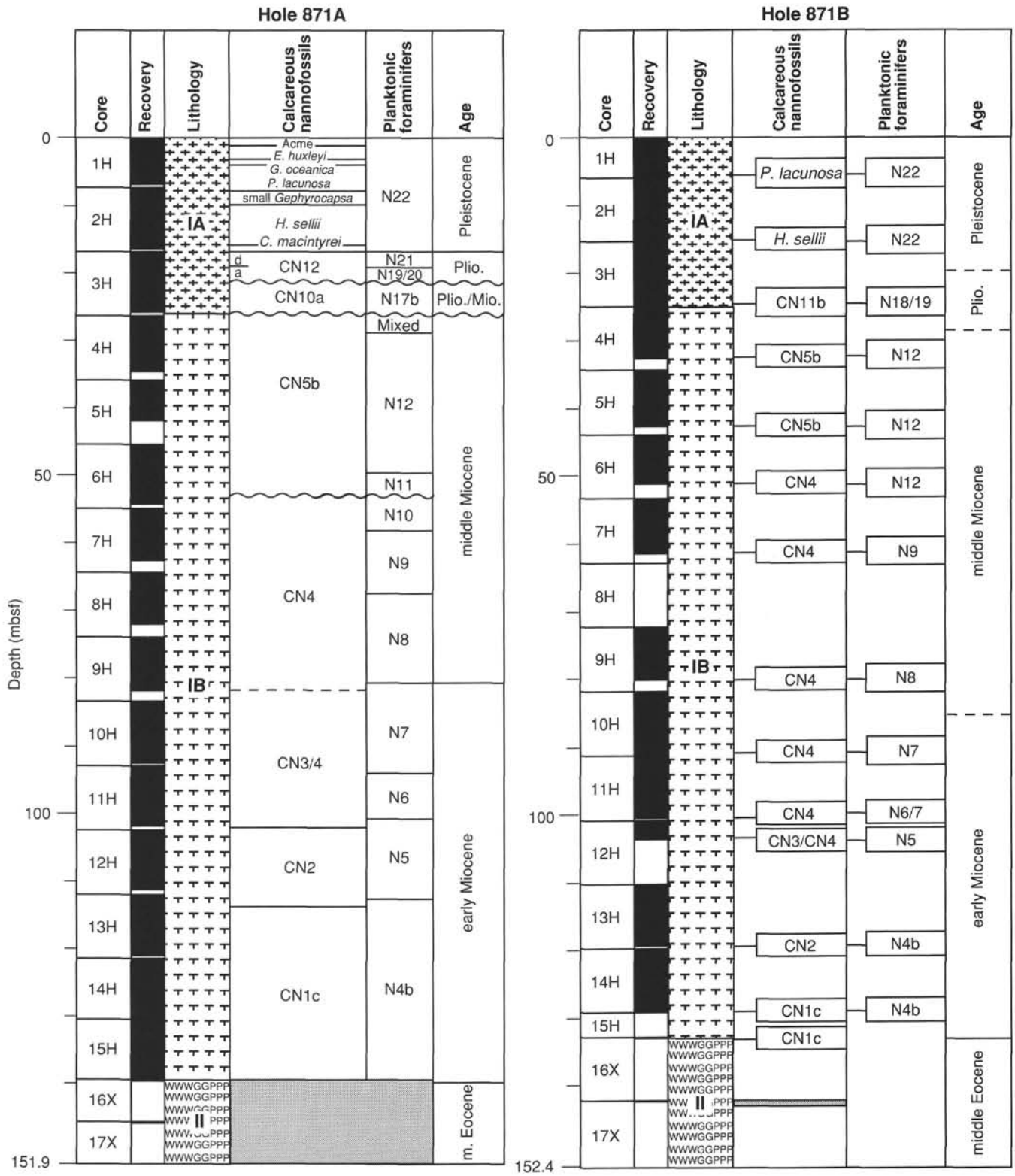


Figure 22. Biostratigraphy of the Neogene pelagic cap in Holes 871A and 871B, Limalok Guyot.

nance of medium-sized, flosculinized *Alveolina*. Other foraminifers, including miliolids, are rare in this interval and macrofossils are poorly represented.

Assemblage IV (Interval 144-871C-21R-1, 0–56 cm, through -23R-1, 45 cm; 317.1–336.3 mbsf) is characterized by the co-occurrence of rare to abundant *Asterocyclina*, rare *Discocyclina*, *Alveolina*

(*Glommoalveolina*) sp., and *Nummulites globulus* gr., and by common to abundant miliolids. The miliolids in Sample 144-871C-21R-1, 72–77 cm, are remarkable for their large size. Minor components of the microfauna consist of rare agglutinated and more common small calcitic foraminifers. Corals become important in this interval, including a whole coral specimen (Interval 144-871C-21R-1, 69–92 cm).

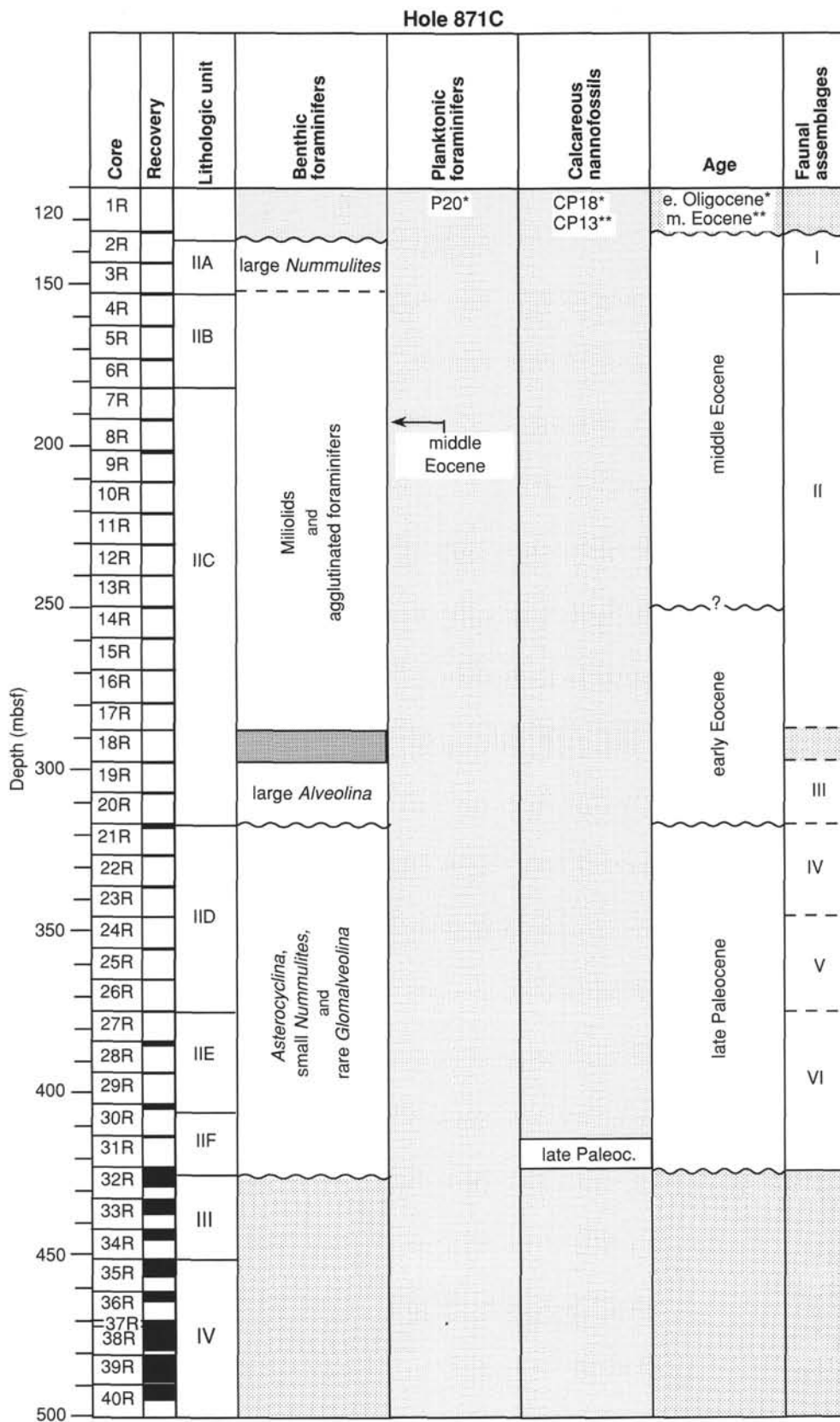


Figure 23. Biostratigraphy of Hole 871C, Limalok Guyot. An asterisk (*) indicates chalk filling cracks in the platform carbonate, and double asterisks (**) indicate manganese crust.

These are associated with few and sparse ostracodes, echinoid and molluscan remains, and melobesian algae, which are common in some layers. Preservation in this interval is rather poor. Larger foraminifers, for instance, are frequently broken, worn, or micritized, and may be included in clasts. This suggests mechanical transport and possible reworking from older layers similar to the lowermost carbonate lithologies.

Assemblage V (Interval 144-871C-24R-1, 0–4 cm, through -26R-1, 4–10 cm; 345.4–364.8 mbsf) is strongly dominated by encrusting algae associated with *Halimeda*. Foraminifer faunas consist of either abundant miliolids and rare small calcitic foraminifers or rare miliolids and more abundant small calcitic foraminifers. Other foraminifers are scattered and rare. It is worth mentioning that the foraminifer fauna is sparse and species-poor in association with abundant encrusting algae. The macrofauna is also sparse, with echinoids as the most consistent component. Rare arthropod remains were also noticed.

Lowermost Assemblage VI (Interval 144-871C-27R-1, 0–4 cm, through -32R-1, 45 cm; 374.3–423.0 mbsf) is characterized by abundant and diverse calcareous algae. The Melobesiae are the most abundant component throughout, although rhodoliths are dominant in some layers such as Sample 144-871C-28R-1, 34–39 cm. Dasy-cladaceans, represented by at least three genera, are common in Sample 144-871C-28R-1, 105–108 cm. *Halimeda*, although present in several samples, is frequent only in the Interval 144-871C-32R-1, 0–45 cm, where they exhibit exceptionally well-preserved aragonitic tests in association with other aragonitic-shelled organisms (see “Lithostratigraphy” section, this chapter). The foraminifer assemblages consist of miliolids (abundant especially in lowermost portion), *Asterocyclina*, *Nummulites*, and rotaliids. Ostracodes, echinoids, corals, and mollusks are present throughout mainly as a minor component of the macrofauna.

Hole 871A

Samples from Sections 144-871A-15H-CC through -17X-CC contain platform carbonate with faunal assemblages including miliolids and small calcitic foraminifers. These faunal elements, as well as fragments of *Nummulites* (Sample 144-871A-16X-CC, 4–7 cm) and the presence of *Praerhapydionina* (Samples 144-871A-17X-CC, 0–4 cm, and -17X-CC, 12–13 cm) indicate a middle Eocene age for these samples. This assemblage is very similar to that encountered in the uppermost interval from Hole 871C.

Hole 871B

Samples of platform carbonate from Section 144-871B-16X-CC contain miliolids and small calcitic foraminifers. The presence of *Praerhapydionina* (Sample 144-871B-16X-CC, 15–18 cm), *Coskino-lina elongata* (Sample 144-871A-16X-CC, 15–18 cm), and *Pseudochrysalidina* (Sample 144-871-16X-CC, 15–18 cm, and cuttings) indicate a middle Eocene age as in the uppermost interval of Hole 871C.

Paleoecologic Interpretation

From a paleoecologic point of view, the foraminifer-algal-macrofossil assemblages recovered in Hole 871C, and to a minor extent in Holes 871A and 871B, are representative of a shallow-water platform environment ranging from a somewhat restricted lagoon to a fully normal marine environment. This preliminary interpretation is supported by the fluctuations in diversity throughout the recovered succession of the micro- and macrofauna and microflora. Despite the very poor recovery, we observed that higher diversity assemblages clearly alternate with poorly diversified fauna and flora. The presence of calcareous nannofossils at the base of the succession and of planktonic foraminifers in the middle of the Assemblage II interval suggests that these two intervals correspond first to the maximum paleodepth, and then to the maximum open-marine influx during the life of the platform. Reworking apparently occurred at the beginning

of the platform growth (Interval 144-871C-32-1, 0–45 cm) and during the deposition of Assemblage IV, where large foraminifers display clear signs of mechanical transport corroborated by their poor preservation and occurrence in clasts with different lithology.

Palynomorphs

Two samples of the white limestone were processed, both being digested in HCl only. Residue from Sample 144-871A-17X-CC, 19–21 cm, representing large, cleaned fragments of limestone contained within foraminifer ooze, was sieved at 10 μ m. Residue from Sample 144-871C-3R-CC, a limestone, was mounted unsieved. Organic residues were lean in both samples.

Sample 144-871A-17X-CC, 19–21 cm, was found to contain small pale fragments of woody tissue and rare algal? palynomorphs. The latter are small (about 27 μ m or less), pale spheres with thin, wrinkled, double- or multi-layered walls. The taxonomic and ecological affinity of these palynomorphs is unknown. Sample 144-871C-3R-CC also contains pale fragments of woody tissue, but a more diverse assemblage of algal? palynomorphs is represented in this sample. Specimens are again pale, thin-walled, and wrinkled; however, they are variable in size (about 10 to 95 μ m diameter) and morphological detail. Some of the larger specimens might be freshwater dinoflagellates.

Two samples from the base of the platform carbonate sequence—a dark marine clay (Sample 144-871C-31R-1, 45–49 cm) and a dark calcareous skeletal packstone (Sample 144-871C-32R-1, 16–20 cm)—are especially rich in angiosperm pollen and other microscopic plant remains (100–10,000 pollen/spores/g sediment). These two samples are also rich in marcasite and pyrite, suggesting a reducing depositional or diagenetic environment. The microfossils include monosulcate pollen (probably *Palmae*) together with triporate, tricolpate, and tricolporate pollen. These probably were derived from plants inhabiting nearby islands during late Paleocene time.

Siliceous Microfossils and Their Diagenetic Products

Two samples from the platform carbonate sequence in Hole 871C were available for acid digestion and analysis of siliceous microfossils. Sample 144-871C-2R-1, 27–44 cm, contains rare diatoms, including *Paralia sulcata* and *Triceratium* sp., probably indicating contamination. The presence of phillipsite, clinoptilolite, opal-CT lepispheres, and volcanic ash in Sample 144-871C-3R-CC suggests extensive silica diagenesis. Whether siliceous microfossils originally existed or not is unclear. However, one well-preserved opal-phytolith was found, indicating that the preservation of relatively dissolution-resistant biosiliceous particles was possible in these sediments. The presence of the phytolith suggests that grass grew nearby, probably on islands associated with the atoll system.

Basal Clay Sequence

Palynology

Four clay samples were processed for palynology using HCl, hot HF, and sieving at 10 μ m: Samples 144-871C-32R-1, 111–113 cm; -32R-2, 20–24 cm; -32R-4, 46–48 cm; and -33R-2, 121–123 cm. All samples contain palynomorphs and other organic debris in varying degrees of preservation, and some samples (notably Sample 144-871C-32R-1, 111–113 cm) contain low-diversity pollen assemblages. Abundant pyrite occurs in all samples, suggesting marine influence during or soon after deposition (see “Organic Geochemistry” section, this chapter). However, the organic debris is predominantly, if not entirely, terrestrial in origin (woody tissues and plant cuticle), and neither dinoflagellates nor other palynomorphs of known marine affinity were found.

Sample 144-871C-32R-1, 111–113 cm, is a light gray clay, the organic component of which is dominated by about equal proportions

of woody tissues and cuticle that greatly dilute the palynomorphs. Unornamented mono- and dicellate fungal spores comprise about 90% of the palynomorph component. Six species of angiosperm pollen were found, of which the two most common were a monosulcate pollen (probably *Palmae*) and a spherical tricolporate? pollen with a microreticulate surface bearing long spines. The latter perhaps belongs to the *Malvaceae*. Small monoletate foveolate fern spores were rarely seen. Conifer pollen were not found. Preservation of the spores and pollen varies from poor to excellent.

Sample 144-871C-32R-2, 20–24 cm, is a light gray-brown clay. The organic residue is well preserved and dominated by woody tissues with subsidiary cuticle. Palynomorphs were very diluted by this terrigenous material such that unornamented mono- and dicellate fungal spores and thin-walled, spheroidal, crumpled, strongly granulate algal? palynomorphs were all that were found.

Sample 144-871C-32R-4, 46–48 cm, a pink clay with gray streaks and patches, yielded a very organically lean and mineral residue. The organic debris is represented by some fragments of woody material and some fragments of what appears to be strongly corroded organic remains. Despite the oxidized appearance of this sample, thin-walled, spheroidal, crumpled, strongly granulate algal? palynomorphs are moderately abundant and show surprisingly little sign of corrosion.

Sample 144-871C-33R-2, 121–123 cm, is a brown clay with light gray streaks. The organic residue is dominated by degraded and strongly pyritized woody tissues. Palynomorphs are rather scarce. They consist almost exclusively of unornamented mono- and dicellate fungal spores and thin-walled, spheroidal, crumpled, strongly granulate algal? palynomorphs, a single monosulcate pollen (probably *Palmae*) being the only other palynomorph found.

The low taxonomic diversity of the embryophyte spore and pollen assemblages found in the clays examined suggests limited habitats for plant growth consistent with a small, low-lying, oceanic island. Low taxonomic diversity among the fungal spores probably indicates a relatively small number of substrates or host plant species available for growth. The abundance of fungal spores points to moist conditions.

Summary and Discussion

The upper part of the clay sequence contains terrestrial organic debris (woody tissues and plant cuticle), pollen, and spores; and the lack of dinoflagellates or other marine palynomorphs suggest preservation of a soil horizon. Low-diversity pollen assemblages from this interval include six angiosperm species, including one that may be related to the *Palmae*. Ferns may have been a minor part of the plant paleocommunity. Abundant fungal spores indicate moist conditions, although the limited diversity of these assemblages implies limited niche space.

Flooding of the island occurred during the early late Paleocene. Sparse, depauperate calcareous nannofossil assemblages preserved in association with dark gray aragonitic grainstones imply that marginal marine conditions existed during the initial stages of inundation. Abundant pollen and spores in this stratum were derived from nearby vegetated islands.

A substantial carbonate platform became established (the "Limalok Atoll") during the late Paleocene. This platform complex persisted throughout the rest of the late Paleocene into the middle Eocene, based upon benthic foraminifer biostratigraphy. Faunal assemblages indicate that the evolution of "Limalok Atoll" was complex. Six distinct faunal assemblages developed during the course of the platform's evolution, with larger foraminifers often playing a major role in the paleocommunity. The occurrence of the planktonic foraminifer *Subbotina praeturritilina* and the diverse nature of the associated fauna suggest at least one period of relatively higher sea level. Benthic foraminifers and very rare diatoms in the uppermost part of the sequence indicate a central lagoonal environment just before the drowning of the platform.

The youngest platform carbonates at Site 871 are early middle Eocene in age, suggesting that the platform was drowned during the middle Eocene. Cessation of platform carbonate sedimentation was followed by deposition of a manganese crust with included pelagic limestone during the middle Eocene (CP13). The ages for both the youngest platform carbonate and the overlying manganese crust precisely date the drowning of the platform as middle Eocene.

Following a hiatus of at least 15 m.y. upper lower Oligocene chalk filled cracks in the top of the carbonate platform. The vast majority of the pelagic cap atop Limalok Guyot accumulated in the Neogene. Calcareous microplankton of the pelagic rain were strongly winnowed by subsurface currents during the early and middle Miocene, resulting in the accumulation and preservation of planktonic foraminifer ooze. Sediment accumulation and preservation was relatively continuous, however, despite the obvious current activity. This phase of sediment accumulation and preservation ended abruptly in the late middle Miocene. A significant period (approximately 6 m.y.) of nondeposition and/or erosion, spanning almost all of the late Miocene, resulted in appreciable reworking of planktonic foraminifers of early and middle Miocene age. In addition, calcareous microplankton of Oligocene age were reworked at this time. The source of this reworked material is unknown, although it must have been derived from the guyot.

The record of latest Miocene and Pliocene deposition is discontinuous, indicating sporadic sediment accumulation and preservation on the Limalok Guyot. Beginning in the latest Pliocene, however, sediment accumulated and was preserved more continuously. The relatively complete, albeit thin, record of the latest Pliocene and Pleistocene suggests a change in the oceanographic conditions controlling sedimentation and sediment preservation on the guyot. This change is corroborated by an apparent decrease in sediment winnowing, attested to by the increase in the ratio of calcareous nannofossil to planktonic foraminifers in the preserved sediment.

PALEOMAGNETISM

Initial magnetic susceptibility was measured at an interval of 10 cm for most cores within the pelagic cap (Lithologic Unit I; 0–133.7 mbsf) and in the lower portion of Hole 871C (422–500 mbsf). The susceptibility in the pelagic sediments is generally low or negative, with larger values probably the result of rust contamination. A down-core decrease in susceptibility at approximately 30 mbsf (Fig. 24A) corresponds to a hiatus separating upper Miocene nannofossil-foraminifer ooze and middle Miocene foraminifer ooze. This reduction may be related to the lower clay content in the lower part of the sequence, where negative susceptibilities indicate an extremely pure carbonate sediment. Susceptibility was not measured in the limestone section (Lithologic Unit II) because of the low core recovery. The claystone (423–452 mbsf) directly overlying volcanic basement is characterized by substantially higher susceptibility than in the pelagic cap (Fig. 24B). Susceptibility values in the basalt (452–500 mbsf) are much higher (ca. 10^{-3} cgs).

Measurements of natural remanent magnetization (NRM) and the remanence after 15-mT alternating-field (AF) demagnetization were made at a spacing of 5 cm on the least disturbed archive halves of Cores 144-871A-3H through -11H and Cores 144-871B-1H through -11H with the pass-through cryogenic magnetometer. The magnetization of the pelagic sediment is weak and most NRM intensities are <10 mA/m. The multishot core orientation device was used to orient Cores 144-871A-3H through -10H (Table 5). Most of the cores are disturbed because the pelagic sediment is too soft and wet.

Despite having azimuthal orientation data, no magnetostratigraphic interpretation is possible for the pelagic sediments. Cores from the pelagic sequence exhibit a bimodal distribution of declinations, often centered on 90° and 270°. Furthermore, the pattern of declination shifts is sometimes systematically related to their position relative to core

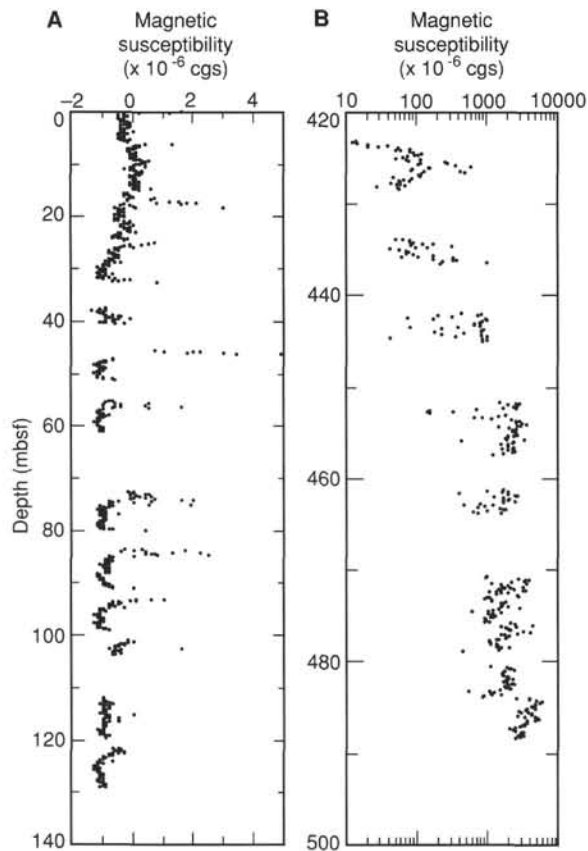


Figure 24. Magnetic susceptibility variations in the pelagic cap from Hole 871B (A) and in the claystone (423–452 mbsf) and basalt of Hole 871C (B).

section boundaries (Fig. 25). This observation prompted a comparison of the remanence directions of the archive and working halves of a test section (Section 144-871B-7H-4). The two halves of the core were each measured twice; once with the core top oriented uphole (along the Z-axis) and once in an inverted position. The declination pattern for all four runs is nearly identical (Fig. 26), suggesting that the apparent “reversals” in the whole-core data are artifacts.

Two discrete samples of limestone (Samples 144-871C-2R-1, 46–48 cm, and -21R-1, 59–61 cm) were stepwise demagnetized with the Schonstedt AF demagnetizer and measured with the pass-through cryogenic magnetometer in single sample mode. Unfortunately, the intensity of NRM was near the effective sensitivity of the cryogenic magnetometer for single sample measurement (ca. 1.0 mA/m). The magnetization remained nearly constant during AF demagnetization, probably because the sample boat dominated the signal. The higher sensitivity of shore-based magnetometers should be sufficient to determine the characteristic magnetization of the limestone samples.

The archive halves of Cores 144-871C-32R and -33R, from 423 to 442 mbsf, were measured in the same way as the APC cores of the pelagic sediments. The intensity of NRM in this claystone subunit of Hole 871C is higher than that of the pelagic cap, ranging from 1.0 to nearly 100 mA/m. Although the inclination values after demagnetization at 15 mT (ca. +30°) are reasonable for deposition at low latitudes in the Southern Hemisphere, the declinations are apparently random (Fig. 27). The within-section variability in declination is difficult to reconcile with an original magnetization, although further shore-based work will evaluate the possible paleolatitudinal information from this lithology.

Nineteen discrete samples of basalt were AF demagnetized and measured with the cryogenic magnetometer (Table 6). The NRM intensity is unusually high, up to 18 A/m, by comparison with similar age crustal lavas (e.g., Van Wagoner and Johnson, 1983). Examples of

Table 5. Multishot orientation data for APC cores, Hole 871A.

Core no.	Azimuth (degrees)
144-871A-	
3H	190
4H	289
5H	349
6H	89
7H	6
8H	24
9H	27
10H	348

the demagnetization behavior are shown in Figures 28 and 29. With the exception of Sample 144-871C-41B-1, 6–8 cm (for which the vertical orientation is unknown), and one sample from Core 144-871C-35R, the characteristic remanence directions have negative inclinations. Five or more distinct inclination groups are present, and the variability in inclination values (+2° to –32°) is compatible with that predicted from recent paleosecular variation (McFadden and McElhinny, 1984). These features suggest the lavas may provide a reasonable estimate of paleolatitude of Limalok Guyot, following more complete shore-based demagnetization and statistical analysis of the data to account for the bias inherent in azimuthally unoriented cores.

Bearing these caveats in mind, the simplest explanation of the basement inclinations is that they represent normal polarity magnetization acquired at low southern paleolatitudes (ca. 10°S). This tentative paleolatitude estimate, together with Sager and Pringle’s (1988) Pacific apparent polar wander path, suggests volcanic construction at ca. 50–60 Ma, which is generally compatible with the oldest recovered sediment (early late Paleocene; see “Biostratigraphy” section, this chapter).

SEDIMENTATION RATES

Neogene Pelagic Cap

Rates of sediment accumulation of the Neogene pelagic cap at Site 871 have been approximated using micropaleontologic data from Hole 871A, which was studied in detail (see “Biostratigraphy” section, this chapter). A calibration to magnetostratigraphy was not possible. No reliable paleomagnetic data were obtained because of the disturbed nature of the pelagic sediments (see “Paleomagnetism” section, this chapter). Age assignments for calcareous nannofossils and planktonic foraminifers are taken from Berggren, Kent, and Van Couvering (1985). The specific biohorizons and their age assignments are given in Table 7. A graphic plot of the sediment accumulation rates is illustrated in Figure 30.

Significant accumulation of pelagic sediment (foraminifer ooze) began atop the drowned Limalok Guyot during the early Miocene (nannofossil Subzone CN1c, planktonic foraminifer Subzone N4b). The initial sediment accumulation rate was approximately 12–15 m/m.y. This rate apparently slowed later in the early Miocene to approximately 2–3 m/m.y. and increased once again to 14–20 m/m.y. by the middle Miocene. The sediments representing the late middle Miocene and most of the late Miocene (5.5–11.5 Ma) are missing at Site 871. Accumulation resumed at a reduced rate (approximately 2 m/m.y.) during the latest Miocene and the Pliocene. Sediment accumulation rates for the Pleistocene were variable but generally on the order of 11–12 m/m.y.

Four distinct unconformities within the Neogene pelagic cap have been identified. The absence of nannofossil Subzone CN5a indicates a hiatus with as much as 1.3 m.y. of the early middle Miocene missing. The most significant unconformity in the pelagic cap sequence separates nannofossil Subzones CN5b from CN10a and planktonic foraminifer Zone N12 from Subzone N17b. The hiatus associated with this unconformity represents approximately 6 m.y. of missing time, encompassing the late middle Miocene and most of the late

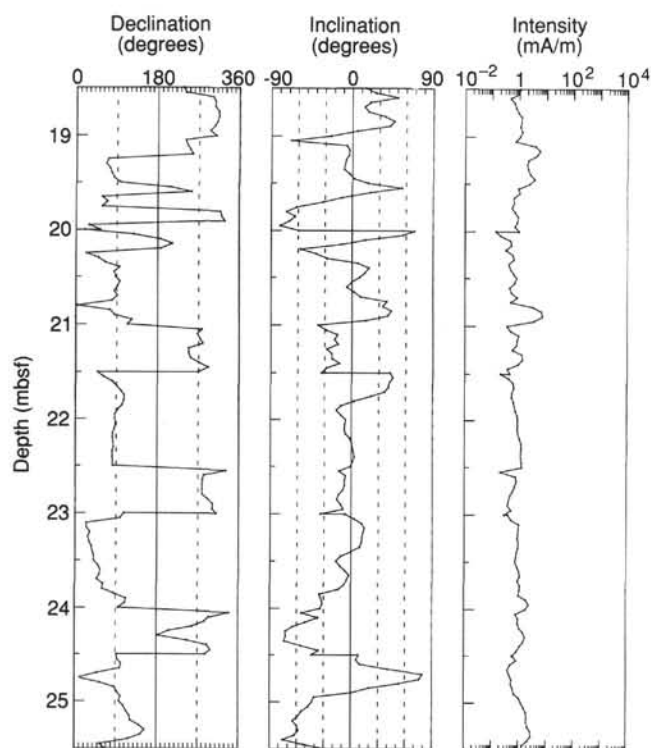


Figure 25. Declination, inclination, and intensity variations for Core 144-871A-3H. Note the bimodal distribution of declinations near 90° and 270° and the similarity of declination variations within Sections 144-871A-3H-3 through -3H-6.

Miocene. Planktonic foraminifer assemblages associated with this disconformity are mixtures of species from the late, middle, and early Miocene as well as some forms from the Oligocene. Calcareous nannofossil assemblages contain common reworked Oligocene species. A third disconformity separates nannofossil Subzones CN10a from CN12a and planktonic foraminifer Subzone N17b from the combined Zone N19/N20. The hiatus at this disconformity is approximately 0.9 m.y., spanning most or all of the early Pliocene. Finally, late Pliocene sediment accumulation was interrupted for approximately 200 k.y., as indicated by the absence of nannofossil Subzones CN12b and CN12c.

Abundance counts of radiolarians provide additional evidence relating to sediment accumulation rates during the Neogene on Limalok Guyot. The presence of siliceous microfossils, despite silica dissolution and diagenesis, can be taken as an indication of increased paleoproductivity in the early and middle Miocene (Fig. 31). However, their abundance is not a direct measure of past productivity because it is likely that, during intervals of slower deposition, non-deposition, or erosion, biogenic silica was more intensely dissolved than during intervals of continuous sedimentation. Silica dissolution is inferred to have occurred during the late Miocene and possibly also during the middle Miocene hiatus.

Carbonate Platform

Sediment accumulation rates for the carbonate platform interval are constrained largely by age assignments based on benthic foraminifer assemblages. Additional constraints are provided by the planktonic foraminifers and calcareous nannofossils (Sample 144-871C-31R-1, 45–49 cm) associated with the gray aragonitic fossil packstone at the base of the carbonate platform sequence. The sediment accumulation values so derived (25–30 m/m.y.) must be viewed as approximate, as poor recovery prevents more exact determinations. It

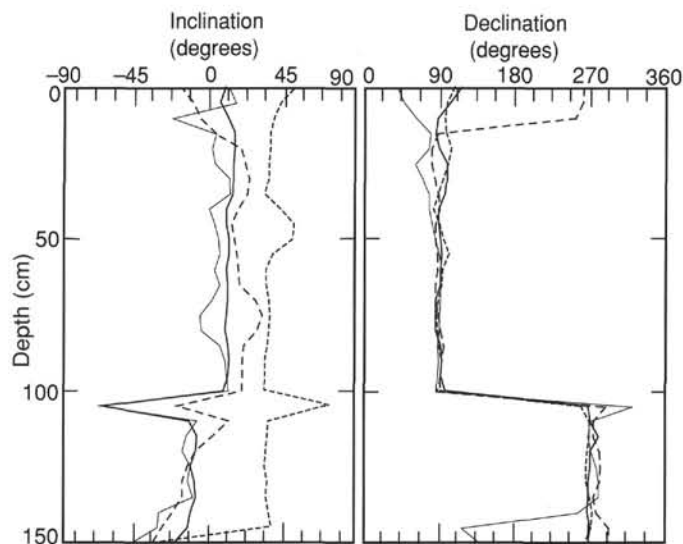


Figure 26. Declination and inclination variations for Section 144-871B-7H-4. Thin lines represent remanence of the archive half measured upright (dashed) and inverted about the Z-axis (solid) of the archive half after demagnetization at 15 mT. Thicker lines represent remanence of working half measured upright (dashed) and inverted (solid). Note the nearly identical declination variation in all four measurements.

should be noted that the logging results suggest numerous disconformities in the sequence that were not identifiable in the recovered material (see “Downhole Measurements and Seismic Stratigraphy” section, this chapter).

INORGANIC GEOCHEMISTRY

Interstitial Waters

Interstitial waters were taken from 15 core samples in Holes 871A and 871C and analyzed according to the methods outlined in the “Explanatory Notes” chapter (this volume). Twelve of these samples came from calcareous oozes in the upper 126 m of the pelagic cap. As limestones were cored from 133 to 427 mbsf, no interstitial samples were extracted from this interval. Interstitial water samples were extracted from soft sediment (primarily clay) recovered from 427 to 443 mbsf. No interstitial water samples were taken from the underlying basalt and basalt breccia. Shipboard interstitial water data from Site 871 are presented in Table 8.

Salinity and Chlorinity

Pore-water salinity values of samples from Holes 871A and 871C are indicative of normal seawater, consistently 35 ppt; Sample 144-871C-34R-2, 0–10 cm, which yielded a value of 34 ppt, is the only exception. The chlorine content is largely that of normal seawater (541–566 mM Cl⁻); however, Cl⁻ values of samples from the calcareous oozes (Samples 144-871A-1H-5, 113–118 cm, through -14H-3, 143–150 cm) are typically 1% higher than surface seawater. The chlorinity values of clay samples (Samples 144-871C-32R-3, 142–150 cm, through -34R-2, 0–10 cm) are the same as surface seawater, and the lowest value (541 mM Cl⁻) is associated with the sample closest to the basalt contact.

Alkalinity, pH, Calcium, Magnesium, Sodium, Potassium, Rubidium, and Lithium

Calcium, magnesium, sodium, potassium, strontium, rubidium, and lithium concentrations of samples from the pelagic cap of the Hole 871A (Lithologic Unit I) remain constant with depth and are

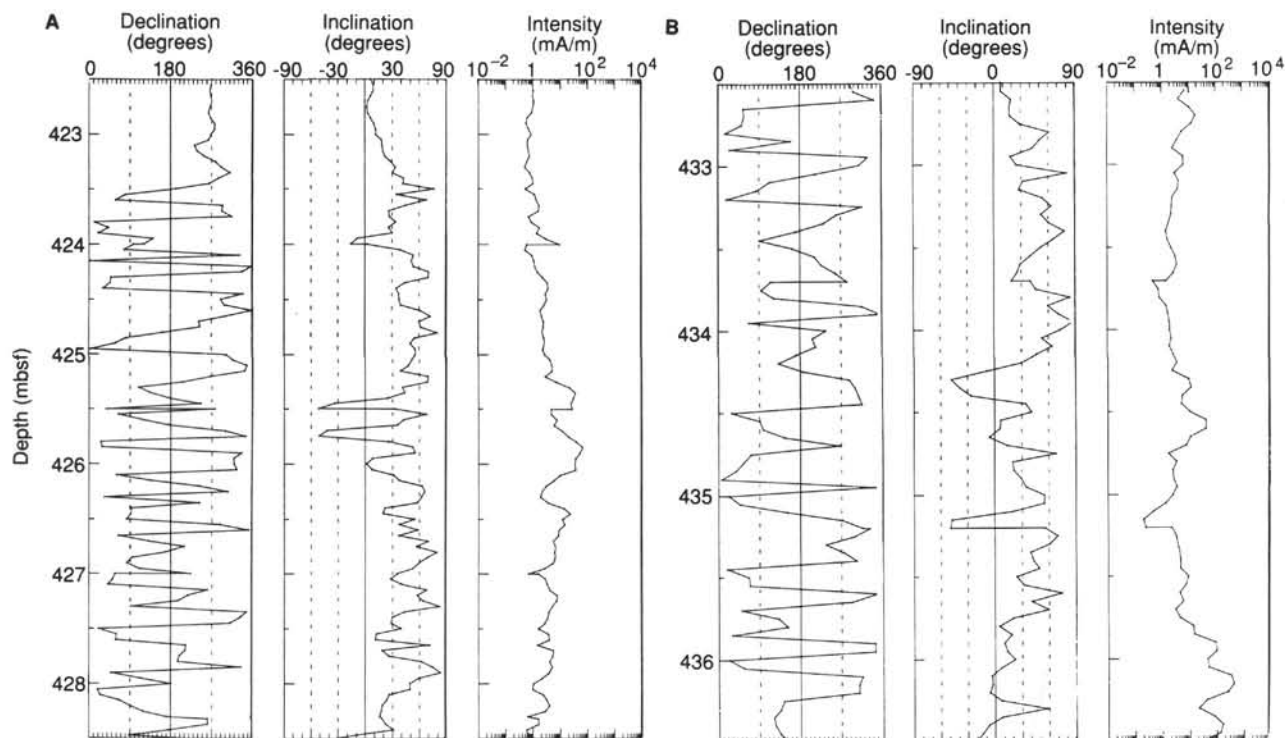


Figure 27. Declination, inclination, and intensity variations of the archive half of Cores 144-871C-32R (A) and -33R (B) after demagnetization at 15 mT with the pass-through cryogenic magnetometer. Both cores are from the claystone unit (423–451 mbsf) and show consistent inclinations but random declinations.

similar to seawater (Fig. 32). Mean values of pH (7.71 ± 0.08) and alkalinity (2.73 ± 0.21) measured on pelagic sediment samples (all samples from Hole 871A) show no depth trend.

Minor element compositions in the clays (all samples from Hole 871C) show the effects of basalt seawater reactions with respect to calcium, magnesium, and potassium. The relative concentrations of calcium increased whereas those of magnesium decreased. The potassium concentration is also lower than ambient seawater. Strontium, rubidium, and lithium concentrations are similar to seawater values.

Silica

Silica concentrations of the interstitial waters from the pelagic cap range from 122 to 169 μM . Silica content of the pore water reflects deep-sea concentrations. Silica contents of the interstitial waters from the clay interval in Hole 871C were elevated relative to seawater, from 156 to 220 μM .

Sulfate and Ammonium

The sulfate contents of the interstitial waters from the pelagic cap are seawater values (30.22 ± 1.5 mM), whereas samples taken from the clays indicate partial sulfate reduction has taken place (27.80 ± 0.37 mM). Ammonium contents vary between 5 and 14 μM in the interstitial waters from the pelagic cap and increase to 17–50 μM in the interstitial waters from the clays, providing additional evidence of locally reducing conditions in the clays (Fig. 32).

Fluoride

Fluoride concentrations within seawater are typically 68 to 70 μM (e.g., Brewer, 1971), whereas F concentrations in interstitial waters from the pelagic cap sediments are consistently near 90 μM (Hole 871A). The F content of interstitial waters from the clays (Hole 871C) are lower than seawater, from 61 to 71 μM (Fig. 32).

ORGANIC GEOCHEMISTRY

At Site 871, in addition to safety monitoring for hydrocarbon gases, 115 samples were analyzed for inorganic carbon content. Of these, 30 samples were used for additional determination of total organic carbon, nitrogen, sulfur, and hydrogen content. The procedures used for the analytical program are described in the "Organic Geochemistry" section of the "Explanatory Notes" chapter (this volume).

Volatile Hydrocarbons

The shipboard safety and pollution monitoring program requires regular measurements of light hydrocarbon gases (C_1 to C_3) in cores immediately after retrieval onto the core deck. Twenty-eight headspace gas samples were obtained from the pelagic carbonate ooze in Holes 871A and 871B, and two headspace gas samples were taken from Hole 871C in the clayey interval of Cores 144-871C-32R and -33R. The low recovery in most of Hole 871C made any further gas sampling meaningless. The results of the headspace gas analyses are given in Table 9. Very low concentrations of volatile hydrocarbon gases were detected. Methane concentrations varied between 2 and 3 ppm without any correlation to sediment type. The concentrations are only slightly higher than the general background of methane in the laboratory and on the core deck, which was found to vary between 1.9 and 2.1 ppm. Traces of ethane and propane were found in a few of the samples. The very low volatile gas concentration in the pelagic cap can be ascribed to the low concentration of organic carbon in these sediments (TOC below 0.5%; see paragraph on organic carbon).

The claystone interval in Cores 144-871C-32R to -34R contains considerable amounts of organic carbon in the uppermost 50 cm of Core 144-871C-32R (up to 12%; see Table 10). Nevertheless, methane concentrations in headspace gas samples from this interval were very low (2.1 ppm), and no indication of increased methanogenesis was observed.

Table 6. Results of demagnetization of basalts from Cores 144-871C-35R- to -41R.

Core, section, interval (cm)	Inclination (degrees)
144-871C-	
35R-1, 44-46	+2.2
35R-2, 4-6	-32.3
36R-1, 36-38	-30.2
36R-2, 57-59	-32.2
36R-3, 25-27	-13.9
37R-1, 85-87	-6.2
37R-2, 16-18	-7.3
37R-2, 87-89	-8.1
38R-1, 85-87	-16.8
38R-3, 84-86	-22.0
38R-5, 56-58	-15.8
38R-6, 96-98	-21.9
39R-1, 81-83	-26.1
39R-4, 11-13	-19.1
39R-5, 113-115	-20.1
39R-6, 118-120	-16.5
40R-1, 141-143	-18.7
40R-4, 62-64	-13.0
*41B-1, 6-8	+18.1

*Vertical orientation unknown.

Carbonate Carbon

Inorganic carbon (IC) content was measured in 115 samples with the Coulometrics carbon dioxide coulometer. In Hole 871A, one sample from each section of the pelagic cap (Lithologic Unit I) was analyzed for IC. The samples were obtained from the split core, freeze-dried, and analyzed directly without desalting. As the porosity of the pelagic oozes is very high (between 65% and 80%; see "Physical Properties" section, this chapter) and no attempts were made to wash the samples before drying, pore-water salt was precipitated in the samples (the actual pore fluids had a composition similar to seawater; see "Inorganic Geochemistry" section, this chapter). Accepting a maximum value of 80% for sample porosity and pore-water salinity values of 35‰, up to 5 wt% of predominantly sodium chloride could have precipitated in the samples. This precipitate provided a systematic error in the determination of both total carbon and inorganic carbon by reducing carbonate carbon values. One sample (Sample 144-871A-12H-2, 72-74 cm), which had an initial IC value of 11.72%, was desalted and rerun for IC. After desalting, inorganic carbon concentration was found to be 0.61% higher. Calculated as calcium carbonate, this difference corresponds to a 5% increase in the calcium carbonate value.

The IC and calcium carbonate values for Hole 871A are given in Table 10. Calcium carbonate content was very high in all samples from the pelagic cap, ranging from 92% to 97% (average = 94.5%, standard deviation = 1.74), corresponding to pure calcium carbonate if desalted. Minor fluctuations with depth were seen in the carbonate concentration (Figs. 33 and 34). These fluctuations may suggest variations in productivity or in clastic input. The quality of the present data does not admit any further interpretation.

No carbon determinations were performed in samples from Hole 871B.

The results for Hole 871C are given in Table 10. Because of low core recovery in this hole, only a limited number of samples (31) were analyzed for carbonate carbon. The samples included the major carbonate facies types encountered within the shallow-water limestone interval (Lithologic Unit II) and the claystone (Lithologic Unit III) overlying the basalt. The amount of sea salt precipitated in the analyzed limestone was negligible.

The shallow-water limestones sampled from Cores 144-871C-1R through -30R are all pure carbonates (>99% CaCO₃). The dark gray skeletal packstone in Core 144-871C-31R-1 (Lithologic Subunit IIF) contained up to 96% calcium carbonate, partly in the form of skeletal aragonite as determined by X-ray diffraction (Table 11).

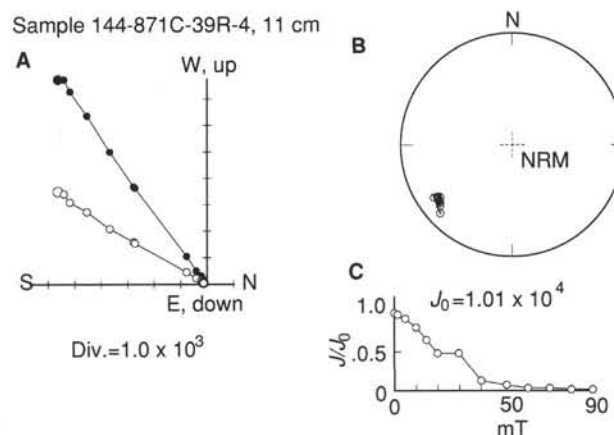


Figure 28. Alternating-field (AF) demagnetization results for basalt Sample 144-871C-39R-4, 11 cm. Demagnetization fields are 0, 2.5, 5, 10, 15, 20, 30, 40, 50, 60, 70, 80, and 90 mT. **A.** Orthogonal vector plot of the progressive AF demagnetization. Closed circles represent horizontal components of the magnetization, and open circles represent vertical components. **B.** Stereonet plot of vector end-points after progressive demagnetization. **C.** Variation of intensity after progressive AF demagnetization.

The topmost 50 cm of the claystone (Lithologic Subunit IIIA) contains variable amounts of carbonate, mainly in the form of aragonitic shells (Fig. 35). The claystone has been strongly bioturbated, and shell fragments were probably redeposited into burrows. Samples taken close to the burrows are virtually free of carbonate. The deeper parts of the claystone (Lithologic Subunits IIIB and IIIC) contain no carbonate.

Organic Carbon and Sulfur

Values of total carbon (TC) and total sulfur (TS) were determined using the Carlo Erba Model NA1500 elemental analyzer. Total organic carbon (TOC) values were calculated from the difference between TC and IC. When the precision of these two values are taken into account, TOC values less than 0.2% can be considered unreliable. The results of the TOC and TS determinations are given in Table 10.

In the pelagic cap (Lithologic Unit I), TOC was below 0.3% in all samples investigated. The quality of the data does not permit any interpretations with regard to secular variations in the TOC. No sulfur was detected in the pelagic cap.

In the shallow-water limestone (Lithologic Unit II), TOC and TS were below detection limits except in the dark gray skeletal packstone (Lithologic Subunit IIF). Sample 144-871C-32R-1, 16-20 cm, from this subunit contained 0.3% TOC and 0.6% TS.

The topmost part of the clay (mottled gray clay in Lithologic Subunit IIIA) below the skeletal packstone is rich in organic matter (TOC up to 10%) and sulfur (TS up to 12%), the latter in the form of pyrite and marcasite. The TS/TOC ratio is remarkably high in some of the samples. A dark gray clay sample obtained from the bottom of Core 144-871C-31R-1 had a composition similar to the clay in Lithologic Subunit IIIA. This sample may represent the only recovered part of a clay unit situated above the skeletal packstone.

The TOC and TS contents decrease rapidly below the mottled gray clay in Subunit IIIA. Neither TOC nor TS were identified in the variegated clay in Lithologic Subunit IIIB. No analyses were made from the basalts in Unit IV.

Organic Matter Type and Thermal Maturation Level

Shipboard geochemical characterization of organic matter is normally performed by Rock-Eval (RE) and pyrolysis gas chromatographic (Py-GC) analyses. During most of the time spent at Site 871, neither the Rock-Eval system nor the Geofina Py-GC were operating

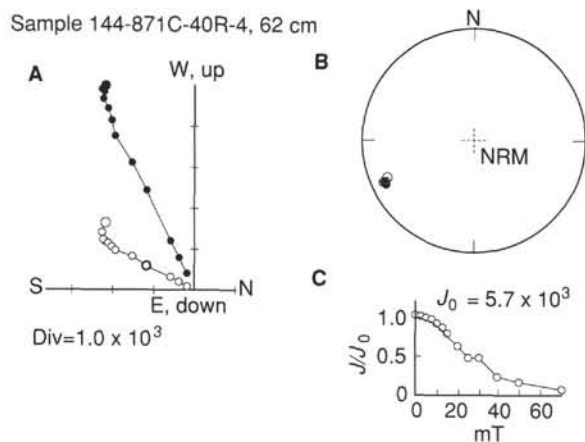


Figure 29. Alternating-field (AF) demagnetization results for basalt Sample 144-871C-40R-4, 62 cm. Demagnetization fields are 0, 2.5, 5, 7.5, 10, 12.5, 15, 20, 25, 30, 40, 50, and 70 mT. Other plot conventions are identified in Figure 28.

properly; therefore, only semi-quantitative RE analyses from the clayey interval at the base of the shallow-water limestone in Hole 871C are reported here.

Sample 144-871C-31R-1, 44–49 cm (Subunit IIF), is a dark gray to black, sticky clay; TOC and TC are high (12.4% and 3.3%, respectively), TS/TOC is low (0.26), S_1 is very low, S_2 is moderate, S_3 is low, and $T_{max} = 425^\circ\text{C}$. The RE data indicate thermally immature to marginally mature organic matter of a composition corresponding to a type II (“herbaceous”) kerogen. The sample represents the clayey interval recovered from the bottom of the core catcher above the dark gray skeletal packstone in Lithologic Subunit IIF.

Sample 144-871C-32R-1, 4–5 cm (Lithologic Subunit IIF) is black material from a dark gray skeletal packstone; S_1 was not detected, S_2 is low to moderate, S_3 is high, and $T_{max} = 415^\circ\text{C}$. The RE data indicate thermally immature organic matter of a composition corresponding predominantly to a type III (woody) kerogen.

Sample 144-871C-32R-1, 41–42 cm (Lithologic Subunit IIIA) is a dark gray clay with shell fragments; TOC and TS are very high (11.5% and 12.6%, respectively), TS/TOC is moderate, S_1 is very low, S_2 is low, S_3 is high, and $T_{max} = 425^\circ\text{C}$. The RE data indicate thermally immature to marginally mature organic matter of a composition corresponding predominantly to a type III (woody) kerogen.

Organic Facies and Depositional Environments

Three major depositional environments are represented in Hole 871: (1) pelagic (foraminifer ooze, Lithologic Unit I), (2) shallow-water marine (platform limestone, Lithologic Unit II), and (3) shallow-water marine to terrestrial (claystone, Lithologic Unit III).

In the first environment, the preservation of organic matter was poor. The TOC values of <0.5% and the TS values below detection limit indicate oxidation of organic matter during or after deposition. Organic matter is mainly autochthonous (linings from foraminifers), but woody tissue has also been reported from most of the samples (see “Biostratigraphy” section, this chapter).

In the second environment, preservation of organic matter was extremely poor. The only exception to this is the dark gray skeletal limestone (Sample 144-871C-32R-1, 16–20 cm, Lithologic Subunit IIF), which will be discussed under the third environment. In the third environment, two distinctive organic facies can be identified. One facies is characterized by very good preservation of organic matter under sulfate-reducing conditions; the other, by poor preservation of organic matter probably under subaerial conditions.

The first facies is represented by the top meter of the gray clay in Interval 144-871C-32R-1, 30–120 cm, the dark gray skeletal pack-

Table 7. Biohorizons used to compute sediment accumulation rates for the Neogene, Hole 871A.

Code	Datum	Age (Ma)	Top depth (mbsf)	Base depth (mbsf)
Calcareous nannofossils:				
C1	FAD <i>E. huxleyi</i> acme	0.085	0.83	1.44
C2	FAD <i>E. huxleyi</i>	0.275	4.41	4.71
C3	LAD <i>P. lacunosa</i>	0.474	4.71	5.30
C4	LAD <i>H. sellii</i>	1.37	12.80	13.35
C5	LAD <i>C. macintyreii</i>	1.45	14.80	15.35
C6	FAD <i>G. oceanica</i>	1.68	17.80	18.35
C7	LAD <i>D. brouweri</i>	1.90	17.80	18.35
C8	LAD <i>D. asymmetricus</i>	2.20	18.75	19.00
C9	LAD <i>D. tamalis</i>	2.60	19.00	19.30
C10	LAD <i>D. variabilis</i>	2.90	19.11	19.61
C11	LAD <i>S. heteromorphus</i>	14.40	52.00	53.50
C12	FAD <i>S. heteromorphus</i>	17.10	102.50	103.00
C13	LAD <i>S. belemnus</i>	17.40	102.50	103.00
C14	FAD <i>S. belemnus</i>	21.50	112.50	115.50
Planktonic foraminifers:				
F1	FAD <i>G. truncatulinoides</i>	1.90	17.00	17.60
F2	FAD <i>G. tosaensis</i>	3.10	19.10	20.60
F3	FAD <i>S. dehiscentis</i>	5.10	20.60	22.10
F4	FAD <i>P. primalis</i>	5.80	25.10	26.50
F5	LAD <i>G. fohsi lobata</i>	11.50	25.10	26.50
F6	FAD <i>G. fohsi lobata</i>	13.10	49.10	50.60
F7	FAD <i>G. praefohsi</i>	13.90	52.10	53.60
F8	FAD <i>G. peripheroacuta</i>	14.90	55.00	58.60
F9	FAD <i>O. suturalis</i>	15.20	66.60	68.30
F10	FAD <i>P. sicana</i>	16.60	77.60	83.50
F11	LAD <i>C. dissimilis</i>	17.60	93.00	96.60
F12	FAD <i>G. insueta</i>	17.90	96.60	102.50
F13	LAD <i>G. kugleri</i>	21.80	102.50	112.00
F14	FAD <i>G. dehiscentis</i>	23.20	130.50	139.50

Note: Ages given are those from Berggren, Kent, and Van Couvering (1985). “Top depth” denotes the lowest sample above a biohorizon; “Base depth” denotes the highest sample below the biohorizon. FAD = first appearance datum, and LAD = last appearance datum.

stone in Interval 144-871C-32R-1, 0–30 cm, and the solitary clay layer in Interval 144-871C-31R-1, 44–49 cm, above the skeletal packstone. In this facies, kerogen of both type II and III has been identified. Thin sections and palynologic slides show precipitation of mainly framboidal marcasite and pyrite in both skeletal and organic remains. Deposition probably took place in a restricted, low-energy environment influenced by seawater. The skeletal packstone may represent a mixture of carbonate grains and shell fragments brought into the depositional environment by storm activity, which for a period created hospitable living conditions for burrowing organisms. Subsequent to this episode, low oxic to anoxic conditions were reestablished and further clay deposition sealed off the skeletal packstone from the influence of diagenetic fluids. This scenario may explain the extraordinary preservation of aragonitic skeletal remains in the packstone. The second organic facies is characterized by poor preservation of mainly terrigenous organic matter under oxic conditions at present.

Conclusions

The following conclusions can be made regarding the organic geochemistry at Site 871:

1. No volatile hydrocarbons were encountered at this site.
2. The pelagic cap sediments (Lithologic Unit I) have a calcium carbonate content of almost 100%. Only very low concentrations of organic matter (TOC below 0.3%), mainly of autochthonous origin, were encountered. The unit was deposited under mildly oxic conditions.
3. The platform limestone (Lithologic Unit II) is made up of pure calcium carbonate with no detectable organic matter. The unit was exposed to oxic conditions during or subsequent to deposition.
4. Lithologic Subunits IIF (dark gray skeletal packstone) and IIIA (gray clay) were deposited under sulfate reducing conditions in a low-energy environment influenced by seawater. The skeletal packstone is interpreted to represent a storm layer.

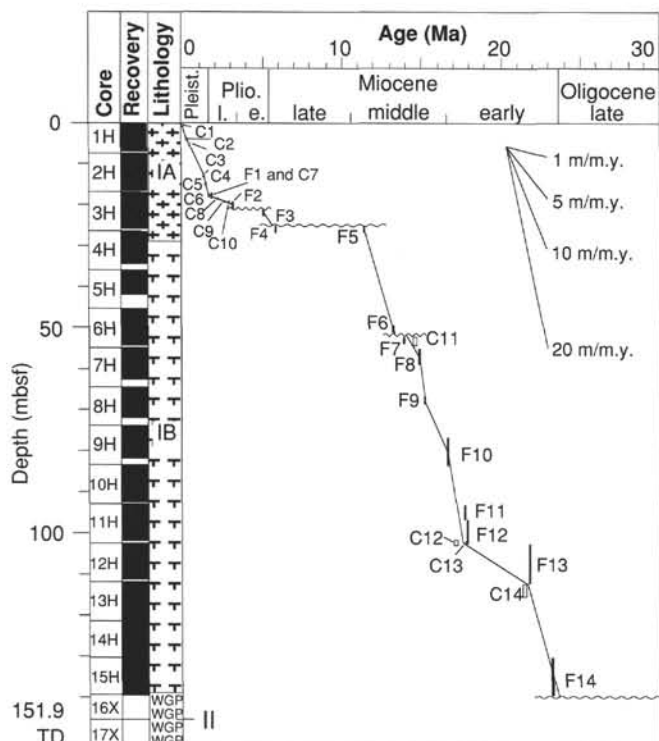


Figure 30. Sediment accumulation rates for the Neogene of Hole 871A. Bars represent the upper and lower limits of a biohorizon as constrained by sampling. Foraminifer biohorizons are indicated by filled bars; calcareous nanofossils by open bars. Codes for foraminifer and nanofossil biohorizons are keyed to Table 7.

5. The extraordinary preservation of the aragonitic shell remains in Lithologic Subunit IIF relates to sealing from percolating waters by subsequent deposition of clay.

6. Organic matter is thermally immature to marginally mature with regard to hydrocarbon formation.

IGNEOUS PETROLOGY

Introduction

Material of clear volcanic origin was first encountered at 436 mbsf (Core 144-871C-33R) in the form of isolated pieces of basalt within the sedimentary section, a few meters above the igneous basement. Except for a single, thin (~1 m thick), basaltic lava unit, the uppermost 6 m of recovered basement consists of a series of volcanogenic breccias. These give way to a sequence of massive flows with recovered thicknesses of 1–4 m, and the hole terminates just beneath the second of two thicker (7.5 m recovered) massive flows. All the flow units have similar mineralogy with only minor variations in texture and phenocryst content. They appear to be nepheline-bearing alkalic basalts.

The basement units (Units 1–23; Table 12) described here make up Lithologic Unit IV (see “Lithostratigraphy” section, this chapter).

Visual Descriptions

Clasts from the Sedimentary Section

Four separate pieces of gray, reasonably fresh basalt, each about 5–10 cm long, were recovered (two each in Intervals 144-871C-33R-3, 90–120 cm, and 144-871C-34R-1, 5–15 cm) from a disturbed, clay-rich section near 436 mbsf. They occur in Lithologic Unit III, at or near the boundary between Subunits IIIB and IIIC, the lowest two subunits of the sedimentary section. Subunit IIIB is a thick (~12 m drilled) sequence of mottled red/blue/olive, semiconsolidated clay-

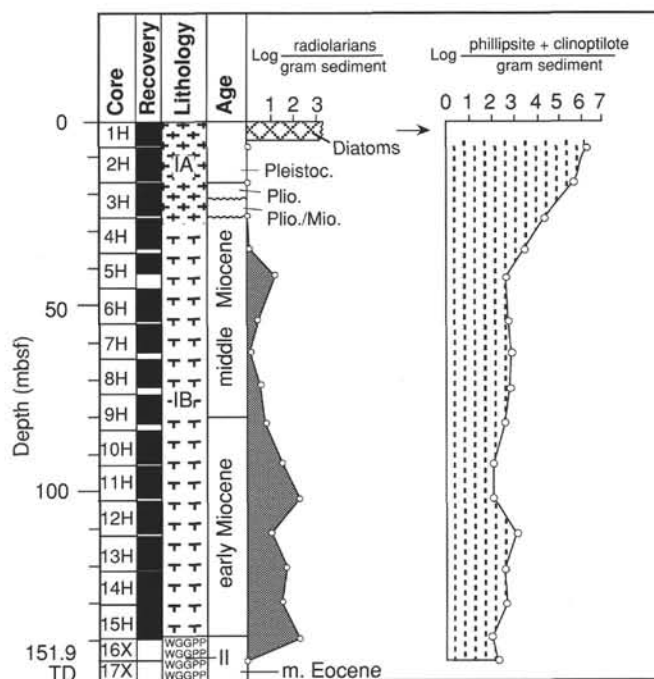


Figure 31. Siliceous microfossil and zeolite abundances for the Neogene of Hole 871A.

stone, and Subunit IIIC is a dark brown claystone in which fragments of highly weathered basalt become increasingly common downhole (see “Lithostratigraphy” section, this chapter). The lowermost claystone is almost certainly attributable to *in-situ* tropical weathering of basaltic material. If this is so, then the overlying claystones encompass a transition from subaerial to marine conditions.

The four basalt fragments encompass three distinct textural variants and are presumed to represent three separate flows. Because their original shapes are not preserved and they occur within a disrupted section of the core, their relationships to one another and to the rest of the sequence are unclear. Perhaps the most likely explanation is that they represent fragments carried downslope as scree or stream bed-load.

Volcaniclastic Units

Volcanogenic Sandstones

Two brick-red volcanogenic sedimentary units occur within the upper part of the igneous basement. The lower of these units (Unit 12; Interval 144-871C-36R-2, 71–81 cm) has been broken up by the drilling and cannot be described in detail. The upper unit, a volcanogenic pebble conglomerate (Unit 3; Interval 144-871C-35R-1, 83–132 cm) appears to have been completely altered to clays and iron oxyhydroxides. It preserves a strong horizontal fabric, imparted both by sedimentary layering and by compaction of angular, vesicular volcanic clasts. In the upper 20 cm of this unit, a distinct upward-fining gradation of clast size occurs.

Volcanic Breccias

Underlying the first three basaltic units is a series of basaltic breccias (452.8–457.8 mbsf; see Table 12) that have been subdivided into four units:

1. Unit 4 (Sections 144-871C-35R-1, 132 cm, to -35R-2, 46 cm) is a coarse, angular basaltic breccia with clast sizes in excess of 5–10 cm and a sand-sized volcanogenic matrix.

2. Unit 5 (Interval 144-871C-35R-2, 46–143 cm) is a much finer (~2 cm), angular, clast-supported basaltic breccia.

Table 8. Surface seawater and interstitial water geochemical data, Site 871.

Core, section, section (cm)	Depth (mbsf)	pH	Alkalinity (mM)	Salinity (g/kg)	Cl ⁻ (mM)	Mg ²⁺ (mM)	Ca ²⁺ (mM)	SO ₄ ²⁻ (mM)	NH ₄ ⁺ (μM)	SiO ₂ (μM)	K ⁺ (mM)	Sr ²⁺ (μM)	Na ⁺ (mM)	F (μM)	Li (μM)
Surface seawater	0	8.12	2.279	35.0	553	53.73	10.51	28.90	5	24	9.72	91	464	70	24
144-871A-															
1H-5, 113-118	7	7.83	2.950	35.0	554	54.09	10.98	31.70	8	159	10.67	94	491	91	24
2H-6, 145-150	16	7.82	2.997	35.0	562	53.50	11.00	29.50	7	169	10.43	101	484	96	24
3H-5, 143-150	24	7.61	2.667	35.0	561	50.82	10.84	30.40	14	152	9.72	98	485	90	24
4H-5, 140-150	34	7.67	2.450	35.0	561	54.29	10.76	29.30	6	139	9.96	96	484	90	24
5H-2, 0-5	38	7.72	2.490	35.0	560	54.21	11.04	31.40	8	122	9.96	98	471	90	24
6H-4, 140-150	51	7.73	3.258	35.0	560	50.86	11.06	28.90	6	154	10.43	103	489	89	26
7H-3, 142-150	59	7.67	2.636	35.0	553	54.14	10.98	29.80	11	154	10.43	98	484	90	24
8H-3, 142-150	69	7.76	2.743	35.0	566	53.90	11.04	29.20	10	159	10.43	101	485	89	26
9H-3, 143-150	78	7.74	2.747	35.0	560	54.16	11.19	34.00	7	158	12.09	101	494	90	24
10H-3, 145-150	88	7.61	2.768	35.0	561	54.34	11.23	28.80	7	156	13.52	106	480	89	24
11H-3, 143-150	97	7.60	2.685	35.0	558	51.56	11.06	31.00	8	156	11.85	106	476	90	24
14H-3, 143-150	126	7.63	2.735	35.0	562	55.03	11.06	28.60	7	156	10.19	100	504	87	24
144-871C-															
32R-3, 142-150	427	7.72	3.300	35.0	553	51.78	13.02	27.30	49	188	8.29	127	482	68	26
33R-2, 145-150	435	7.69	2.497	35.0	545	50.75	12.43	28.20	17	156	9.01	117	470	71	24
34R-2, 0-10	443	7.84	2.868	34.0	541	49.70	12.60	27.90	50	220	8.53	133	464	61	24

3. Unit 6 (Interval 144-871C-35R-3, 0-124 cm) is a more matrix-rich, possibly matrix-supported breccia with somewhat rounded basaltic clasts and a sand-sized volcanogenic matrix (Fig. 36).

4. Unit 7 (Sections 144-871C-35R-3, 124 cm, to -35R-5, 28 cm) is a very coarse basaltic breccia with clast sizes in excess of 20 cm.

In all cases the breccias are highly altered and the samples are too friable to permit detailed study. With the possible exception of Unit 5, however, the majority of clasts appear not to have been highly vesicular; they appear more likely to represent talus or other erosional debris rather than the products of explosive eruptions.

Major Basaltic Units

The first basalt unit from Hole 871C (Unit 1; Interval 144-871C-35R-1, 6-58 cm) was recovered immediately beneath the lowermost claystone of Lithologic Unit III and above the volcanoclastic pebble conglomerate of Unit 2. Unit 1 is a relatively thin (50 cm), medium-gray basalt, crisscrossed by a stockwork of 1-2 mm calcite veins spaced about 5 cm apart (Fig. 36). Like the majority of basalts at this site, it contains small (1-2 mm) phenocrysts of clinopyroxene in a microcrystalline groundmass. A notable feature of this unit is the presence of a number of small (<4 cm), highly altered, rusty brown xenoliths (Fig. 37). Because it occurs between two sedimentary layers, it is possible that this basalt is intrusive in origin, but distinct contact features and orientations are not preserved in the core.

Beneath the breccia units, we have identified 11 distinct massive flows (Units 13-23) that complete the basement section (Table 12). The upper eight flows (Units 13-20) are relatively thin, with recovered thicknesses between 1 and 4 m. Beneath these are two thick flows (Units 21 and 22), each with a recovered thickness of 7.5 m, and a final flow is represented by Core 144-871C-41B, which was retrieved from the bit on recovery of the drill string. In all except the latter case, the core recovered from each unit appears continuous, and it is likely that the recovered intervals are close to the actual flow thicknesses. Unfortunately, the overlying clays closed the hole and prevented logging, so this assumption cannot be verified.

Individual flow units are distinguished by changes in phenocryst content and/or in texture, or by the presence of intervening zones of broken and/or highly altered material. Where more than one or two pieces of such intervening material occur, we have given unit numbers to these broken zones because they do not, for the most part, appear to represent rubbly or weathered flow tops such as those encountered at Site 872 (see "Igneous Petrology" section, "Site 872" chapter, this volume). In no case was a distinct chilled margin or other flow margin feature recovered in Hole 871C, although a number of the thinner flows appear more vesicular near their tops. In the thicker flows near

the bottom of the hole, zones of high vesicularity occur within the flow interiors but are not conspicuous near the margins.

All the basaltic units for which recovery was significant at this site are very similar, differing only slightly from one another in textural detail and in phenocryst abundances. The largest phenocrysts are invariably olivine, typically euhedral to rounded in shape, and 3-5 mm in size, they constitute >5% of the lava. Occasional larger, angular olivines appear to be xenocrysts related to small, olivine-rich xenoliths that occur sporadically throughout the section. Virtually all olivines are at least partially altered to rusty brown iddingsite margins with a variety of phyllosilicates and/or calcite in their interiors; fresh olivine is only occasionally present. Small phenocrysts of clinopyroxene (1-4 mm) are almost ubiquitous and typically constitute 10%-20% of the lava. They are dark green to black in color and commonly appear to be quite fresh, although alteration to a soft green layer silicate, presumably chlorite, or to dark red-brown clay(?) is also common. Thin section examination shows that these are almost always pinkish titanite.

Alteration and Weathering Features

The entire basaltic section has been pervasively, but patchily altered by low-temperature hydrothermal fluids. Alteration features are of three main types:

1. Veins of calcite are generally 1-2 mm thick, but they can range up to 8 mm. They commonly include a light green phyllosilicate that swells rapidly on exposure to air and/or fresh water; this is presumably a smectite.

2. Vesicles are invariably filled with one or more of several minerals including calcite, smectite (as above), dark green celadonite(?), and an unidentified white zeolite.

3. Basalt groundmass is patchily altered to a deep purplish brown. This type of alteration is ubiquitous in the matrixes of the breccias and common in the lower basaltic units, where continuous purplish alteration surrounds isolated, gray, less altered domains. In these cases, the basalt has developed a distinctly mottled appearance that resembles, at first glance, some of the breccias higher in the section.

As a consequence of this alteration, much of the core, although it appeared fresh when first opened, deteriorated rapidly on exposure to air. Subsequent handling led to complete disintegration of the core into irregular, friable fragments only a few millimeters in size. This degradation precludes any meaningful petrographic or analytical study of the primary features of the affected material. Fortunately, all of the major flow units appear to have retained some regions of relatively unaltered material suitable for further study. D.M. Christie

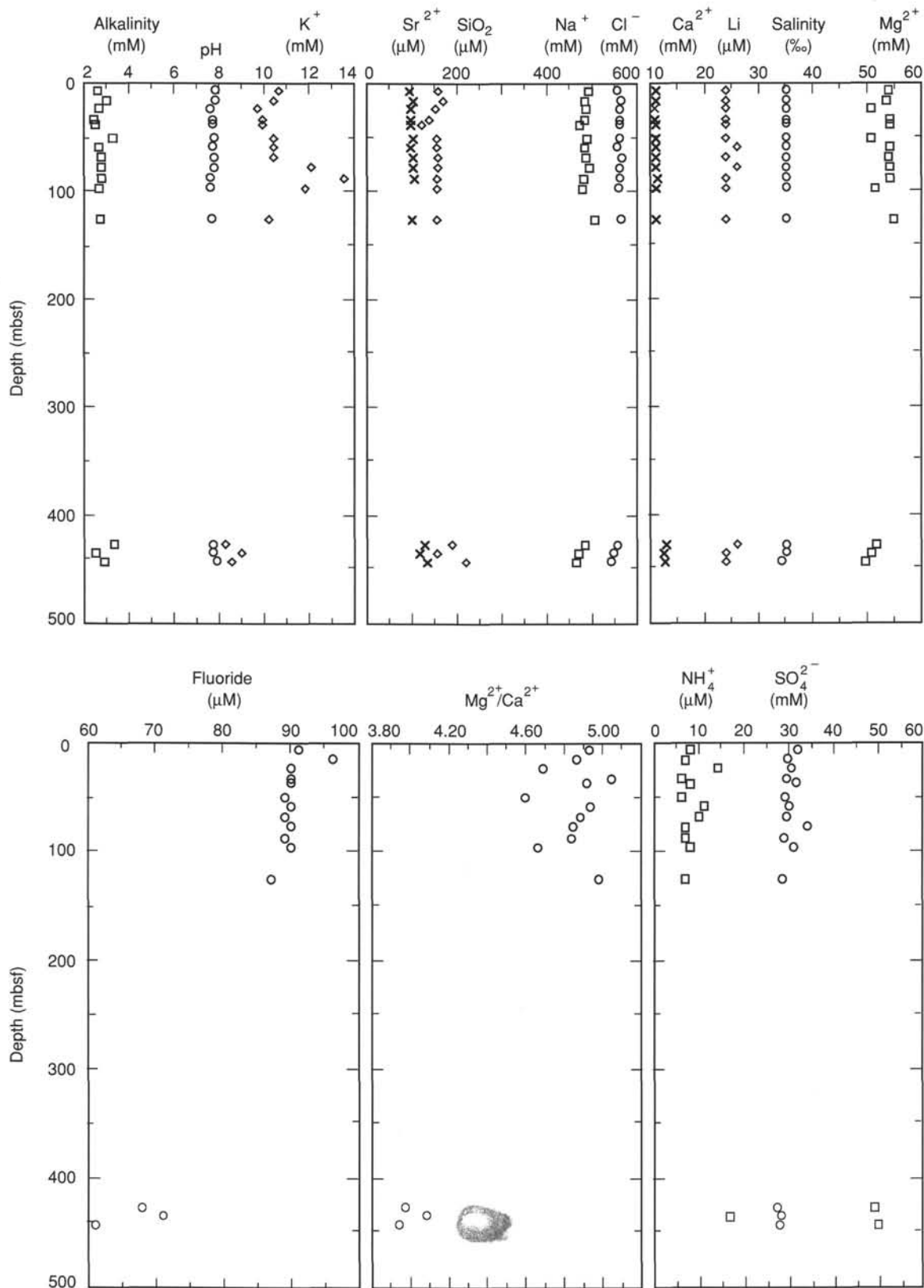


Figure 32. Concentrations of interstitial pore-water parameters vs. depth, Holes 871A and 871C. The concentration values of alkalinity, pH, Sr, SiO_2 , Na^+ , Cl^- , Ca^{2+} , Li, salinity, and Mg^{2+} remain constant at near seawater values throughout the 126 m of the pelagic cap. The contents of K^+ , Sr^{2+} , SiO_2 , Cl^- , Ca^{2+} , and Mg^{2+} in the interstitial waters of Hole 871C are altered by chemical reactions between seawater and the basalt. Fluoride concentrations are elevated by 20 μM over seawater values in Hole 871A, whereas fluoride contents from Hole 871C are close to seawater values. Basalt-seawater interaction can be clearly seen by comparing the molar ratio of Mg^{2+} and Ca^{2+} . Concentrations of SO_4^{2-} and NH_4^+ change noticeably in Hole 871C because of reducing conditions.

Table 9. Results of headspace gas analyses, Holes 871A and 871B.

Core, section, interval (cm)	Methane (ppm)	Ethane (ppm)	Propane (ppm)
144-871A-			
1H-5, 0-5	2.5	Tr	Tr
2H-6, 0-5	2.5	None	None
3H-6, 0-5	2.5	None	0.4
4H-6, 0-5	2.4	None	Tr
5H-5, 0-5	2.1	None	None
6H-6, 0-5	2.1	Tr	None
7H-5, 0-5	2.6	None	None
8H-5, 0-5	2.8	None	None
9H-5, 0-5	2.5	None	None
10H-4, 0-5	2.5	Tr	None
11H-6, 0-5	2.2	Tr	Tr
12H-6, 0-5	2.8	Tr	Tr
13H-6, 0-5	2.2	Tr	None
14H-6, 0-5	2.1	Tr	None
15H-4, 145-150	2.8	Tr	None
17H-CC	2.6	Tr	None
144-871B-			
1H-4, 0-5	2.6	None	None
2H-5, 0-5	2.0	None	None
3H-6, 0-5	2.1	None	None
4H-5, 0-5	2.2	None	None
5H-5, 0-5	2.0	None	None
6H-5, 0-5	2.0	None	None
7H-5, 0-5	2.0	None	None
9H-5, 0-5	2.1	None	None
10H-6, 0-5	2.1	None	None
11H-6, 0-5	2.3	None	None
13H-6, 0-5	2.2	Tr	Tr
14H-6, 0-5	2.2	None	None
Laboratory background	2.1	None	None

Note: Tr = trace, and None = no gas detected.

has previously witnessed a similar remarkable, rapid deterioration of drill core. In the former case, the core was from deeply buried, seemingly pristine leucite-bearing lavas that degraded to clay in a matter of weeks. We speculate that this phenomenon is related to the presence of abundant feldspathoids within the groundmass of the lavas.

Petrography

Fifteen thin sections were examined covering most of the major flow units. All the flows examined have very similar mineralogy with only minor variations in texture and mineral proportions, particularly phenocryst abundance. The basaltic sequence is characterized by an abundance of olivine microphenocrysts, commonly around 15%, set in a microcrystalline, titanite-rich groundmass. Plagioclase is present only as anhedral, poikilitic or interstitial crystals in the groundmass, never as phenocrysts or euhedral groundmass laths.

In most thin sections, the groundmass is characterized by abundant prisms of titanite, abundant cubes of magnetite and fine needles of apatite. Irregular patches of plagioclase and/or a clear, low-relief, low-birefringent material are interstitial to, and frequently poikilitically enclosed, the titanite. The low-birefringent material can be identified as nepheline by its negative, uniaxial optical character in some samples, but it appears partially cloudy and almost isotropic in others. In the latter case, optical determination is not possible and we have tentatively identified this cloudy material as partially altered nepheline, although it may include some alkali feldspar, plagioclase, or even analcime.

Fresh plagioclase is present in a number of samples as both small interstitial patches and as larger (up to 0.5 mm), optically continuous, poikilitic regions. It is sparsely twinned, but the few grains suitable for optical determination consistently yield values close to An_{35} .

The textures of the lavas appear to vary with flow thickness. The thinner lavas (Units 9, 13 and 15; Table 12) are very fine grained with intersertal textures in which the characteristic titanite and magnetite are separated by an unresolvable, cloudy, colorless matrix, presumably dominated by partially altered plagioclase and/or neph-

line. The thicker lavas (Units 21 and 22) are, by contrast, well crystallized and less fine grained with intergranular textures.

Based on their mineralogy, we infer that these lavas are distinctly alkalic and most likely strongly undersaturated in nature. If our identification of nepheline is correct, the majority are best termed "basanites" as they contain modal nepheline and plagioclase. Some of the finer grained samples are basanitoids because their mineralogy is not resolvable, and a single clast (Interval 144-871C-33R-1, 5-20 cm) from the claystone unit is a nephelinite because it lacks plagioclase.

Summary and Conclusions

As recorded in Hole 871C, the earliest events in the geologic history of Limalok Guyot are a series of eruptions of highly alkalic basalts, basanites, and nephelinites that form a series of at least 11 massive flows, ranging from 1 m to more than 7 m in thickness. The margins of these flow units are not apparent in the drill core, so it is not known whether they are submarine or subaerial. A conventional interpretation based on lava compositions and flow thicknesses would be that these lavas represent a posterosional, valley-filling sequence. However, the effects of pervasive, low-temperature hydrothermal alteration are apparent throughout the sequence. Such attenuation is unlikely in flows produced by short-lived low-volume host erosional events. Rather, it seems to imply that magmatic activity continued in the vicinity for some time, perhaps indicating that these lavas represent part of the main constructional phase of the volcano.

Angular volcanic breccias and a thick overlying sequence of dense, mottled claystone record a (long?) period of weathering and erosion of the volcanic pile that most likely was subaerial initially but which ended with unequivocally marine conditions.

PHYSICAL PROPERTIES

Introduction

The objectives of the physical properties measurement program at Site 871 were (1) to measure the standard shipboard physical properties, including nondestructive, whole-core measurements of bulk density, compressional wave velocity, magnetic susceptibility and thermal conductivity, and discrete measurements of index properties, shear strength and compressional wave velocity (see "Explanatory Notes" chapter, this volume); and (2) to identify geotechnical units for downhole and cross-hole correlations.

Discrete Measurements

The sedimentary sequence recovered at Site 871 consists of the following lithologic units: Unit I, un lithified nannofossil foraminifer ooze and foraminifer ooze (0-133.7 mbsf); Unit II, platform carbonates consisting of packstones, wackestones, and grainstones (133.7-422.9 mbsf); Unit III, mottled gray and variegated clay (422.9-451.6 mbsf); and Unit IV, altered olivine phyric basalt with basalt breccia and volcanoclastic sandstone intervals (451.6-500 mbsf).

Measurements of index properties were made on representative samples of the pelagic ooze, as well as on limestones, clays, and basalts where recovery permitted. These samples were shared with other shipboard investigators (e.g., paleomagnetism and geochemistry) to preserve the small amount of available material. The index properties measurements from Site 871 are summarized in Figure 38 and Table 13. The distribution of these measurements was constrained by the relative core recovery in each unit. There was good core recovery in the pelagic cap (70%-100%); in contrast, core recovery from the platform carbonates was poor, ranging from 0% to 17%. In the lower part of Unit III and in Unit IV there was 30% to 100% core recovery.

The pelagic sediments at Site 871 were sampled at regular intervals, averaging one sample every 1.5 to 4.0 m. These sediments are comprised of approximately 96% calcium carbonate, with the remaining solids consisting of salt (see "Inorganic Geochemistry" section,

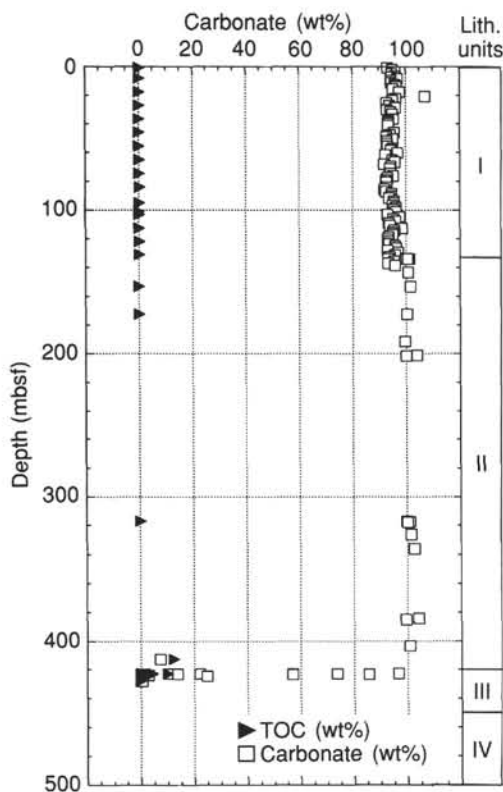


Figure 33. Carbonate content of sediments in Holes 871A and 871C, calculated as calcium carbonate. Also shown are the major lithologic units, as given in the "Lithostratigraphy" section (this chapter).

this chapter). These sediments suffered considerable disturbance from drilling, handling, and splitting operations before the discrete measurements were made.

Within the pelagic cap, values of dry-bulk density range from 0.7 to 1.0 g/cm³, wet-bulk density values are between 1.5 and 1.7 g/cm³, porosity values are between 67% and 81%, and values of water content (% dry wt) range from 70% to 143% (see Table 13 and Fig. 39). Thermal conductivity values in the oozes show moderate scatter but a clear trend with depth (Table 13). Values of conductivity in the pelagic cap lie between 1.0 and 1.5 W/(m · K), with a relative conductivity peak located between 20 and 30 mbsf. This is consistent with the higher density values and lower water contents measured within this interval.

Few discrete measurements of index properties in the platform carbonate sequence from 134 to 420 mbsf were made on account of the poor core recovery, (Table 13 and Fig. 38). In these rocks, porosity values (2%–23%) and water contents (0%–12%) were low, whereas wet and dry bulk density (1.85–2.99 and 1.19–2.97 g/cm³, respectively), and grain density values (2.3–3.0 g/cm³) are higher than in the overlying pelagic cap.

The digital sound velocimeter (DSV) data are scattered; furthermore, because of the high water content and soupy texture of the cores, values are often equal to, or lower than, the velocity of seawater (i.e., 1531 m/s at 24°C; Weast, 1984). A general, but inconclusive, trend toward higher velocity values at increasing sub-bottom depths is present in Unit I (Table 14 and Fig. 40), as the void ratio (volume of voids/volume of solids; a measure of porosity) of the sediment gradually decreases in the foraminifer ooze. The *P*-wave logger (PWL) data was considered to be unreliable at this site because of disturbed intervals in the cores, and because "voids" between the core liner and the sediment being measured served to attenuate the acoustic pulse.

The velocity values measured in Hole 871C on the platform carbonates, clays, and basalts are given in Table 15. These velocities were measured on cubic samples of rock or indurated sediment using the Hamilton Frame device. Problems with ascertaining the orientation of pieces of rock in the core resulted in few determinations of velocity anisotropy.

The Wykeham-Farrance vane apparatus was used to make shear strength measurements in the pelagic ooze. These sediments exhibited very low vane shear strengths, ranging from 0 to 15 kPa (Table 16 and Fig. 39). In light of the sampling disturbance referred to earlier, the vane strength parameters may realistically be described as "re-molded" values. In some instances, insufficient material existed to fill the split core liner, and, hence, the vane could not be inserted to the prescribed depth. No shear strength determinations were made on the carbonates. The frequency of measurements subsequently improved in the clays and basalts near the base of the section because of improved core recovery. A small number of hand-held Torvane measurements were made in the upper part of the clay interval in Unit III, between 423 and 426 mbsf. These sediments had undrained shear strengths of 40 to 240 kPa (Table 16).

Magnetic susceptibility was measured using the Bartington susceptibility loop mounted on the MST. These data are displayed in Figure 41 for Holes 871A and 871B. The susceptibility of the sediment is generally positive in the upper 30 mbsf of each hole and assumes negative values below, to about 140 mbsf at the base of the pelagic cap. These negative values of susceptibility correspond to the high percentage of calcium carbonate in the foraminifer ooze below this level. Higher values of susceptibility below 30 mbsf generally reflect contamination or small rust particles near the top of each core.

Geotechnical Units

The measurements of physical properties were used to define the characteristics of the sediment and rock at Site 871 and to define geotechnical units. Five major geotechnical units are identified; the boundaries of these units, for the most part, correspond to the lithologic unit boundaries described in the "Lithostratigraphy" section (this chapter).

Pelagic Cap

Geotechnical Unit 1 (0 to ~25 mbsf), is characterized by higher density values and lower porosity and water content values than Geotechnical Unit 2 (~25 to 140 mbsf) as seen in Figures 38 and 39. Using the discrete index properties measurements and the GRAPE bulk density profiles (Fig. 42), it is possible to divide this upper geotechnical unit into two subunits. The boundary between Geotechnical Subunits IA and IB is placed at about 25 mbsf, near a sharp change in the trends of index properties. Geotechnical Subunit IB is marked by relatively large changes in properties at both its upper and lower boundaries; these changes seem to correspond to the positions of stratigraphic disconformities and hiatuses in sediment accumulation (see "Biostratigraphy" section, this chapter).

From Samples 144-871A-3H-2, 109 cm, to -3H-4, 43 cm (19.6–22.0 mbsf), there are sharp increases in wet-bulk and dry-bulk density values (1.55–1.67, and 0.81–0.98 g/cm³, respectively); these are accompanied by decreases in water content (% dry wt) and porosity (90%–70% and 72%–67%, respectively). Below ~22 mbsf, these trends are reversed, as wet and dry bulk density values decrease (to 1.40 and 0.58 g/cm³, respectively), whereas both water content and porosity values increase sharply (to 143% and 80%, respectively) downhole to Sample 144-871A-4H-4, 89 cm. Similar changes in the relative trends of GRAPE bulk density are also observed in Holes 871A and 871B (Fig. 41).

Geotechnical Unit 2 (~25 to 140 mbsf) represents the remainder of the pelagic cap, a thick sequence of virtually uniform sediment

Table 10. Results of geochemical analyses, Holes 871A and 871C.

Core, section, interval (cm)	Lithology	Depth (mbsf)	IC (wt%)	CaCO ₃ (wt%)	TC (wt%)	TOC (wt%)	N (wt%)	H (wt%)	S (wt%)	TS/TOC
144-871A-										
1H-1, 68-71	Calcareous ooze	0.68	11.19	93.24	11.39	0.20	0.01	0.09	0	0
1H-2, 68-70	Calcareous ooze	2.08	11.42	95.15						
1H-3, 68-70	Calcareous ooze	3.58	11.53	96.07						
1H-4, 68-70	Calcareous ooze	5.08	11.39	94.90						
1H-5, 68-70	Calcareous ooze	6.58	11.51	95.90						
1H-CC, 10-11	Calcareous ooze	7.18	11.35	94.57						
2H-1, 69-71	Calcareous ooze	8.19	11.63	96.90	11.53	0	0	0.06	0	0
2H-2, 69-71	Calcareous ooze	9.69	11.34	94.48						
2H-3, 69-71	Calcareous ooze	11.19	11.35	94.57						
2H-4, 69-71	Calcareous ooze	12.69	11.52	95.98						
2H-5, 69-71	Calcareous ooze	14.19	11.57	96.40						
2H-6, 69-71	Calcareous ooze	15.69	11.43	95.23						
3H-1, 69-71	Calcareous ooze	17.69	11.71	97.57	11.45	0	0.01	0.04	0	0
3H-3, 69-71	Calcareous ooze	20.69	12.86	107.15						
3H-4, 69-71	Calcareous ooze	22.19	11.55	96.23						
3H-5, 69-71	Calcareous ooze	23.69	11.41	95.07						
3H-6, 69-71	Calcareous ooze	25.19	11.14	92.82						
4H-1, 69-71	Calcareous ooze	27.19	11.27	93.90	11.39	0.12	0	0.09	0	0
4H-2, 69-71	Calcareous ooze	28.69	11.54	96.15						
4H-3, 69-71	Calcareous ooze	30.19	11.16	92.99						
4H-4, 69-71	Calcareous ooze	31.69	11.32	94.32						
4H-5, 69-71	Calcareous ooze	33.19	11.40	94.98						
5H-1, 69-71	Calcareous ooze	36.69	11.45	95.40	11.28	0	0	0.08	0	0
5H-2, 69-71	Calcareous ooze	38.19	11.23	93.57						
5H-3, 69-71	Calcareous ooze	39.69	11.22	93.49						
5H-4, 69-71	Calcareous ooze	41.19	11.21	93.40						
6H-1, 69-71	Calcareous ooze	46.19	11.48	95.65	11.42	0	0.01	0.08	0	0
6H-2, 69-71	Calcareous ooze	47.69	11.30	94.15						
6H-3, 69-71	Calcareous ooze	49.19	11.15	92.90						
6H-4, 69-71	Calcareous ooze	50.69	11.44	95.32						
6H-5, 69-71	Calcareous ooze	52.19	11.16	92.99						
6H-6, 69-71	Calcareous ooze	53.69	11.16	92.99						
7H-1, 70-72	Calcareous ooze	55.70	11.20	93.32	11.30	0.10	0	0.09	0	0
7H-2, 70-72	Calcareous ooze	57.20	11.41	95.07						
7H-3, 70-72	Calcareous ooze	58.70	11.34	94.48						
7H-4, 70-72	Calcareous ooze	60.20	11.63	96.90						
7H-5, 69-71	Calcareous ooze	61.69	11.08	92.32						
8H-1, 69-71	Calcareous ooze	65.19	11.38	94.82	11.40	0.02	0	0.09	0	0
8H-2, 69-71	Calcareous ooze	66.69	11.50	95.82						
8H-3, 69-71	Calcareous ooze	68.19	11.02	91.82						
8H-4, 69-71	Calcareous ooze	69.69	11.33	94.40						
8H-5, 69-71	Calcareous ooze	71.19	11.28	93.98						
9H-1, 71-73	Calcareous ooze	74.71	11.32	94.32	11.46	0.14	0	0.06	0	0
9H-2, 71-73	Calcareous ooze	76.21	11.43	95.23						
9H-3, 70-72	Calcareous ooze	77.70	11.17	93.07						
9H-4, 69-71	Calcareous ooze	79.19	11.10	92.49						
9H-5, 69-71	Calcareous ooze	80.69	11.13	92.74						
10H-1, 70-72	Calcareous ooze	84.20	11.14	92.82	11.45	0.31	0	0.09	0	0
10H-2, 70-72	Calcareous ooze	85.70	11.04	91.99						
10H-3, 70-72	Calcareous ooze	87.20	11.11	92.57						
10H-4, 70-72	Calcareous ooze	88.70	11.37	94.73						
10H-5, 70-72	Calcareous ooze	90.20	11.35	94.57						
10H-6, 70-72	Calcareous ooze	91.70	11.25	93.74						
11H-1, 72-74	Calcareous ooze	93.72	11.46	95.48						
11H-2, 72-74	Calcareous ooze	95.22	11.47	95.57	11.67	0.20	0	0.07	0	0
11H-3, 72-74	Calcareous ooze	96.72	11.40	94.98						
11H-4, 72-74	Calcareous ooze	98.22	11.55	96.23						
11H-5, 72-74	Calcareous ooze	99.72	11.46	95.48						
11H-6, 69-71	Calcareous ooze	101.19	11.55	96.23	11.47	0	0.01	0		
12H-1, 72-74	Calcareous ooze	103.22	11.18	93.15	11.39	0.21	0	0.06	0	0
12H-2, 72-74	Calcareous ooze	104.72	11.72	97.65						
12H-3, 72-74	Calcareous ooze	106.22	11.45	95.40						
12H-4, 72-74	Calcareous ooze	107.72	11.54	96.15						
12H-5, 72-74	Calcareous ooze	109.22	11.23	93.57						
12H-6, 72-74	Calcareous ooze	110.72	11.29	94.07						
13H-1, 69-71	Calcareous ooze	112.69	11.81	98.40	11.22	0	0	0.07	0	0
13H-2, 69-71	Calcareous ooze	114.19	11.48	95.65						
13H-3, 69-71	Calcareous ooze	115.69	11.41	95.07						
13H-4, 69-71	Calcareous ooze	117.19	11.40	94.98						
13H-5, 69-71	Calcareous ooze	118.69	11.22	93.49						
13H-6, 69-71	Calcareous ooze	120.19	11.17	93.07						
14H-1, 69-71	Calcareous ooze	122.19	11.22	93.49	11.49	0.27	0	0.05	0	0
14H-2, 69-71	Calcareous ooze	123.69	11.23	93.57						
14H-3, 69-71	Calcareous ooze	125.19	11.51	95.90						
14H-4, 69-71	Calcareous ooze	126.69	11.55	96.23						
14H-5, 69-71	Calcareous ooze	128.19	11.17	93.07						
14H-6, 69-72	Calcareous ooze	129.69	11.64	96.98						
15H-1, 69-71	Calcareous ooze	131.19	11.51	95.90	11.78	0.27	0	0.07	0	0
15H-2, 69-71	Calcareous ooze	132.69	11.26	93.82						
15H-3, 69-71	Calcareous ooze	134.19	11.19	93.24						
15H-4, 69-71	Calcareous ooze	135.69	11.46	95.48						
15H-5, 69-71	Calcareous ooze	137.19	11.19	93.24						
15H-6, 69-71	Calcareous ooze	138.69	11.51	95.90						

Table 10 (Continued).

Core, section, interval (cm)	Lithology	Depth (mbsf)	IC (wt%)	CaCO ₃ (wt%)	TC (wt%)	TOC (wt%)	N (wt%)	H (wt%)	S (wt%)	TS/TOC
144-871C-										
2R-1, 17-21	Limestone	133.87	11.99	99.90						
2R-1, 46-48	Limestone	134.16	12.14	101.15						
2R-1, 54-59	Limestone	134.24	12.08	100.65						
3R-1, 12-18	Limestone	143.42	12.09	100.73						
4R-1, 48-52	Limestone	153.38	12.20	101.63	12.34	0.14	0		0	0
6R-1, 24-29	Limestone	172.54	12.03	100.21	11.70	0	0		0	0
8R-1, 7-14	Limestone	191.57	11.95	99.50						
9R-1, 5-12	Limestone	201.25	12.48	103.96						
9R-1, 46-53	Limestone	201.66	12.00	99.98						
21R-1, 59-61	Limestone	317.09	11.97	99.91	12.23	0.26	0		0	0
21R-1, 90-96	Limestone	317.40	12.15	101.23						
21R-1, 130-136	Limestone	317.80	12.03	100.23						
22R-1, 19-26	Limestone	326.39	12.19	101.57						
23R-1, 37-45	Limestone	336.17	12.31	102.57						
28R-1, 34-39	Limestone	384.04	12.51	104.23						
28R-1, 123-128	Limestone	384.93	11.94	99.46						
30R-1, 34-39	Limestone	403.44	12.10	100.82						
31R-CC, 44-49	Clay	412.80	0.88	7.33	13.36	12.48	0.09	0.78	3.29	0.26
32R-1, 16-20	Limestone	422.66	11.59	96.57	11.90	0.31	0.01	0.21	0.61	1.97
32R-1, 41-42	Clay	422.91	1.25	10.42	11.46	10.21	0.14	1.50	12.63	1.24
32R-1, 44-49	Clay	422.94	8.83	73.60	13.36	4.53	0.09		3.29	0.73
32R-1, 52-53	Clay	423.02	6.83	56.91	7.70	0.87	0.02	0.55	3.20	3.69
32R-1, 53-54	Clay	423.03	2.66	22.16	4.98	2.32	0.03	0.90	11.54	4.99
32R-1, 58-60	Clay	423.08	1.66	13.83	2.74	1.08	0.01	0.96	7.50	6.98
32R-1, 68-69	Clay	423.18	0.11	0.92	0.68	0.57	0.01	1.37	8.30	14.52
32R-1, 82-83	Clay	423.32	10.24	85.50	10.20	0	0.01	0.27	1.64	0
32R-1, 98-99	Clay	423.48	6.83	56.90	0.46	0	0.01	1.66	0.60	0
32R-1, 125-126	Clay	423.75	0.10	0.83	0.44	0.34	0	1.27	1.48	4.33
32R-1, 143-144	Clay	423.93	0.35	2.90	0.52	0.17	0.01		0.07	0.41
32R-2, 55-57	Clay	424.55	2.99	24.90	1.74	0	0.01	1.22	1.94	0
32R-3, 75-77	Clay	426.25	0.01	0.08	0	0	0	1.67	0	0
32R-4, 94-96	Clay	427.94	0.07	0.58	0.06	0	0	1.60	0.01	0

Notes: All numbers are in weight percent (wt%). IC = inorganic carbon, TC = total carbon, and TOC = total organic carbon.

which exhibits a narrow range of index properties. Below the sharp change in index properties at ~25 mbsf, and continuing to 140 mbsf, values of bulk density gradually increase with depth as porosity and water content trends gradually decrease to the base of the pelagic cap. The GRAPE density data do not show such a clear trend, but it is nevertheless distinguishable. The discrete values of bulk density are slightly lower than the bulk densities measured with the GRAPE, but the trends are consistent. The lower values of the discrete measurements may be a disturbance-related effect caused by splitting the core into two halves. The increase in dry-bulk density over this interval represents a downhole gradient of approximately $0.09 \text{ g/cm}^3/100 \text{ m}$ (Fig. 39).

Velocities measured with the DSV apparatus in the pelagic cap generally range from 1400 to 1600 m/s. A very slight trend of increasing velocity may occur in the pelagic cap with depth; somewhat higher velocities were measured between 90 mbsf and 130 mbsf (Table 14 and Fig. 40).

Shallow-water Limestones

Geotechnical Unit 3 (140–422 mbsf) includes the whole of the carbonate sequence out of necessity, because so few data are available within this interval. Wet-bulk, dry-bulk, and grain densities cluster closely together between 2.5 and 3.0 g/cm^3 . Low porosity values (2%–22%) are typical for this type of limestone. Water contents are very low (0%–10%) but, again, are typical for limestones (Table 13 and Fig. 38).

Velocities are high (3440–5700 m/s) compared with reported values from downhole measurements. These values are not unusual for limestones of this type. Tests on orthogonal faces of the cubes suggested, in some cases, a higher velocity parallel to the core axis, however in many cases, the orientation of limestone core pieces was uncertain.

Clays

Geotechnical Unit 4 (422–450 mbsf) consists of a highly heterogeneous basalt weathering profile made up of dense plastic clays with

partially weathered basalt clasts. A feature of these clays is their very high grain density ($3.0\text{--}3.5 \text{ g/cm}^3$). The clays are probably moderately over-consolidated. Torvane shear strength values range from 40 to 220 kPa with a peak in the profile at 428 mbsf (Table 16).

Basalts

Geotechnical Unit 5 (450–500 mbsf) consists of basalts. These have closely clustered density values in the range 2.9 to 3.0 g/cm^3 . Water contents are between 0% and 5% (Table 13). Velocities are widely scattered between 3100 and 5200 m/s, the lower values being mainly in the more weathered and brecciated rock (Table 15). The scatter is probably the result of voids and discontinuities within the rock and the small size of test specimens relative to these features. Some of the basalts are highly brecciated with a dominant and relatively weak matrix. These are prone to disintegration on exposure to air.

Discussion

The physical properties determinations at Site 871 included a wide assortment of rock and soil types. Core recovery was good in the pelagic cap sediments, poor in the platform carbonates, and moderate in the underlying clay and basalts. Core disturbance was obvious in the pelagic sediments and continued through the coring, handling, and sampling processes. Nevertheless, clear trends in index properties appear to delineate at least one important sedimentological boundary, that is between the late and middle Miocene at approximately 25 mbsf. This probably represents a nondepositional or erosional hiatus.

DOWNHOLE MEASUREMENTS AND SEISMIC STRATIGRAPHY

Log Types, Processing, Reliability, and Resolution

Logs were obtained from the entire carbonate platform succession in Hole 871C with the geophysical, Formation MicroScanner (two passes), and geochemical tool strings. These logs are valuable for interpreting the sedimentary succession and possible discontinuities

Table 11. Results of semiquantitative X-ray diffraction analyses of clay and limestone from Lithologic Subunits IIF and IIIA, Section 144-871C-32R-1.

Depth in section (cm)	Subunit IIF		Subunit IIIA	
	23–28	47–49	77–79	130–135
Lithology	Limestone	Clay	Clay	Clay
Calcite	XXX	X		
Aragonite	XX	XXX	X	
Siderite		X		
Dolomite (ferroan)				X
Pyrite	XXX	XXX	XXX	
Marcasite		XX	XXX	
Illite	X	X	X	X
Vermiculite	X	X	X	
Kaolinite	X	X	X	X
Goethite		X		X

Notes: Only sedimentary minerals are shown. XXX = abundant, XX = moderate, and X = observed.

in accumulation, because core recovery within this 289-m interval (Cores 144-871C-2R through -31R) averaged only 3.5%.

We first attempted to lower the borehole magnetometer into the underlying basalt flows, but this tool string was unable to pass the 30-m clay interval (423–452 mbsf) between the basaltic basement and the carbonate platform succession. To avoid similar problems with tool sticking, the other logging tool runs were halted above this clay zone. Because of the different positions of tools on the various strings, the lower boundary of logging data from each tool varies from approximately 425 mbsf (top of clays) for the gamma spectrometry and resistivity tools, to approximately 410 mbsf for the sonic velocity measurements. The upper limit to all logging runs was the base of the drill string at 118.7 mbsf, located within the overlying pelagic sediments.

The natural gamma tool (NGT) run on each string provided numerous distinct peaks throughout the carbonate platform facies. The location of these natural gamma events are at identical logging depths among the various runs; therefore, it was unnecessary to make any relative depth shifting between logs. However, the measured position of the end of the drill string according to the cable indicator on the logging runs was 2.2 m higher than the total length of the drill pipe below the rig floor during coring operations. Because core depths are recorded relative to the drill string, we lowered all logging depths by 2.2 m to make the logging data consistent with the corresponding cored interval. The resulting steps to convert from logging depths (meters below rig floor) to mbsf (meters below seafloor) are as follows: (1) subtraction of 10.9 m (distance from rig floor to mean sea surface); (2) subtraction of 1254.6 m (depth from sea surface to seafloor according to drilling operations); and (3) addition of 2.2 m to adjust for the offset between logging depths and drilling depths, or a composite conversion factor of 1263.3 m.

The geophysics tool was not continuously run, so the records from the lower part of the hole were spliced to the main run from the upper part of the hole at 244.7 mbsf. No overlap occurred in the data from some tools on this long geophysics string, so some records have a 5–10 m gap just above this splice.

Hole size is the most important control on the accuracy of logs from Hole 871C. Where the hole diameter exceeds 38 cm (15 in.), the FMS pads are no longer in complete contact with the borehole walls and one or more of the four traces may be incoherent. Where the diameter exceeds 46 cm (18 in.), the lithodensity tool has incomplete contact against the borehole wall and the logs of density and photoelectric effect show swings to unreliably low values; the density compensation factor, which attempts to correct for inadequate pad contact, is applying corrections so large that the compensation is only approximate. The natural gamma and resistivity tool measurements are affected by varying borehole diameter, so correction factors will be applied to these logs during post-cruise processing. The irregular borehole diameter caused severe problems for the sonic velocity tool; therefore, despite systematic editing of the measurements, post-cruise

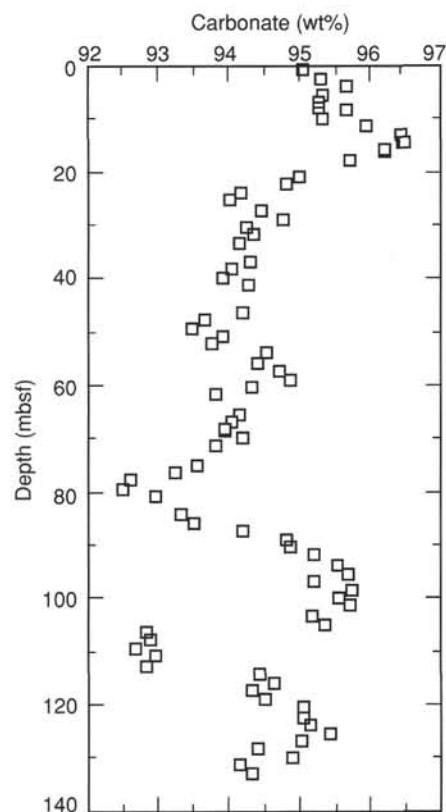


Figure 34. Carbonate content of sediments from the pelagic cap in Hole 871A. Values are calculated as five-point running averages.

total-waveform analysis will be necessary to produce reasonable velocity values. Most of the other logging tools do not require pad contact; therefore, they are rather insensitive to changes in borehole size.

The caliper log of the borehole diameter can be interpreted in terms of the relative degree of consolidation and cementation of the limestone facies. The main extended “washout” interval is from about 250 to 280 mbsf, and it coincides with a packstone facies that developed a chalky texture during late-stage diagenesis. Another severe washout is at 186–192 mbsf in a skeletal grainstone facies; several other wide intervals are also present in the hole.

Vertical resolutions by the various logging tools are generally on the order of 50–60 cm, except for the medium and deep resistivity tools, which have 1.5 and 2 m resolutions, and the FMS, which has a resolution of 0.5–1.0 cm (see “Explanatory Notes” chapter, this volume). Data is collected at 15 cm (0.50-ft) intervals, except for the FMS runs, which have a 2.-mm (0.10 in.) sampling rate.

Resistivity, Density, and Velocity Relationships

Resistivity, density, and sonic velocity are strongly correlated throughout the logged interval at Hole 871C (Fig. 43). The composition of the carbonate platform and overlying foraminifer ooze is nearly pure calcite carbonate; therefore, these geophysical measurements are mainly responding to differences in porosity within the facies, rather than indicating mineralogical changes. Three scales of fluctuations correlate among these logs: (1) short-wavelength peaks at the meter-scale, (2) a general downward trend to higher values, and (3) broad features on the scale of tens of meters.

The various short-wavelength peaks and fluctuations are probably associated with meter-scale variations in porosity and cementation. In carbonates where the relative abundance of lime mud to larger grains is the only variable, there is a progressive increase in density

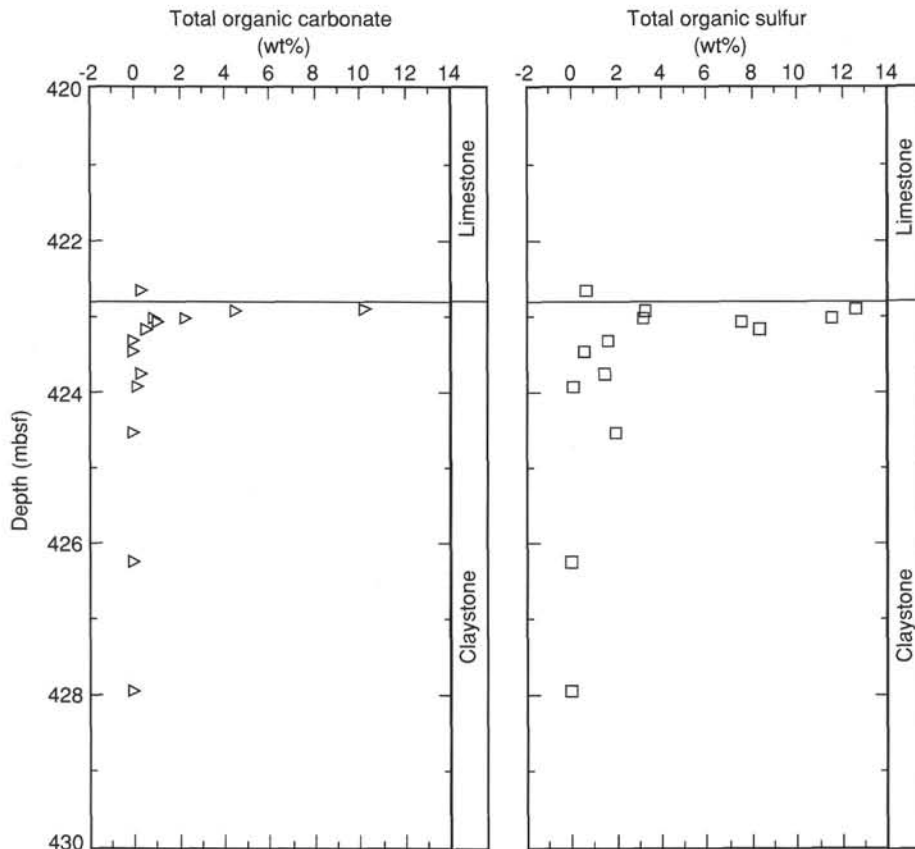


Figure 35. Total organic carbon (TOC) and total sulfur (TS) in sediments at the transition from claystone to limestone in Core 144-871C-32R. Note the marked increase in TOC and TS in the topmost 50 cm below the claystone/limestone boundary.

and resistivity from grainstone facies through packstone and wackestone to mudstone facies (e.g., Asquith, 1979; Dorfman et al., 1990). In those intervals where variations in cementation are present, lower resistivity values commonly also coincide with lower velocity values and larger hole diameters because the weaker, less lithified material has been preferentially removed during the drilling process. The recovered core material suggests that the composition of the limestones also influenced the degree of cementation, with grainstones being less cemented than micritic mudstones. As a result, the corresponding responses of the resistivity and density tools are magnified by these changes in facies.

The shallowest penetrating resistivity tool, the spherical-focused sonde (SFLU log) has the highest resolution but generally lower values than the medium or deep phasor induction resistivity sondes (IMPH and IDPH logs, respectively), which have greater depths of investigation. The differences between the three resistivity log types are attributable to the different responses of the three sondes, accentuated by the irregular hole diameter. The apparent resistivity increase with greater penetration may primarily be an artifact of the relatively large hole diameter, an effect commonly observed in past ODP logging of platform carbonates (e.g., Shipboard Scientific Party, 1991). Therefore, the deepest penetrating devices will provide the most reliable data when the beds are thick, but all values are likely to be degraded in the presence of large borehole diameters and thin beds. We display the medium-penetration resistivity log in Figure 43, which has smoothed some of the higher frequency bed-to-bed variations in resistivity, is more directly comparable to the density log in resolution, and is probably a more accurate representation of major resistivity fluctuations independent of hole diameter. The FMS provides the highest resolution mapping (about 5 mm) of the resistivity variations of the

borehole wall; thus, it indicates that many of these short-wavelength features have internal complexity, such as groupings of thin beds or irregular patterns of cementation. However, the FMS record is incomplete in several intervals as a result of the enlarged borehole diameters.

Some of the high-density, high-resistivity peaks also correlate with peaks in natural gamma intensity (Fig. 43); for example, the phosphatic hardground at the top of the carbonate platform at 138 mbsf. Strong natural gamma intensities were observed from more cemented beds in the carbonate platform of the Great Barrier Reef region, where uranium mimicked the porosity pattern of the density and resistivity logs (e.g., Shipboard Scientific Party, 1991). However, these correlations were the exceptions rather than the rule in Hole 871C. Indeed, some of the strongest natural gamma peaks, which are mainly caused by uranium enrichment, do not appear to have any corresponding features displayed in resistivity or density logs. We suspect that some of these uranium enrichments are associated with unconformities or condensed sedimentary intervals. In such circumstances, exposure-related dissolution or leaching of aragonitic bioclasts within the limestone beds may have partially canceled porosity changes resulting from grain-to-grain cementation, therefore, a condensed limestone interval will not necessarily have a net increase in bulk resistivity and density.

In addition to these high-frequency, meter-scale fluctuations, a general downhole increase in average resistivity, density, and velocity is present (Fig. 44). This trend may be partially caused by the effects of greater compaction and diagenetic cementation with depth. Superimposed on this average trend are broad (tens of meters) variations in the average resistivity and, to a lesser degree, in the density. The corresponding core recovery suggests that these multimeter-scale variations are caused by changes in facies type and by diagenesis. For example, an interval of relatively low resistivity from 250 to 295 mbsf

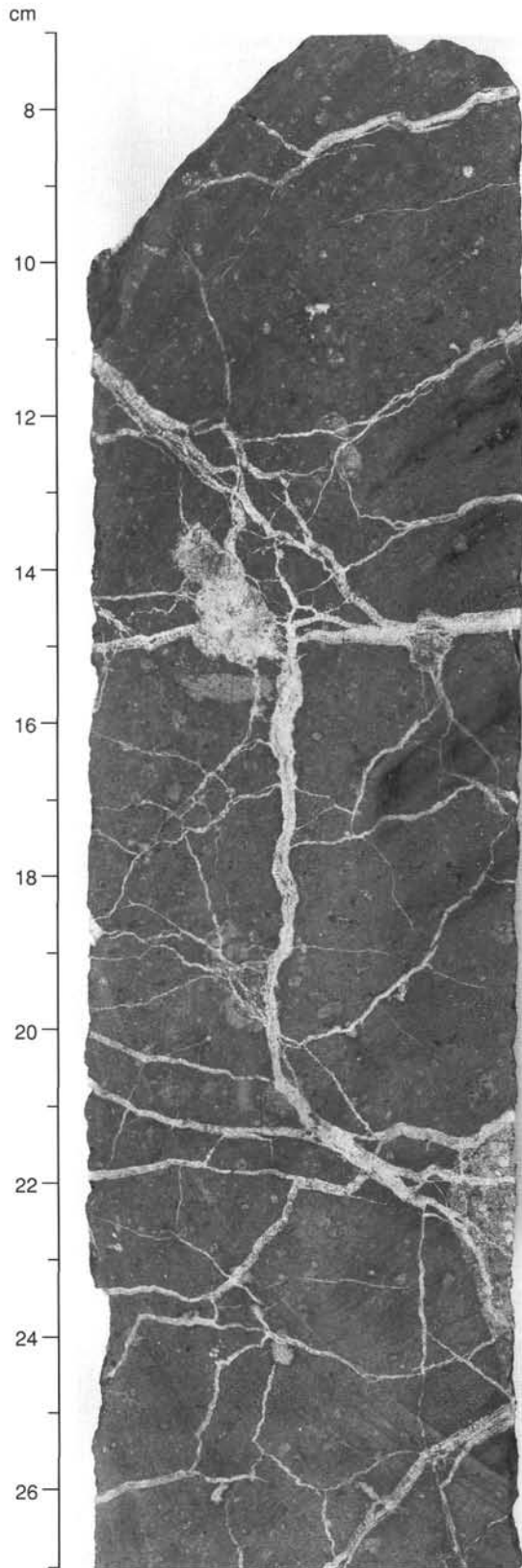


Figure 36. Interval 144-871C-35R-1, 7-27 cm, part of Igneous Unit 1. Note the extensive calcite veining and the numerous small xenoliths. Three larger xenoliths are present between 13 and 15 cm, and a larger one occurs at the edge of the core between 21 and 25 cm.

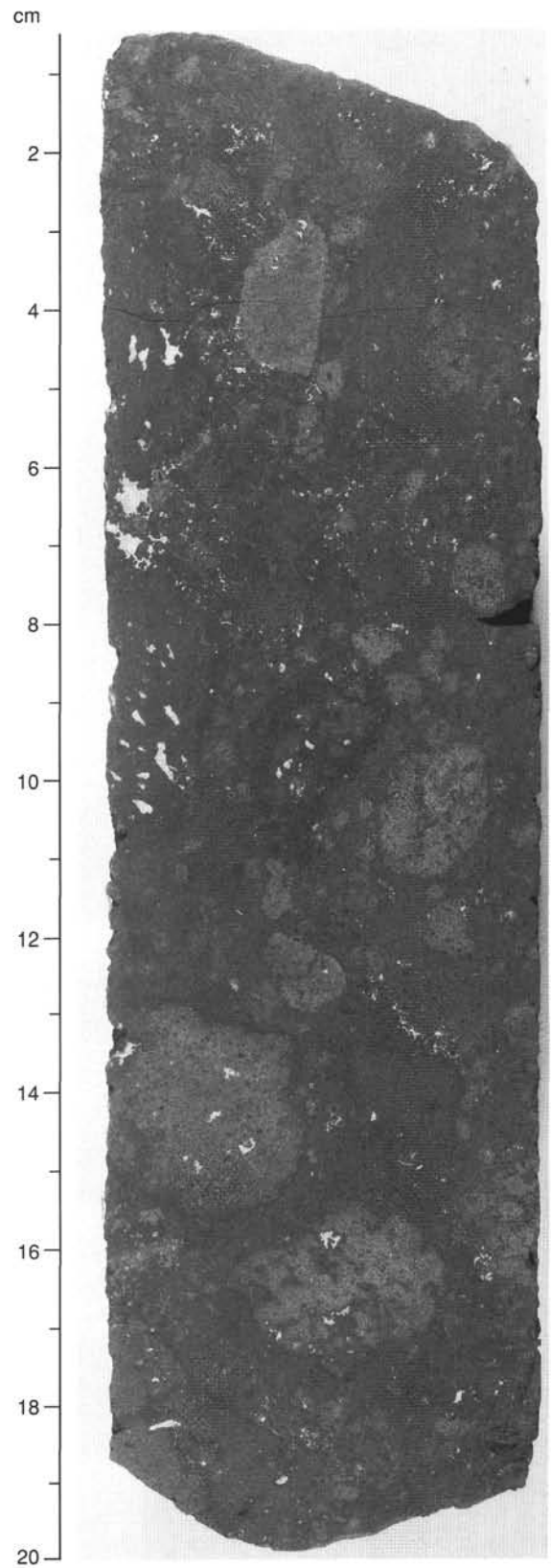


Figure 37. Interval 144-871C-35R-3, 0-20 cm, part of the basalt breccia of Igneous Unit 6. Note the generally rounded clasts and the indistinct (owing to alteration) outlines of some clasts such as the one between 15.5 and 17.5 cm.

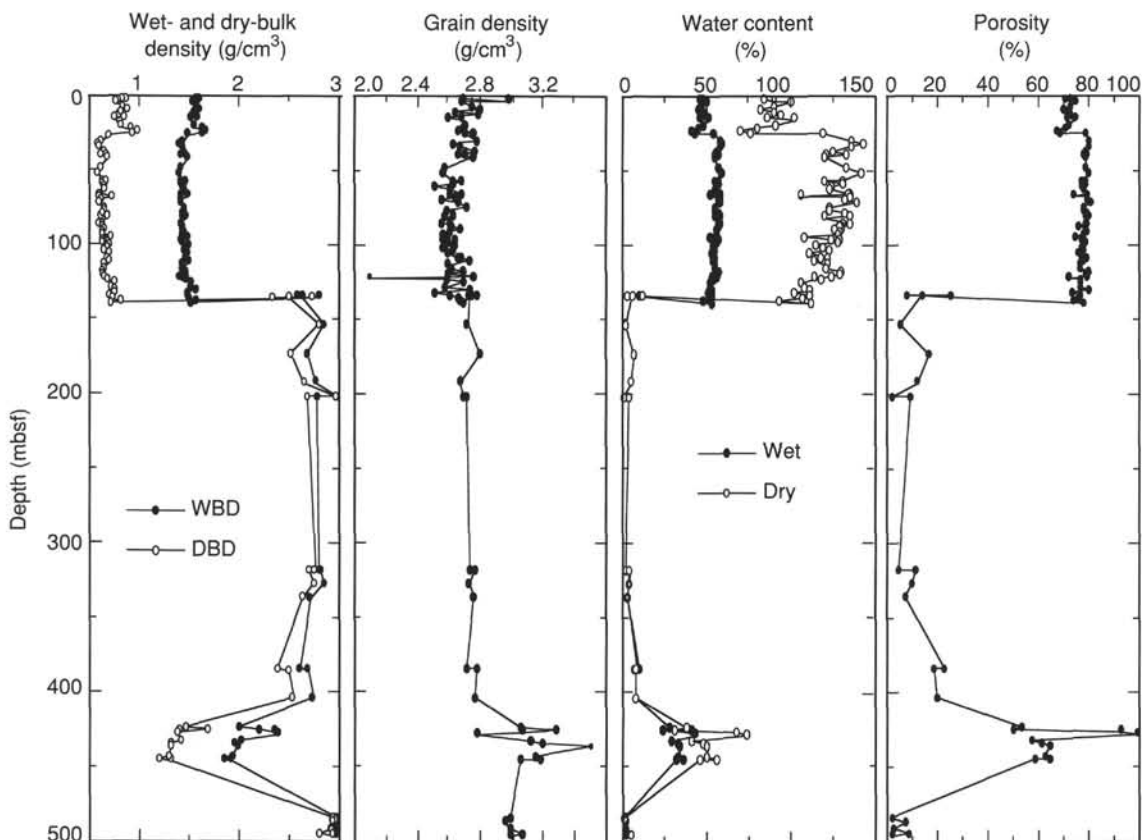


Figure 38. Measurements of index properties (wet- and dry-bulk density, grain density, water content, and porosity) vs. depth, Site 871.

corresponds to a limestone that underwent chalkification to form a low-density porous rock. The lowest 35 m of the logging runs (385–420 mbsf) is characterized by high resistivity with frequent peaks, which corresponds to a rhodolith grainstone in which encrusting red algae have created a denser rock fabric.

Sonic Traveltime Computations

An attempt was made to recover the seismic velocity profile of the platform limestones (420–138 mbsf) from the sonic log by picking the fastest of the four traveltimes from each sonic log measurement and removing unreasonably large traveltime spikes. The remaining traveltimes were summed (integrated) to obtain two-way traveltime (TWT) as a function of depth in the hole (mbsf) (Fig. 45). This curve was calibrated to the well-established top of the carbonate platform at 138 mbsf and 1.85 s TWT. This traveltime-depth plot can be checked by comparing it to some event that can be confidently correlated at a deeper level on the seismic reflection profile (see “Seismic Stratigraphy Interpretation” section, below). Our most confident (and deepest) reflection is the top of basaltic basement at 2.09 s TWT. This corresponds to a depth on the traveltime-depth plot of 365 mbsf, although the top of the solid basalts actually occurs at 450 mbsf in the cored section. This appears to be unreasonably shallow, so we conclude that the traveltime-depth plot is not a good estimate of the situation. Washed-out hole conditions throughout the logged section allowed large traveltimes to be averaged into the total profile, yielding an average logged velocity of 1.9 km/s from 1.85 to 2.09 s TWT.

Log-facies Comparisons

Lithologic units and subunits defined on the basis of the limited core recovery are generally recognized in the composite logs. How-

ever, these logs indicate that the boundaries between facies are often demarcated by natural gamma intensity peaks induced by uranium concentrations, and that the lithologic units display considerable internal lithologic variation. The logging signatures of the different lithologic units can be used to set more precise boundaries between these facies (Table 17). The combined FMS resistivity maps of the borehole, coupled with the natural gamma and medium-penetration resistivity signals, provide details of sedimentary structures on the meter to centimeter level. Some of the major features within the carbonate platform succession are summarized in terms of the ship-board-defined lithologic units.

Lithologic Unit I

Nature: foraminifer ooze
Age: Pleistocene to early Miocene

The pelagic cap on the carbonate platform consists of white, homogeneous foraminifer ooze. Only the lowermost 15 m of this facies were logged, and, as expected, this noncemented unit is characterized by very low bulk density (averaging approximately 1.4 g/cm³), very low resistivity (averaging approximately 0.7 Ωm), and negligible natural gamma intensity (approximately 1 to 3 API units). Minor fluctuations in the geochemical logs of radiogenic and stable elements (Figs. 46 and 47) are near the noise levels. The FMS imagery supports the lack of significant sedimentary structure in this winnowed foraminifer sand facies.

Lithologic Unit II

The 289-m-thick carbonate platform that comprises Lithologic Unit II is divided into six distinct facies or subunits. The characteristics and internal features of each of these facies on downhole logs are discussed separately.

Table 12. Summary of igneous units, Hole 871C.

Unit	Section/interval number	Description
1	Interval 144-871C-35R-1, 6–58 cm	Xenolith-bearing clinopyroxene phyric basalt, possible dike
2	Interval 144-871C-35R-1, 58–83 cm	Altered basalt fragments
3	Interval 144-871C-35R-1, 83–132 cm	Volcaniclastic pebble conglomerate
4	Sections 144-871C-35R-1, 132 cm, to -35R-2, 46 cm	Coarse, angular basalt breccia
5	Interval 144-871C-35R-2, 46–163 cm	Angular basalt breccia
6	Interval 144-871C-35R-3, 0–124 cm	Subrounded basalt breccia
7	Sections 144-871C-35R-3, 124 cm, to -35R-5, 28 cm	Very coarse basalt breccia
8	Interval 144-871C-36R-1, 1–22 cm	Altered basalt fragment
9	Sections 144-871C-36R-1, 22 cm, to -36R-2, 49 cm	Olivine phyric basalt
10	Interval 144-871C-36R-2, 50–60 cm	Altered basalt fragment
11	Interval 144-871C-36R-2, 61–70 cm	Red altered basalt fragment
12	Interval 144-871C-36R-2, 71–81 cm	Volcaniclastic sandstone
13	Sections 144-871C-36R-2, 82 cm, to -36R-3, 51 cm	Sparsely olivine phyric basalt
14	Sections 144-871C-36R-3, 51 cm, to -37R-1, 20 cm	Altered olivine phyric basalt
15	Sections 144-871C-37R-1, 20 cm, to -37R-2, 24 cm	Olivine clinopyroxene phyric basalt
16	Sections 144-871C-37R-2, 24 cm, to -36R-1, 18 cm	Altered clinopyroxene phyric basalt
17	Sections 144-871C-38R-1, 18 cm, to -38R-4, 17 cm	Clinopyroxene phyric basalt
18	Sections 144-871C-38R-4, 11 cm, to -38R-5, 30 cm	Altered clinopyroxene phyric basalt
19	Sections 144-871C-38R-5, 30 cm, to -38R-6, 135 cm	Sparsely clinopyroxene phyric basalt
20	Section 144-871C-38R-CC	Olivine phyric basalt
21	Sections 144-871C-39R-1, 0 cm, to -39R-5, 149 cm	Clinopyroxene olivine phyric basalt
22	Sections 144-871C-39R-6, 0 cm, to -40R-4, 110 cm	Clinopyroxene phyric basalt
23	Interval 144-871C-41B-1, 0–42 cm	Olivine clinopyroxene microphyric basalt

Lithologic Subunit IIA

Nature: benthic foraminifer packstone and wackestone
 Intervals: Sections 144-871-2R-1 to -4R-4, 33 cm
 Recovery depth: 133.7–153.2 mbsf
 Age: middle Eocene

The top of Unit II is marked by a black, laminated, iron-manganese oxide, and phosphatic crust. This surface and the indurated hard-ground limestone immediately below are recognized by distinct peaks in natural gamma intensity (approximately 45 API units, mainly induced by uranium with a possible thorium contribution, no potassium; see Fig. 46), density (peaking at 2.3 g/cm³), and resistivity (2.5 Ωm) at approximately 138 mbsf. The Fe enrichment in this layer is too small to register in the iron geochemical log (Fig. 47). In the FMS imagery, the top of this hardground is placed at 138 mbsf; it consists of 1 m of high-resistivity limestone overlying a relatively lower resistivity zone with internal 10-cm-scale mottling by higher resistivity material (Fig. 48A). This mottled zone probably corresponds to the burrow-mottled limestone recovered in the corresponding cored interval (lower portion of Core 144-871C-2R).

The underlying packstone to wackestone exhibits relatively low density and resistivity values compared to the underlying Subunit IIB. It does not display coherent bedding in the FMS imagery, but it does appear to have mottles of slightly more cemented material.

Lithologic Subunit IIB

Nature: skeletal grainstone
 Interval: Sections 144-871-4R-1, 33 cm, through Core 144-871-6R
 Recovery depth: 153.2–182.5 mbsf
 Age: middle Eocene

The top of this subunit corresponds closely with a peak in natural gamma intensity at approximately 152 mbsf (Fig. 43). This peak is larger (65 vs. 45 API units) than the peak associated with the hard-ground at the top of the carbonate platform. This uranium enrichment event is not associated with a significant change in either resistivity or bulk density, and is expressed as a non-unique, 1-m-thick interval of relatively low resistivity in the FMS imagery. This low-resistivity interval may correspond to the very coarse, miliolid-intraclast sand with keystone vugs in the uppermost portion of Subunit IIB, which represents a possible intertidal setting (see “Lithostratigraphy” section, this chapter). A manganese-coated pebble recovered at the top of Core 144-871C-4R, if not displaced downhole, suggests that the uranium-enrichment peak may correspond to a hardground, similar to the one noted at 138 mbsf.

The upper half of this lithologic subunit is characterized by high resistivity and bulk density relative to the overlying Subunit IIA and to the underlying half of this subunit. This signature suggests that the upper portion of this grainstone is comparably better cemented, especially with respect to the packstone-wackestone facies of Subunit IIA. The FMS imagery indicates meter-scale alternations of higher and lower resistivity, but no bedding structures within this subunit. All intervals have a centimeter-scale mottled appearance in the FMS images.

Another uranium-enrichment natural gamma peak that occurs at about 168 mbsf in the middle of Subunit IIB corresponds to a low-density excursion (Fig. 46). The FMS imagery indicates 20-cm-thick patches of very high-resistivity material within a low-resistivity matrix; these features may indicate localized cementation.

The FMS imagery of the basal 4 m (179–183 mbsf) of this subunit indicates four 10-cm-thick, horizontal, high-resistivity layers.

Lithologic Subunit IIC

Nature: foraminifer packstone and wackestone
 Interval: Core 144-871C-6R to Section 144-871C-21R-1, 16 cm
 Recovered depth: 181.9–316.7 mbsf
 Age: middle to early Eocene

This subunit has moderate resistivity (averaging 1–2 Ωm) and bulk density values (averaging about 2.0–2.1 g/cm³). Considerable fluctuations occur in the physical properties above approximately 243 mbsf, but relatively constant values are found below this depth, except for the basal 20 m of this subunit. The FMS images of the upper logging facies display either intervals of relative homogeneity or indications of meter-scale intervals containing centimeter-scale mottling. The recovered interval of Core 144-871C-9R included fragments of dense micritic mudstone, but no definite indication of this is present in the FMS imagery of these beds. There is a minor natural gamma intensity peak at 209 mbsf, which appears to correlate with a peak in resistivity; the FMS imagery indicates a 1.8-m-thick interval (208.2–210.0 mbsf) of relatively high resistivity containing centimeter-scale lenticular mottling. Within this upper facies, the thorium log, which is generally near noise levels throughout the carbonate platform succession, displays a low, broad, 60-m-thick zone of gradual increases in concentration and then decreases, but without distinct peaks (Fig. 46).

A sharp peak in natural gamma intensity at 243 mbsf (corresponding to the middle of Core 144-871C-13R) coincides with the change from the upper logging facies characterized by variable physical parameters to the lower homogenous facies (Fig. 43). This uranium-concentration event seems to coincide with a possible hiatus between

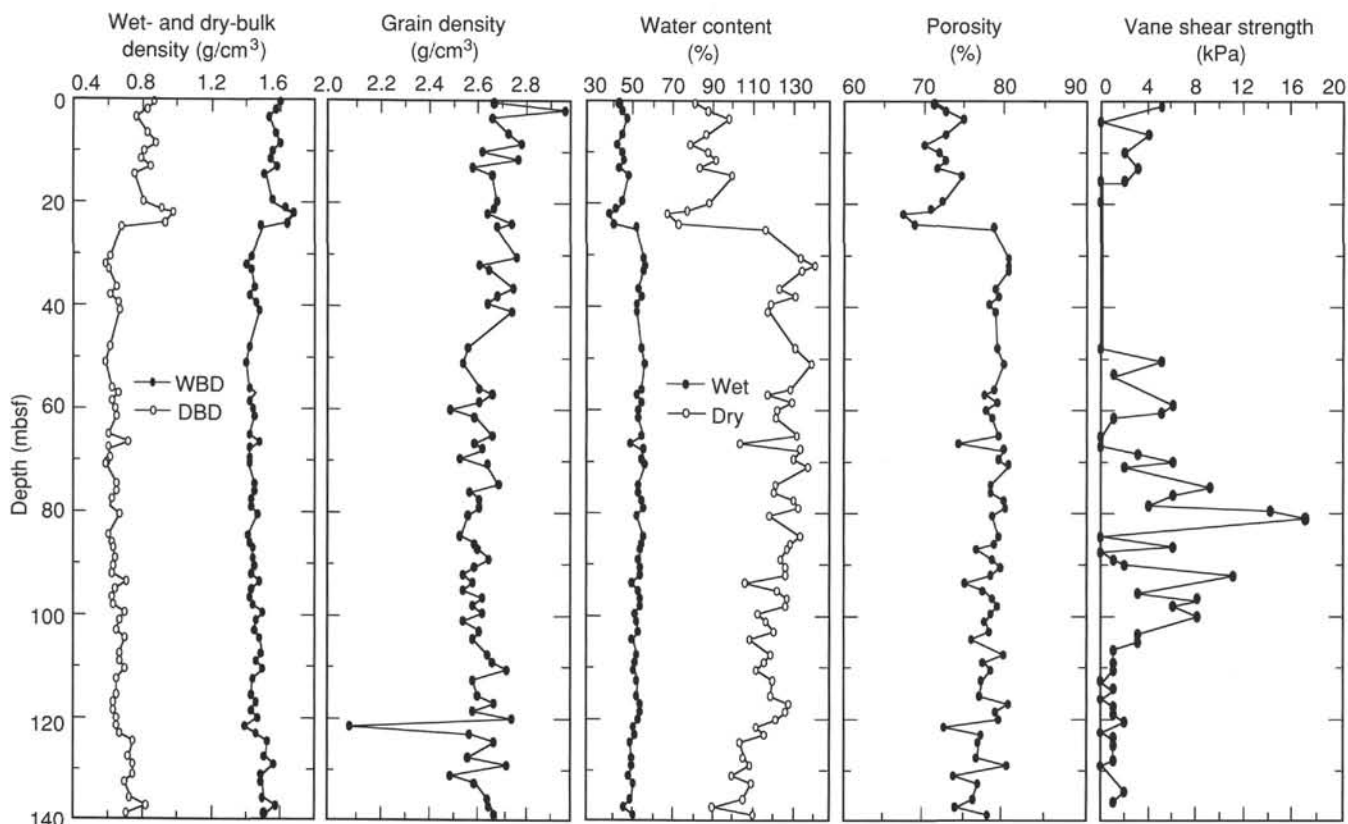


Figure 39. Measurements of index properties and vane shear strength vs. depth, Hole 871A.

the early and middle Eocene. The FMS imagery across this level displays a 40-cm-thick, high-resistivity band centered at about 243.5 mbsf, which overlies relatively low-resistivity material. Unfortunately, the widened hole diameter below 247 mbsf renders the next 30 m unreliable; it appears, nonetheless, that this underlying facies has fairly uniform low resistivity. This 30-m zone (~247 to 277 mbsf) corresponds to a "chalky" interval with moldic porosity.

In the lowermost 20 m of this lithologic subunit, the FMS imagery reveals numerous, 5- to 10-cm-wide lenses or blocks of very high-resistivity material. Some of these may correspond to coral bioclasts (as was recovered in Core 144-871C-20R). Some centimeter- to meter-scale regions or "voids" with very low resistivity are also present.

Lithologic Subunit IID

Nature: foraminifer packstone, coral rudstone, and algal-coral grainstone
Interval: Section 144-871C-21R-1, 16 cm, through Core 144-871-26R
Recovered depth: 316.7–374.3 mbsf
Age: late Paleocene

The upper 10 m of this subunit are characterized by two adjacent large maxima in natural gamma intensity caused by uranium concentrations and by a similar double peak in resistivity (Fig. 43). The upper peak in the FMS imagery is a 3-m-thick zone of increased resistivity, containing at least ten 10-cm-thick beds of very high resistivity, with a sharp upper limit at 319.0 mbsf. The lower resistivity peak extends from about 324 to 328 mbsf and has similar thin bedding. These two peaks are separated by a poorly resolved 2-m-thick interval of relatively low resistivity. Corresponding recovery in Core 144-871C-21R consists of foraminifer grainstone and coral-shell rudstone. It appears that the top of the uppermost peak in uranium and resistivity at 319.0 mbsf coincides with the boundary between the late Paleocene and early Eocene age sediments (= Subunit IIC/IID boundary).

A similar interval of elevated uranium concentration and high-resistivity peaks occurs between 341 and 350 mbsf (Fig. 43). The FMS imagery of this interval indicates a more diffuse zone of moderate relative resistivity containing 10-cm-scale patches of very high resistivity, and lacking the thin bedding that characterized the higher interval of uranium enrichment. These blocks may be either compact coralline fragments or pockets of cementation.

Between and below these peaks in natural gamma intensity, the facies have a higher average resistivity (approximately 2–3 Ωm) and bulk density (approximately 2.1–2.2 g/cm^3) than in the overlying lithologic subunits. The FMS imagery indicates a 1- to 10-cm scale of mottling by higher resistivity.

Lithologic Subunit IIE

Nature: rhodolith-rich grainstone
Interval: Core 144-871C-27R to Section 144-871C-31R-1, 21 cm
Recovered depth: 374.3–413.0 mbsf
Age: late Paleocene

This subunit is characterized by high-amplitude fluctuations in resistivity and in natural gamma intensity with wavelengths on the order of 5 m (Fig. 43). The uppermost peak in natural gamma intensity at 374 mbsf appears to correspond to the top of this algal-rich subunit. Uranium is often enriched in limestones precipitated in depositional environments where organic matter or phosphate was originally present (Serra, 1985). Therefore, uranium can display higher relative concentrations in algal carbonate mats because their reducing microenvironments are conducive to redox scavenging of uranium from seawater. Although this uranium concentration process is usually associated with blue-green algal mats, it may also be applicable to red algal encrustations and concretions (rhodoliths). Another process that may contribute to peaks in uranium enrichment is condensed sedi-

Table 13. Index properties and thermal conductivity data, Holes 871A and 871C.

Core, section, interval (cm)	Depth (mbsf)	Wet-bulk density (g/cm ³)	Dry-bulk density (g/cm ³)	Grain density (g/cm ³)	Porosity (%)	Water content (% dry wt)	Thermal conductivity (W/[m · K])
144-871A-							
1H-1, 48-49	0.48	1.60	0.87	2.69	71.10	83.60	
1H-2, 45-46	1.85	1.57	0.83	2.98	72.70	90.10	1.87
1H-3, 48-49	3.38	1.53	0.76	2.68	74.80	100.50	1.45
1H-5, 48-49	6.38	1.57	0.83	2.75	72.50	89.60	1.15
2H-1, 89-90	8.39	1.60	0.88	2.80	70.00	81.50	
2H-2, 89-90	9.89	1.55	0.81	2.64	71.70	90.20	1.37
2H-3, 89-90	11.39	1.54	0.79	2.79	72.70	93.90	1.48
2H-4, 92-93	12.92	1.58	0.85	2.60	71.50	86.00	
2H-5, 89-90	14.39	1.51	0.75	2.68	74.70	102.50	1.23
3H-2, 109-110	19.59	1.55	0.81	2.70	72.20	90.80	1.50
3H-3, 109-110	21.09	1.63	0.91	2.69	70.70	79.70	1.59
3H-4, 43-44	21.93	1.67	0.98	2.66	67.40	70.10	
3H-5, 69-70	23.69	1.64	0.93	2.76	68.80	75.70	1.35
3H-6, 14-15	24.64	1.49	0.68	2.70	78.70	118.70	1.11
4H-3, 89-90	30.39	1.43	0.61	2.78	80.40	136.00	1.22
4H-4, 89-90	31.89	1.40	0.58	2.63	80.40	143.00	
4H-5, 59-60	33.09	1.43	0.60	2.67	80.40	136.50	1.16
5H-1, 59-60	36.59	1.45	0.65	2.77	78.90	125.30	1.50
5H-2, 59-60	38.09	1.42	0.61	2.70	79.30	133.60	
5H-3, 59-60	39.59	1.46	0.66	2.66	78.00	121.30	1.23
5H-4, 59-60	41.09	1.48	0.67	2.76	78.90	120.20	1.02
6H-2, 79-80	47.79	1.42	0.61	2.58	79.10	133.40	1.06
6H-4, 79-80	50.79	1.40	0.58	2.56	79.90	141.80	1.13
7H-1, 114-115	56.14	1.42	0.62	2.63	78.70	130.80	
7H-2, 57-58	57.07	1.46	0.66	2.68	77.50	119.70	1.26
7H-3, 57-58	58.57	1.42	0.62	2.63	79.00	131.60	1.25
7H-4, 57-58	60.07	1.44	0.64	2.51	77.70	124.50	0.97
7H-5, 57-58	61.57	1.45	0.65	2.61	78.40	123.50	1.09
8H-1, 31-32	64.81	1.42	0.60	2.68	79.30	134.70	
8H-2, 36-37	66.36	1.48	0.72	2.61	74.20	106.00	1.23
8H-3, 26-27	67.76	1.42	0.60	2.64	79.80	135.70	1.16
8H-4, 32-33	69.32	1.42	0.61	2.55	79.20	132.70	1.09
8H-5, 30-31	70.80	1.42	0.59	2.66	80.50	139.50	1.02
9H-1, 70-71	74.70	1.45	0.65	2.71	78.30	123.40	1.24
9H-2, 70-71	76.20	1.45	0.65	2.59	78.30	122.90	1.33
9H-3, 66-67	77.66	1.43	0.62	2.63	79.80	132.50	1.05
9H-4, 65-66	79.15	1.43	0.61	2.63	80.00	135.20	1.03
9H-5, 69-70	80.69	1.47	0.67	2.58	78.50	120.50	
10H-1, 110-111	84.60	1.41	0.60	2.55	79.20	135.60	1.57
10H-2, 90-91	85.90	1.42	0.62	2.61	78.70	130.80	1.15
10H-3, 80-81	87.30	1.44	0.63	2.62	76.40	129.10	1.18
10H-4, 110-111	89.10	1.44	0.64	2.67	78.50	126.20	1.04
10H-5, 110-111	90.60	1.45	0.63	2.61	79.40	128.90	
10H-6, 101-102	92.01	1.43	0.62	2.56	78.30	128.30	
11H-1, 78-79	93.78	1.48	0.71	2.60	75.00	108.50	0.79
11H-2, 78-79	95.28	1.43	0.64	2.56	77.30	124.40	0.82
11H-3, 78-79	96.78	1.42	0.62	2.64	78.40	129.60	1.19
11H-4, 78-79	98.28	1.44	0.63	2.60	79.10	128.40	1.07
11H-5, 78-79	99.78	1.50	0.70	2.64	78.30	114.90	
11H-6, 78-79	101.30	1.46	0.67	2.56	77.50	118.80	
12H-1, 70-71	103.20	1.45	0.65	2.63	78.00	122.80	
12H-2, 70-71	104.70	1.48	0.70	2.60	75.80	110.80	1.25
12H-4, 70-71	107.70	1.49	0.67	2.66	79.80	121.70	
12H-5, 70-71	109.20	1.46	0.67	2.68	77.30	117.90	1.19
12H-6, 70-71	110.70	1.50	0.70	2.74	78.30	114.40	1.03
13H-1, 80-81	112.80	1.44	0.65	2.60	77.10	122.20	
13H-3, 80-81	115.80	1.43	0.65	2.62	76.80	121.60	1.19
13H-4, 80-81	117.30	1.46	0.63	2.69	80.40	130.20	1.10
13H-5, 80-81	118.80	1.43	0.63	2.60	78.80	129.00	1.06
13H-6, 80-81	120.30	1.47	0.65	2.76	79.30	124.20	
14H-1, 28-29	121.80	1.39	0.65	2.09	72.40	114.30	
14H-2, 28-29	123.30	1.46	0.67	2.59	77.00	118.40	1.74
14H-3, 28-29	124.80	1.52	0.74	2.69	76.70	106.40	1.35
14H-5, 28-29	127.80	1.51	0.72	2.58	76.50	108.10	1.15
14H-6, 28-29	129.30	1.56	0.74	2.74	80.20	111.00	1.18
15H-1, 90-91	131.40	1.49	0.74	2.51	73.60	102.00	
15H-2, 90-91	132.90	1.49	0.70	2.61	76.60	111.40	0.47
15H-4, 90-91	135.90	1.50	0.73	2.66	76.00	107.40	
15H-5, 90-91	137.40	1.57	0.82	2.67	73.90	92.80	
15H-6, 90-91	138.90	1.51	0.71	2.69	77.90	112.20	1.12

mentation and/or enhanced cementation. The FMS imagery indicates that the resistivity peaks correspond to 1-m-thick intervals of higher average resistivity, spaced at 2-4 m intervals (Fig. 48B); imagery was not obtained from the uppermost peaks. These high-resistivity intervals contain discontinuous horizontal banding and centimeter-scale mottling. Some of these centimeter-scale mottles probably represent algal rhodoliths. Thorium content increases above background levels in the lower half of Subunit IIE (Fig. 46), which indicates a minor contribution from clay.

Lithologic Subunit IIF

Nature: dark gray and skeletal packstone
Interval: Sections 144-871C-31R-1, 21 cm, to -32R-1, 40 cm
Recovered depth: 413.0-422.9 mbsf
Age: early late Paleocene

Below approximately 418 mbsf in the geochemical log, iron and aluminum concentrations increase (Fig. 47). Lithologic Subunit IIF

Table 13 (Continued).

Core, section, interval (cm)	Depth (mbsf)	Wet-bulk density (g/cm ³)	Dry-bulk density (g/cm ³)	Grain density (g/cm ³)	Porosity (%)	Water content (% dry wt)	Thermal conductivity (W/m · K)
144-871C-							
2R-1, 17-19	133.90	2.81	2.73	2.75	7.90	3.00	
2R-1, 38-40	134.10	2.59	2.33	2.78	25.50	11.20	
2R-1, 54-56	134.20	2.63	2.50	2.73	13.50	5.50	
4R-1, 48-50	153.40	2.85	2.80	2.72	5.10	1.90	
6R-1, 24-26	172.50	2.68	2.51	2.80	16.60	6.70	
8R-1, 7-9	191.60	2.77	2.65	2.67	11.60	4.50	
9R-1, 5-7	201.30	2.99	2.97	2.69	2.10	0.70	
9R-1, 46-48	201.70	2.78	2.68	2.71	9.30	3.50	
21R-1, 90-92	317.40	2.80	2.76	2.74	4.30	1.60	
21R-1, 130-132	317.80	2.82	2.70	2.77	10.90	4.10	
22R-1, 19-21	326.40	2.85	2.75	2.73	9.60	3.60	
23R-1, 37-39	336.20	2.71	2.63	2.76	7.30	2.90	
28R-1, 34-36	384.00	2.61	2.38	2.71	22.60	9.70	
28R-1, 123-125	384.90	2.69	2.50	2.78	18.60	7.60	
30R-1, 39-41	403.50	2.74	2.54	2.77	19.90	8.00	
32R-1, 59-61	423.10	2.00	1.46	3.06	53.30	37.50	
32R-2, 56-58	424.60	2.20	1.68	3.28	50.10	30.50	
32R-3, 76-78	426.30	1.97	1.41	3.06	55.03	40.01	
32R-4, 95-97	428.00	1.95	1.39	2.77	53.96	39.67	
33R-1, 43-45	432.60	2.01	1.42	3.12	57.20	41.20	
33R-2, 78-80	434.50	1.95	1.32	3.20	61.30	47.60	
33R-3, 35-37	435.60	1.98	1.31	3.51	64.50	50.30	
34R-1, 78-80	442.60	1.93	1.29	3.15	62.50	49.80	
34R-2, 122-124	444.50	1.85	1.19	3.19	64.50	55.70	
34R-3, 91-93	445.70	1.92	1.32	3.06	58.70	45.50	
39R-4, 11-13	484.60	2.97	2.94	2.99	1.82	0.90	
39R-5, 113-115	487.10	2.99	2.95	2.96	7.33	1.41	
40R-1, 141-143	491.10	2.97	2.93	2.99	2.12	1.34	
40R-4, 62-64	494.80	2.93	2.81	3.07	8.62	4.50	
41R-1, 6-8	496.00	2.98	2.93	2.99	1.81	1.57	

is a skeletal packstone, colored dark gray by pyrite. This downward increase in iron content probably marks the transition from the algal-dominated grainstone above, to this skeletal packstone below. The FMS imagery indicates that this facies is bedded at the 10–30 cm scale, with bedding contacts dipping at 2°–3° toward the southwest. There is a sharp lower contact to a very low-resistivity facies at 424.3 mbsf, which may mark the top of the clay facies of Lithologic Unit III; however, this is near the lower limit of reliable FMS imagery. If these interpretations are valid, then this dark gray skeletal packstone facies at the base of the carbonate platform succession is 6 m thick and extends approximately from 418 to 424 mbsf.

Seismic Stratigraphy Interpretation

An excellent single-channel seismic profile was obtained on two crossings of Hole 871C using a 200 in.³ water gun as a sound source. These data were recorded on a Masscomp computer, refiltered and displayed (Fig. 49). Comparison with the coring results suggest that several internal reflectors can be correlated to the recovered lithologic section and downhole measurements.

First, and most easily identified, is the base of the foraminifer ooze (pelagic cap; Lithologic Unit I) at 138 mbsf from the logging section, and 1.85 s TWT on the seismic record. This reflector is easily substantiated by the 3.5-kHz record, which also shows a pronounced “hard-ground” reflector at the same two-way traveltime. Below this distinct horizon are two or three flat-lying horizons between 1.85 and 1.93 s TWT that probably are images of additional, underlying nondepositional surfaces suggested by several distinct anomalies in the natural gamma intensity (mostly uranium) that occur between 150 and 210 mbsf and that span the entire middle Eocene portion of the sequence. Although the general correlation of several reflectors to several gamma ray intensity anomalies seems reasonable we do not choose to speculate on the specific correlations among events of the two records.

A faint reflector at 2.01 s TWT may correlate with the upper Paleocene/lower Eocene boundary at about 320 mbsf. It is also possible that this reflector correlated to another unrecovered unconformity within the coralline rudstone (Lithologic Subunit IID) sug-

gested by a large natural gamma-ray (mainly uranium) anomaly at about 345 mbsf (Fig. 43). A fairly strong reflector at 2.07 s TWT tends to drape over the underlying basement on the illustrated profile (Fig. 49), but it is correlated with a more flat-lying reflector with a sedimentary appearance to the south. We suggest that this is the top of the 26-m-thick unit of clay and volcanics (Lithologic Unit III) that lies in the interval from 424 to 450 mbsf. A strong, broken reflection occurs at 2.09 s TWT that is underlain by more strong, discontinuous reflectors subparallel to the upper one. We interpret this sequence as basement reverberation, with the uppermost of these reflectors at 2.09 s correlating with the first solid basalts recovered at 450 mbsf.

Because the sonic log appears to be biased toward anomalously low velocities, two average interval velocities were calculated from the events on the seismic reflection record correlated to the drilled section. By this method, the 138 m, 0.17-s-thick section of foraminifer ooze has a formation velocity of 1.6 km/s. The underlying units of platform limestones, claystones, and volcanics have a total thickness of 283 m and 0.24 s, down to the top of basaltic basement at 450 mbsf and 2.09 s TWT. This yields an average formation velocity of 2.6 km/s for the integrated, shallow-water (?) sedimentary sequence. Because the general tendency is for sonic log velocities to increase downward throughout this sequence (Fig. 44), although the overall velocity average is anomalously low, we suspect that this sequence is characterized by a velocity gradient that also increases downward. We have somewhat arbitrarily broken the average 2.6 km/s velocity into an upper section at 2.5 km/s and a lower section at 2.7 km/s. This places the reflection event at 2.01 s TWT at the Paleocene/Eocene boundary at 319 mbsf.

The above correlations and formation velocities are considered to be reasonable estimates of in-situ conditions in Hole 871C. As such, they can be used with regional seismic surveys to construct a seismic stratigraphic map of the entire platform on Limalok Guyot.

In summary, the seismic stratigraphy section at Site 871 may be divided into three main parts:

1. A lower volcanic edifice terminates at 450 mbsf in soil horizons and localized pockets of organic-rich clay.

Table 14. DSV compressional wave velocity measurements of pelagic sediments, Holes 871A and 871C.

Core, section, interval (cm)	Depth (mbsf)	Temperature (°C)	Velocity (m/s)
144-871A-			
2H-2, 60-70	9.60	23.90	1465.20
2H-6, 90-100	15.90	23.10	1455.80
3H-2, 100-110	19.50	23.40	1542.50
3H-3, 100-110	21.00	23.20	1482.60
3H-4, 100-110	22.50	23.30	1551.20
4H-2, 126-136	29.26	24.20	1431.60
4H-3, 126-136	30.76	23.80	1492.20
4H-4, 100-110	32.00	23.70	1505.30
6H-6, 33-43	53.33	23.30	1497.10
7H-4, 102-112	60.52	23.40	1465.20
7H-5, 40-50	61.40	23.40	1493.80
8H-1, 96-106	65.46	23.10	1473.00
8H-2, 44-54	66.44	22.80	1411.00
8H-4, 40-50	69.40	23.20	1549.40
8H-5, 48-58	70.98	23.10	1506.90
9H-1, 108-118	75.08	23.40	1471.40
9H-2, 50-60	76.00	23.40	1477.80
9H-3, 78-88	77.78	23.60	1539.00
9H-3, 101-111	78.01	23.20	1495.50
9H-4, 69-79	79.19	23.30	1433.10
9H-5, 68-78	80.68	23.00	1502.00
10H-1, 120-130	84.70	23.90	1492.20
10H-3, 82-92	87.32	23.60	1506.90
10H-5, 43-53	89.93	23.60	1551.20
11H-2, 87-97	95.37	24.20	1460.50
11H-3, 33-43	96.33	24.20	1431.60
11H-4, 47-57	97.97	24.00	1497.10
11H-5, 87-97	99.87	23.40	1508.60
12H-1, 51-61	103.01	24.20	1416.80
12H-3, 74-84	106.24	23.90	1510.20
12H-4, 61-71	107.61	23.00	1523.60
12H-5, 45-55	108.95	23.20	1523.60
12H-6, 50-60	110.50	22.90	1576.10
13H-1, 35-45	112.35	22.90	1574.30
13H-2, 35-45	113.85	22.80	1527.00
13H-3, 34-44	115.34	22.80	1568.90
13H-4, 114-124	117.64	22.80	1583.30
13H-5, 93-103	118.93	22.80	1565.30
13H-6, 39-49	119.89	22.80	1556.40
14H-1, 35-45	121.85	22.80	1516.90
14H-2, 62-72	123.62	22.80	1585.20
14H-3, 31-41	124.81	22.80	1528.70
14H-5, 35-45	127.85	22.80	1585.20
14H-6, 29-39	129.29	22.80	1520.30
14H-6, 31-41	129.31	22.80	1419.80
15H-3, 50-60	134.00	22.80	1474.60
15H-4, 100-110	136.00	22.80	1563.50
144-871C-			
21R-1, 59-69	317.09	23.00	3328.00
21R-1, 59-69	317.09	23.00	3328.00

Note: DSV = digital sound velocimeter.

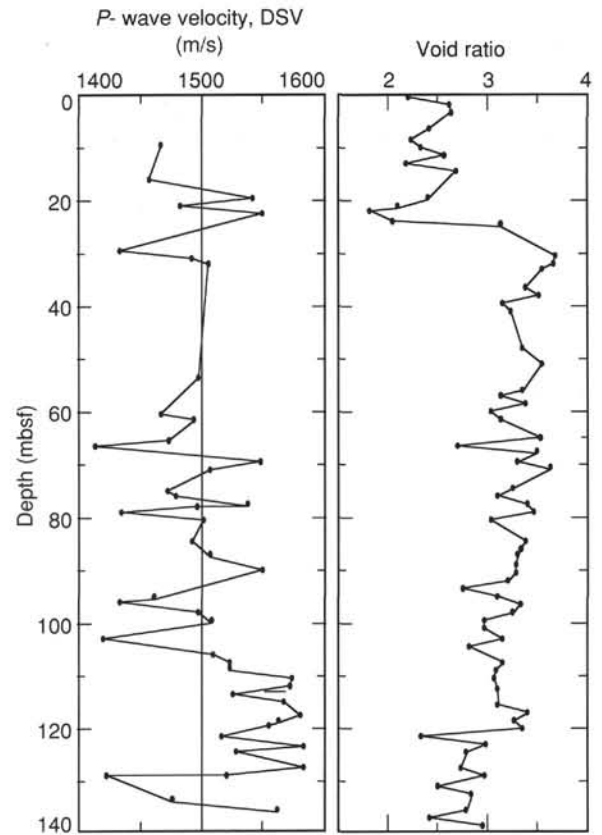


Figure 40. Digital sound velocimeter (DSV) measurements of compressional wave velocity and calculated void ratio of pelagic sediment (volume of voids/volume of solids) vs. depth, Hole 871A.

The angular volcanic breccias and the thick overlying sequence of dense variegated clay record a period of weathering and erosion of the volcanic pile. The weathering and erosion most likely occurred in subaerial conditions, as exhibited by the poor preservation of terrestrial-derived organic matter. The low-diversity pollen assemblage represents the limited floral diversity; the assemblage is dominated by angiosperms and abundant fungal spores. The poor preservation and low-diversity assemblage are suggestive of a moist tropical island with limited floral diversity.

Flooding of the island occurred during the early late Paleocene, with the initial stages of inundation characterized by marginal marine conditions. The color transition near the top of the clay from a light to an increasingly darker gray reflects an increase in organic matter (TOC up to 10%), and sulfur (TS up to 12%); the sulfur is observed as pyrite and marcasite. This gray clay was deposited in a low-energy environment, under sulfate-reducing conditions that were influenced by seawater. The organic-rich clay was burrowed and infilled with skeletal debris, which still preserves its aragonitic composition, and with calcareous nannofossils of early late Paleocene age. This clay horizon is interpreted as being a basal transgressive marine deposit.

The overlying carbonate sequence records the development and demise of a Paleocene to Eocene carbonate platform. The lowermost limestones have a well-sorted packstone texture, with coarse sand-sized grains; the constituent grains exhibit a high biotic diversity. These characteristics suggest that a well-oxygenated, turbulent, shallow-marine depositional environment existed on Limalok Guyot during the early late Paleocene. The presence of pyrite and carbon fragments within these limestones suggests that there was sulfate reduction occurred in this early diagenetic marine environment.

The upper Paleocene packstones and grainstones contain a normal marine biota and rhodoliths, denoting deposition on an open shelf or

2. A series of platform limestones is present from 424 to 138 mbsf. The development of this carbonate platform appears to have been interrupted at a depth of 319 mbsf, corresponding to the Paleocene/Eocene boundary. The carbonate platform was terminated at a depth of 138 mbsf in the middle Eocene. In addition to these two major surfaces, there may be lesser condensations or disconformities that correlate with some of the uranium-enriched horizons and may be related to lowstand or transgressive sea level fluctuations.

3. A pelagic cap of Miocene through Pleistocene age indicates substantial subsidence of Limalok Guyot.

SUMMARY AND CONCLUSIONS

Initial interpretations of the cores obtained at Site 871 indicate that the upper portion of the igneous basement of Limalok Guyot was formed by a series of eruptions of highly alkalic basalts, basanites, and nephelinites. These are probably related to the constructional phase of the volcano rather than a short-lived posterosional phase. The basalt has basement inclinations that appear to represent normal polarity magnetization acquired at a low southern paleolatitude of approximately 10°S.

Table 15. Hamilton Frame measurements of compressional wave velocity on limestones, clays, and basalts, Hole 871C.

Core, section, interval (cm)	Depth (mbsf)	Distance (mm)	Axes of measurement	Traveltime (μ s)	Corrected traveltime (μ s)	Measured velocity (m/s)	Velocity anisotropy index
144-871C-							
2R-1, 17-21	133.87	20.19	a	7.68	4.68	4314.10	
2R-1, 17-21	133.87	21.67	l	7.95	4.95	4377.78	
2R-1, 17-21	133.87	21.44	2	7.40	4.40	4872.73	
2R-1, 46-48	134.16	21.54	a	8.72	5.72	3765.73	
2R-1, 46-48	134.16	21.46	b	8.96	5.96	3600.67	
2R-1, 46-48	134.16	21.21	c	8.71	5.71	3714.54	-0.01
2R-1, 49-54	134.19	21.70	a	8.12	5.12	4238.28	
2R-1, 49-54	134.19	20.78	b	8.07	5.07	4098.62	
2R-1, 49-54	134.19	21.70	c	8.11	5.11	4246.58	-0.02
3R-CC, 12-18	152.80	21.56	l	8.69	5.69	3789.10	
3R-CC, 12-18	152.80	20.72	2	8.48	5.48	3781.02	
3R-CC, 12-18	152.80	21.95	3	8.74	5.74	3824.04	
4R-1, 48-52	153.38	19.48	a	7.11	4.11	4739.66	
4R-1, 48-52	153.38	21.45	b	7.13	4.13	5193.71	
4R-1, 48-52	153.38	21.44	c	7.59	4.59	4671.02	0.06
6R-1, 24-29	172.54	20.39	a	7.78	4.78	4265.69	
6R-1, 24-29	172.54	21.47	l	8.39	5.39	3983.30	
6R-1, 24-29	172.54	21.56	2	8.14	5.14	4194.55	
8R-1, 7-14	191.57	20.86	a	6.72	3.72	5607.53	
8R-1, 7-14	191.57	21.86	l	7.03	4.03	5424.32	
8R-1, 7-14	191.57	21.66	2	7.21	4.21	5144.89	
9R-1, 5-12	201.25	19.07	a	6.48	3.48	5479.89	
9R-1, 5-12	201.25	21.83	l	7.05	4.05	5390.12	
9R-1, 5-12	201.25	21.53	2	6.71	3.71	5803.24	
9R-1, 46-53	201.66	21.50	a	8.66	5.66	3798.59	
9R-1, 46-53	201.66	21.48	l	8.82	5.82	3690.72	
9R-1, 46-53	201.66	20.17	2	8.85	5.85	3447.86	
21R-1, 59-61	317.09	21.48	a	8.02	5.02	4278.88	
21R-1, 59-61	317.09	21.42	b	7.52	4.52	4738.94	
21R-1, 59-61	317.09	21.44	c	7.88	4.88	4393.44	0.03
21R-1, 90-96	317.40	21.47	a	7.14	4.14	5185.99	
21R-1, 90-96	317.40	21.51	b	7.02	4.02	5350.75	
21R-1, 90-96	317.40	21.74	c	7.06	4.06	5354.68	-0.02
21R-1, 130-136	317.80	19.30	a	8.07	5.07	3806.71	
21R-1, 130-136	317.80	21.43	l	7.71	4.71	4549.89	
21R-1, 130-136	317.80	21.51	2	7.81	4.81	4471.93	
22R-1, 19-26	326.39	21.72	a	7.41	4.41	4925.17	
22R-1, 19-26	326.39	21.62	l	7.18	4.18	5172.25	
22R-1, 19-26	326.39	21.54	2	7.11	4.11	5240.88	
23R-1, 37-45	336.17	21.61	l	7.76	4.76	4539.92	
23R-1, 37-45	336.17	21.70	2	7.93	4.93	4401.62	
23R-1, 37-45	336.17	21.40	3	7.63	4.63	4622.03	
28R-1, 34-39	384.04	17.72	a	8.62	5.62	3153.03	
28R-1, 34-39	384.04	21.40	l	9.28	6.28	3407.64	
28R-1, 34-39	384.04	21.53	2	9.15	6.15	3500.81	
28R-1, 123-128	384.93	18.91	a	8.11	5.11	3700.59	
28R-1, 123-128	384.93	21.41	l	8.26	5.26	4070.34	
28R-1, 123-128	384.93	21.61	2	8.27	5.27	4100.57	
30R-1, 34-39	403.44	9.44	a	5.51	2.51	3760.96	
30R-1, 34-39	403.44	21.62	l	7.85	4.85	4457.73	
30R-1, 34-39	403.44	21.51	2	7.72	4.72	4557.20	
32R-1, 16-20	422.66	14.65	a	6.55	3.55	4126.76	
32R-1, 16-20	422.66	21.49	b	7.92	4.92	4367.89	
32R-1, 16-20	422.66	12.85	c	6.19	3.19	4028.21	
39R-1, 11-13	480.51	22.61	a	7.96	4.96	4558.47	
39R-1, 11-13	480.51	21.57	b	7.70	4.70	4589.36	
39R-1, 11-13	480.51	21.39	c	7.70	4.70	4551.06	0.01
39R-1, 81-83	481.21	23.25	a	8.04	5.04	4613.10	
39R-1, 81-83	481.21	21.41	b	7.52	4.52	4736.73	
39R-1, 81-83	481.21	21.43	c	7.32	4.32	4960.65	-0.06
39R-1, 113-115	481.53	20.40	a	7.92	4.92	4146.34	
39R-1, 113-115	481.53	21.37	b	8.07	5.07	4214.99	
39R-1, 113-115	481.53	21.51	c	7.94	4.94	4354.25	-0.04
40R-1, 141-143	491.11	23.20	a	8.42	5.42	4280.44	
40R-1, 141-143	491.11	21.39	b	7.72	4.72	4531.78	
40R-1, 141-143	491.11	21.39	c	7.96	4.96	4312.50	0.02
40R-4, 62-64	494.82	22.31	a	8.65	5.65	3948.67	
40R-4, 62-64	494.82	21.46	b	7.79	4.79	4480.17	
40R-4, 62-64	494.82	21.28	c	8.77	5.77	3688.04	0.13
41R-1, 6-8	496.00	21.85	a	7.95	4.95	4414.14	
41R-1, 6-8	496.00	21.70	b	7.73	4.73	4587.74	
41R-1, 6-8	496.00	21.47	c	7.53	4.53	4739.51	-0.05

Notes: a = direction perpendicular to split core plane, b = direction transverse to split core plane, and c = core axis; 1, 2, and 3 = unoriented axes; all axes orthogonal.

Table 16. Wykeham-Farrance and Torvane shear strength data, Holes 871A and 871C.

Core, section, interval (cm)	Depth (mbsf)	Test type	Spring constant	Vane constant	Torsion angle (degree)	Torsion ² (kg/cm ²)	Undrained shear strength (kPa)
144-871A-							
1H-1, 60-61	0.60	WF	31.27	0.23	7		5.00
1H-3, 71-72	3.61	WF	31.27	0.23	0		0
1H-5, 52-53	6.42	WF	31.27	0.23	6		4.00
2H-2, 70-71	9.70	WF	31.27	0.23	3		2.00
2H-4, 66-67	12.66	WF	31.27	0.23	5		3.00
2H-6, 58-59	15.58	WF	31.27	0.23	8		2.00
2H-6, 58.5-59.5	15.59	WF	10.91	0.23	0		0
3H-2, 103-104	19.53	WF	10.91	0.23	1		0
6H-2, 104-105	48.04	WF	10.91	0.23	0		0
6H-4, 55-56	50.55	WF	10.91	0.23	21		5.00
6H-6, 25-26	53.25	WF	10.91	0.23	6		1.00
7H-3, 87-88	58.87	WF	10.91	0.23	25		6.00
7H-4, 103-104	60.53	WF	10.91	0.23	22		5.00
7H-5, 31-32	61.31	WF	10.91	0.23	5		1.00
8H-1, 36-37	64.86	WF	10.91	0.23	2		0
8H-2, 100-101	67.00	WF	10.91	0.23	0		0
8H-3, 88-89	68.38	WF	10.91	0.23	13		3.00
8H-4, 96-97	69.96	WF	10.91	0.23	25		6.00
8H-5, 57-58	71.07	WF	10.91	0.23	10		2.00
9H-1, 121-122	75.21	WF	10.91	0.23	39		9.00
9H-2, 88-89	76.38	WF	10.91	0.23	23		6.00
9H-3, 140-141	78.40	WF	10.91	0.23	17		4.00
9H-4, 89-90	79.39	WF	10.91	0.23	58		14.00
9H-5, 95-96	80.95	WF	10.91	0.23	69		17.00
10H-1, 130-131	84.80	WF	10.91	0.23	0		0
10H-2, 139-140	86.39	WF	10.91	0.23	23		6.00
10H-3, 107-108	87.57	WF	10.91	0.23	0		0
10H-4, 96-97	88.96	WF	10.91	0.23	6		1.00
10H-5, 64-65	90.14	WF	10.91	0.23	8		2.00
10H-6, 89-90	91.89	WF	10.91	0.23	45		11.00
11H-2, 93-94	95.43	WF	10.91	0.23	12		3.00
11H-3, 89-90	96.89	WF	10.91	0.23	31		8.00
11H-4, 58-59	98.08	WF	10.91	0.23	26		6.00
11H-5, 125-126	100.25	WF	10.91	0.23	32		8.00
12H-1, 99-100	103.49	WF	10.91	0.23	13		3.00
12H-2, 101-102	105.01	WF	10.91	0.23	11		3.00
12H-3, 120-121	106.70	WF	10.91	0.23	5		1.00
12H-5, 90-91	109.40	WF	10.91	0.23	5		1.00
12H-6, 80-81	110.80	WF	10.91	0.23	3		1.00
13H-1, 92-93	112.92	WF	10.91	0.23	2		0
13H-2, 91-92	114.41	WF	10.91	0.23	6		1.00
13H-3, 109-110	116.09	WF	10.91	0.23	2		0
13H-4, 122-123	117.72	WF	10.91	0.23	6		1.00
13H-5, 116-117	119.16	WF	10.91	0.23	6		1.00
13H-6, 128-129	120.78	WF	10.91	0.23	7		2.00
14H-1, 140-141	122.90	WF	10.91	0.23	2		0
14H-2, 97-98	123.97	WF	10.91	0.23	5		1.00
14H-3, 79-80	125.29	WF	10.91	0.23	4		1.00
14H-5, 93-94	128.43	WF	10.91	0.23	6		1.00
14H-6, 17-18	129.17	WF	10.91	0.23	2		0
15H-3, 63-64	134.13	WF	10.91	0.23	8		2.00
15H-4, 118-119	136.18	WF	10.91	0.23	5		1.00
144-871C-							
32R-1, 100-101	423.50	WF	31.27	0.23	119		83.00
32R-1, 117-118	423.67	TV				0.50	123.00
32R-1, 56-57	423.06	TV				0.40	98.00
32R-2, 16-17	424.16	TV				0.70	172.00
32R-2, 80-81	424.80	TV				0.16	39.00
32R-2, 99-100	424.99	WF	31.27	0.23	90		63.00
32R-3, 13-14	425.63	TV				0.25	61.00
32R-3, 70-71	426.20	TV				0.57	140.00
32R-3, 127-128	426.77	TV				0.86	211.00
32R-4, 15-16	427.15	TV				0.85	208.00
32R-4, 61-62	427.61	TV				0.69	169.00
32R-4, 101-102	428.01	TV				0.90	221.00
33R-1, 40-41	432.60	TV				0.67	164.00
33R-1, 90-91	433.10	TV				0.35	86.00
33R-2, 75-76	434.45	TV				0.23	56.00
33R-3, 30-31	435.50	TV				0.18	44.00

Notes: WF = Wykeham-Farrance vane, and TV = Soil-test Torvane.

steep ramp. These packstones give way to grainstones, rudstones, and some boundstones, which contain abundant miliolids, scleractinian corals, red and green algae, echinoids, and larger foraminifers (*Nummulites*, Discocylinidae). The facies signify the presence of a nearby reef, and they represent deposition in a back-reef environment during the late Paleocene.

A period of deposition in a protected lagoon during the early Eocene is represented by lower Eocene packstones that contain low-

spired gastropods and miliolids in a low-diversity assemblage. The overlying lower and middle Eocene burrowed skeletal wackestones and packstones contain *Alveolina* and miliolids; these low-energy facies indicate continued deposition in a protected, shallow-lagoon setting during early to middle Eocene time. The presence of middle Eocene grainstones signifies the return of higher energy conditions. Some of the grainstones exhibit low-angle cross laminations composed of coarse-sand-sized grains and keystone vugs; these grain-

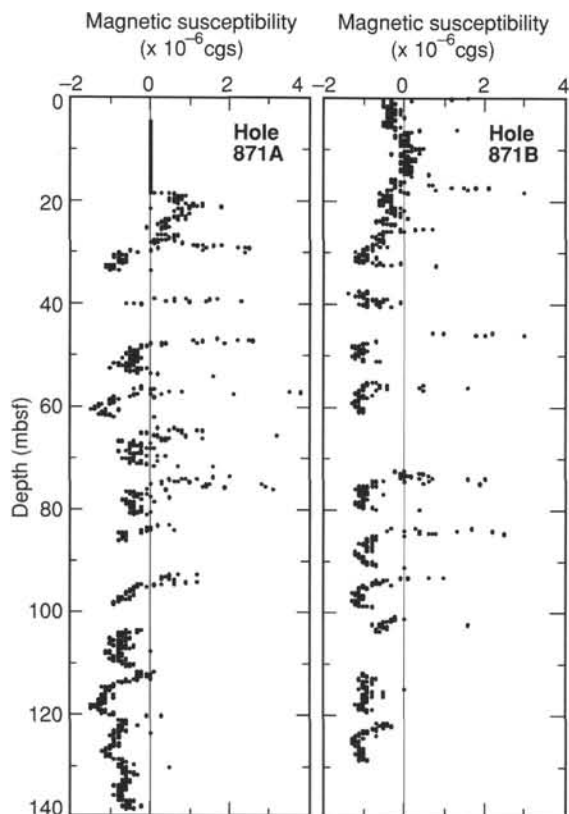


Figure 41. Magnetic susceptibility variations in pelagic sediment vs. depth, Holes 871A and 871B.

stones are interpreted as beach or sand-bar deposits. The uppermost limestones are middle Eocene packstone and wackestone containing *Nummulites* and miliolids that were deposited in a protected, shallow lagoon.

The platform limestones on Limalok Guyot represent a shallowing-upward sequence, with changes in depositional environment from open subtidal to a shallow-lagoonal depositional setting. A peak in faunal diversity, coupled with the presence of planktonic foraminifers, marks at least one period of higher sea level during the early middle Eocene. Benthic foraminifers and rare diatoms in the uppermost part of the sequence are indicative of a central lagoonal environment just before platform drowning.

The carbonate platform is overlain by an iron-manganese oxide and phosphatic crust containing middle Eocene calcareous plankton. This planktonic assemblage tightly constrains the date of the platform drowning and indicates that oceanic, poorly oxygenated waters covered the relict platform immediately after its demise. Manganese-oxide encrustation and phosphatization possibly continued through some part of the late Eocene and early Oligocene.

The carbonate platform subsided into the pelagic realm by the early Oligocene, as demonstrated by the presence of planktonic foraminifers and nannofossils that infill borings in the marine hardground. The accumulation of pelagic sediments did not begin until the early Miocene. Lower and middle Miocene sediments were strongly winnowed by bottom currents, although sediment preservation was relatively continuous with accumulation rates of 5–20 m/m.y. A prominent disconformity, spanning the late middle Miocene through most of the late Miocene (approximately 6 m.y.), resulted in appreciable reworking of calcareous microplankton of Oligocene and early to middle Miocene age. Sediment accumulation during the latest Miocene and Pliocene was slow (2–3 m/m.y.) and discontinuous. The relatively complete, albeit thin, uppermost Pliocene and Pleistocene suggests a change in oceanographic conditions. This change was accompanied by higher

sediment accumulation rates (11–12 m/m.y.) and a decrease in sediment winnowing.

REFERENCES*

- Asquith, G.D., 1979. *Subsurface Carbonate Depositional Models: A Concise Review*. Tulsa, OK (Petroleum Publ. Co.).
- Berggren, W.A., Kent, D.V., and Flynn, J.J., 1985. Jurassic to Paleogene: Part 2. Paleogene geochronology and chronostratigraphy. In Snelling, N.J. (Ed.), *The Chronology of the Geological Record*. Geol. Soc. London Mem., 10:141–195.
- Berggren, W.A., Kent, D.V., and Van Couvering, J.A., 1985. The Neogene: Part 2. Neogene geochronology and chronostratigraphy. In Snelling, N.J. (Ed.), *The Chronology of the Geological Record*. Geol. Soc. London Mem., 10:211–260.
- Brewer, J.M., 1971. North Atlantic fluoride profiles. *Deep-Sea Res. Part A*, 18:237–241.
- Camoin, G., Bernet-Rollande, M.C., and Philip, J., 1988. Rudist-coral frameworks associated with submarine volcanism in the Maastrichtian strata from Pachino area (S.E. Sicily). *Sedimentology*, 23:128–143.
- Collot, J.-Y., Greene, H.G., Stokking, L.B., et al., 1992. *Proc. ODP, Init. Repts.*, 134: College Station, TX (Ocean Drilling Program).
- Davis, A.S., Pringle, M.S., Pickthorn, L.B.G., Clague, D.A., and Schwab, W.C., 1989. Petrology and age of alkalic lava from the Ratak Chain of the Marshall Islands. *J. Geophys. Res.*, 94:5757–5774.
- Dorfman, M.H., Newey, J.-J., and Coates, G.R., 1990. New techniques in lithofacies determination and permeability prediction in carbonates using well logs. In Hurst, A., Lovell, M.A., and Morton, A.C. (Eds.), *Geological Applications of Wireline Logs*. Geol. Soc. Publ. London, 48:113–120.
- Dunham, R.J., 1970. Meniscus cement. In Bricker, O.P. (Ed.), *Carbonate Cements*. Johns Hopkins Univ., Stud. Geol., 19:297–300.
- Folk, R.L., 1965. Some aspects of recrystallization in ancient limestones. In Pray, L.C., and Murray, R.C. (Eds.), *Dolomitization and Limestone Diagenesis*. Spec. Publ.—Soc. Econ. Paleontol. Mineral., 13:13–48.
- Gartner, S., 1977. Calcareous nannofossil biostratigraphy and revised zonation of the Pleistocene. *Mar. Micropaleontol.*, 2:1–25.
- Hein, J.R., Kang, J.K., et al., 1990. Geological, geochemical, geophysical, and oceanographic data and interpretations of seamounts and C-rich ferromanganese crusts from the Marshall Islands, KORDI-USGS R.V. *Faranella* Cruise F10-89-CP. *Open-File Rep.—U.S. Geol. Surv.*, 90-407.
- Hottinger, L., 1960. Recherches sur les alvéolines du Paléocène et de l'Eocène. *Schweiz. Palaeontol. Abh. (Mem. Soc. Paleontol. Suisse)*, 75/76:1–243.
- Lincoln, J.M., Pringle, M.S., and Premoli Silva, I., in press. Early and Late Cretaceous volcanism and reef-building in the Marshall Islands. In Pringle, M.S., Sager, W.W., Sliter, W.V., and Stein, S. (Eds.), *The Mesozoic Pacific*. Am. Geophys. Union, Geophys. Monogr. Ser.
- McFadden, P.L., and McElhinny, M.W., 1984. A physical model for paleosecular variation. *Geophys. J. R. Astron. Soc.*, 78:809–830.
- Nakanishi, M., Tamaki, K., and Kobayashi, K., 1992. A new Mesozoic isochron chart of the northwestern Pacific Ocean: paleomagnetic and tectonic implications. *Geophys. Res. Lett.*, 19:693–696.
- Pringle, M.S., Jr., 1992. Geochronology and petrology of the Musicians Seamounts, and the search for hot spot volcanism in the Cretaceous Pacific [Ph.D. dissert.]. Univ. of Hawaii, Honolulu.
- Rio, D., Fornaciari, E., and Raffi, I., 1990. Late Oligocene through early Pleistocene calcareous nannofossils from western equatorial Indian Ocean (Leg 115). In Duncan, R.A., Backman, J., Peterson, L.C., et al., *Proc. ODP, Sci. Results*, 115: College Station, TX (Ocean Drilling Program), 175–235.
- Sager, W.W., and Pringle, M.S., 1988. Mid-Cretaceous to Early Tertiary apparent polar wander path of the Pacific Plate. *J. Geophys. Res.*, 93:11753–11771.
- Schaub, H., 1981. *Nummulites et Assilines de la Téthys paléogène*. Taxonomie, phylogénèse et biostratigraphie. *Mem. Suisses Paleontol.*, 104.
- Schlanger, S.O., Campbell, J.F., and Jackson, M.W., 1987. Post-Eocene subsidence of the Marshall Islands recorded by drowned atolls on Harrie and Sylvania guyots. In Keating, B.H., Fryer, P., Batiza, R., and Boelert, G.W. (Eds.), *Seamounts, Islands, and Atolls*. Am. Geophys. Union, Geophys. Monogr. Ser., 43:165–174.
- Serra, O., 1985. 5.8 shallow-water carbonate environment. *Sedimentary Environments from Wireline Logs*: Houston (Schlumberger Educ. Services), 143–154.

* Abbreviations for names of organizations and publication titles in ODP reference lists follow the style given in *Chemical Abstracts Service Source Index* (published by American Chemical Society).

Shipboard Scientific Party, 1991. Site 812. In Davies, P.J., McKenzie, J.A., Palmer-Julson, A., et al., *Proc. ODP, Init. Repts.*, 133 (Pt. 1): College Station, TX (Ocean Drilling Program), 135–176.

Van Wagoner, N.A., and Johnson, H.P., 1983. Magnetic properties of three segments of the Mid-Atlantic Ridge at 37°N: FAMOUS, Narrowgate and AMAR:AMAR 2. *J. Geophys. Res.*, 88:5065–5082.

Weast, R.C. (Ed.), 1984. *CRC Handbook of Chemistry and Physics*: Boca Raton, FL (CRC Press).

White, M.R., 1992. On species identification in the foraminiferal genus *Alveolina* (late Paleocene–middle Eocene). *J. Foraminiferal Res.*, 22:52–70.

Ms 144IR-104

NOTE: For all sites drilled, core-description forms (“barrel sheets”) and core photographs can be found in Section 3, beginning on page 453. Forms containing smear-slide data can be found in Section 4, beginning on page 1017. Thin-section data are given in Section 5, beginning on page 1037. Conventional log, FMS, dipmeter, and geochemical log (element and oxide weight %) data can be found in CD-ROM form (back pocket).

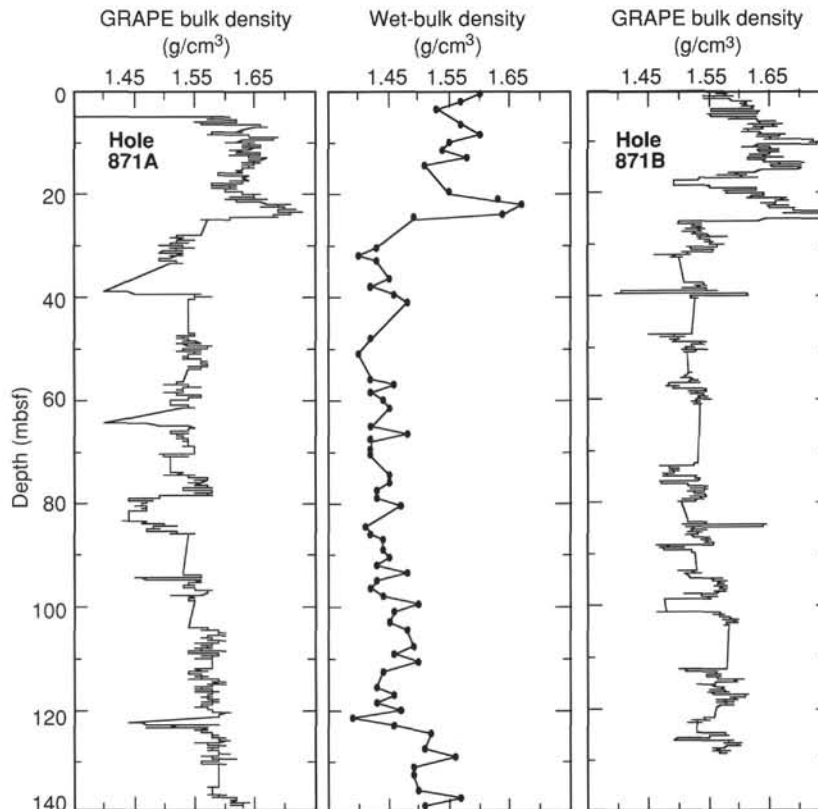


Figure 42. Comparison of downhole profiles of GRAPE bulk density vs. depth, Holes 871A and 871B. Center figure illustrates discrete wet-bulk density measurements vs. depth, Hole 871A.

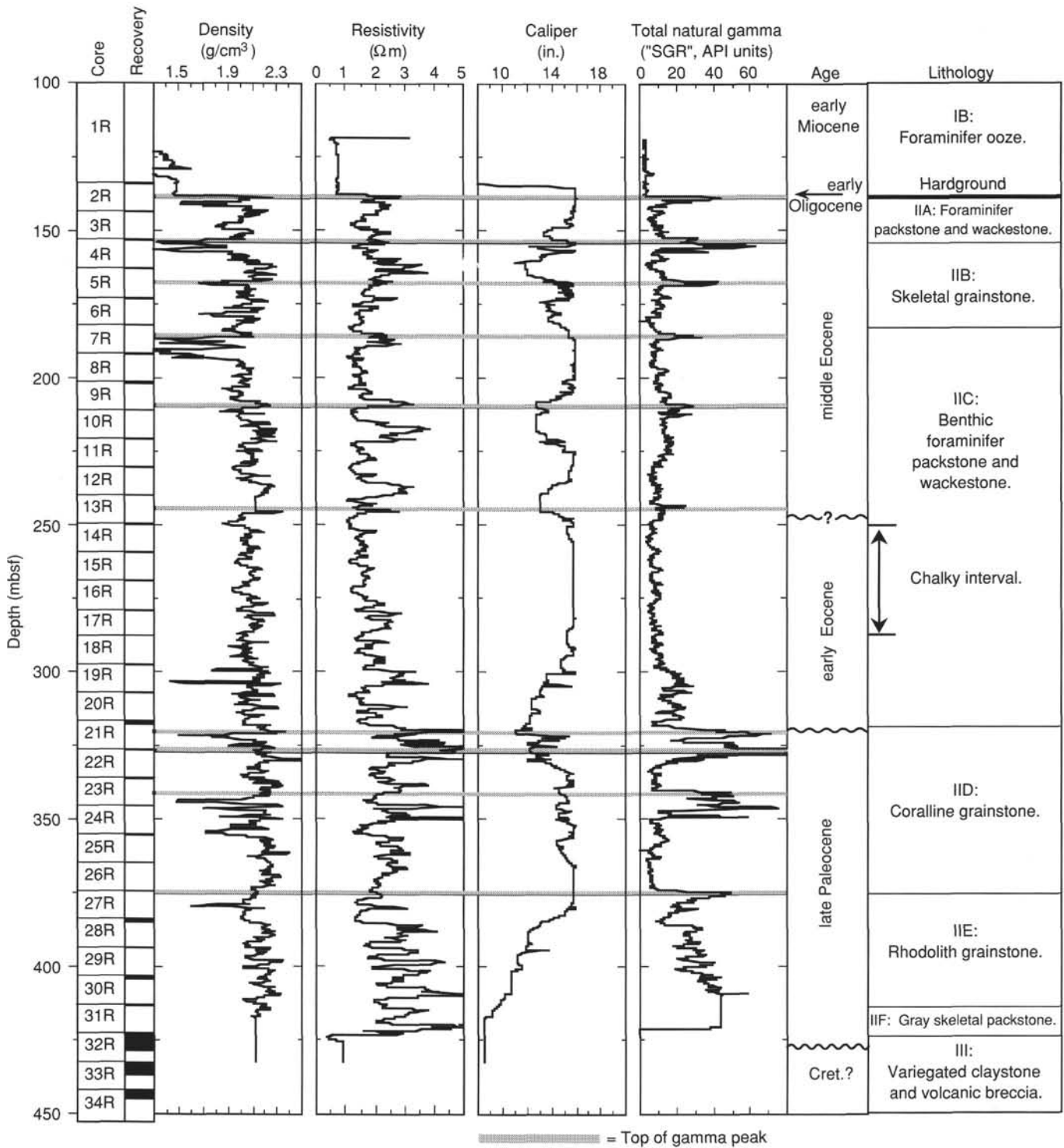


Figure 43. Stratigraphy of Hole 871C from selected geophysical logs compared to cored intervals, lithostratigraphy, and biostratigraphic ages within Hole 871C. Resistivity is from the ILM (medium-penetration resistivity) tool. Total natural gamma ("SGR") has been taken from the geochemistry run. Caliper, or apparent hole diameter, does not record values greater than 16 in. (40.6 cm); drill-bit diameter is 9.9 in. (25 cm). Fluctuations in density and resistivity generally coincide; therefore, these variations provide a record of relative porosity of different limestone beds within the carbonate platform. Peaks in total natural gamma are marked by shaded lines; these events are mainly a result of concentrations of radioactive uranium and have no discernible correlation to the minor clay contents. Major events in total natural gamma (uranium concentration) appear to coincide with biostratigraphic boundaries and facies changes, and may be associated with hiatuses in sedimentation or exposure surfaces.

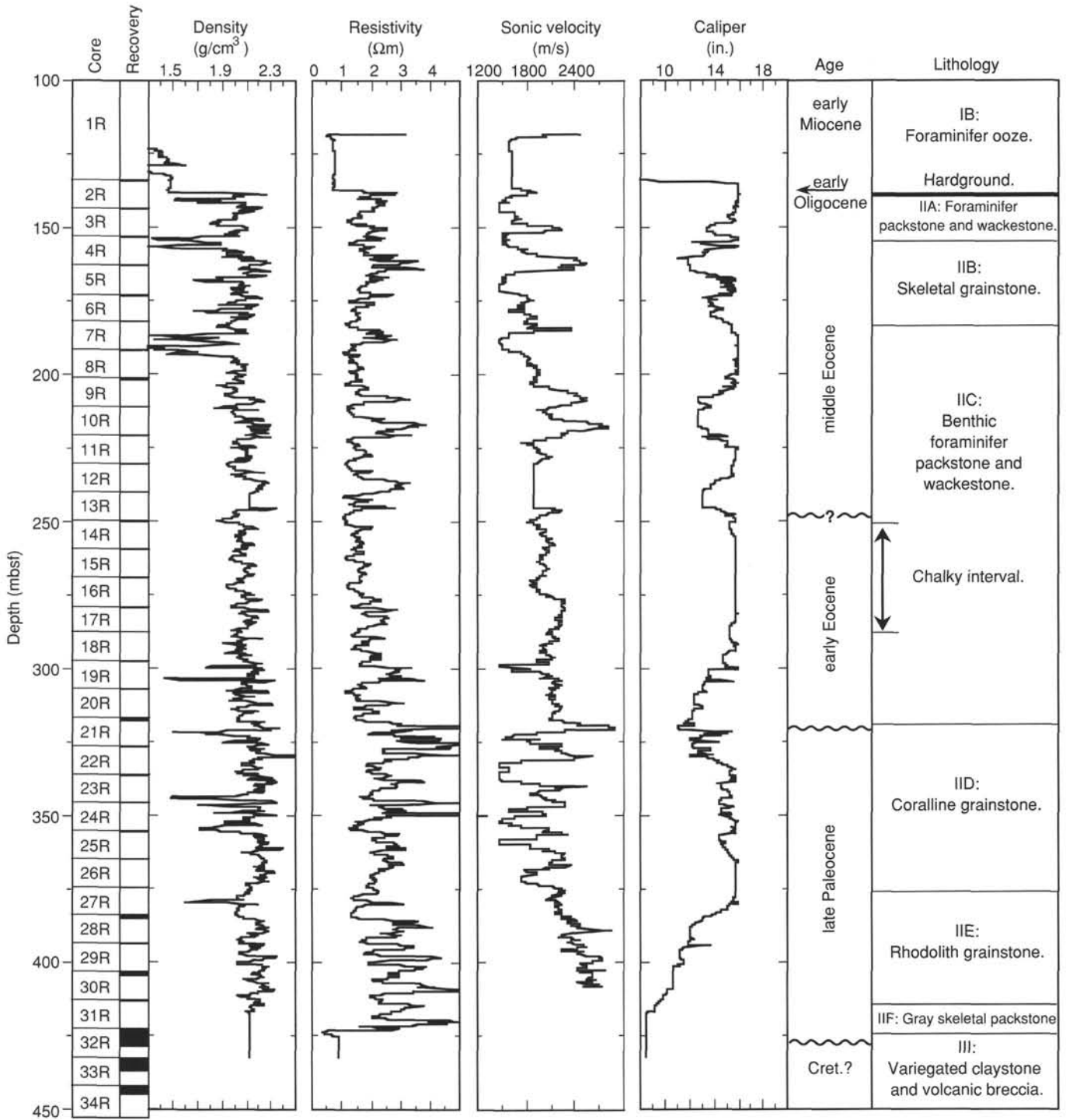


Figure 44. Geophysics logging measurements in the carbonate platform in Hole 871C. Density, medium-penetration resistivity, and sonic velocity signals show a general downhole increase in these parameters, indicating a lower porosity. Individual peaks generally correlate among these logs and probably correspond to less porous intervals within the carbonate platform facies.

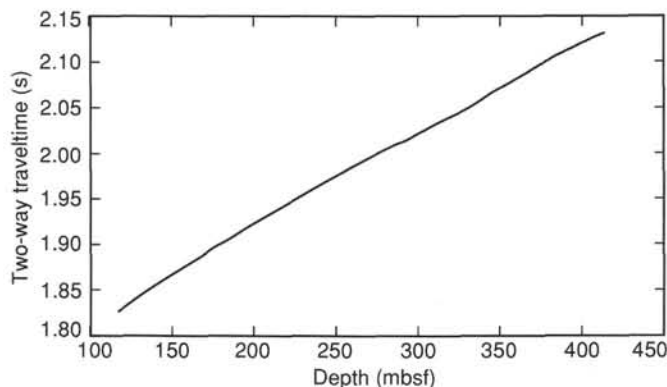


Figure 45. Integrated sonic traveltime vs. depth in the carbonate platform in Hole 871C. These interval velocities appear to have been biased to slower values because of the irregular borehole conditions.

Table 17. Main features of carbonate platform stratigraphy from downhole logging, Site 871.

Feature or lithologic unit	Facies	Log-defined boundaries (mbsf, nearest meter)	Core-recovery defined boundaries (mbsf, nearest meter)	Logging feature used to identify
Top of carbonate platform	Phosphatic hardground	138	134	Formation MicroScanner imagery shows very low relative resistivity in sharp contact to underlying high resistivity layer.
Lithologic Subunit IIA	Burrowed foraminifer packstone to wackestone	138–152	134–153	Formation MicroScanner imagery shows mottled, relatively low resistivity; base of subunit placed at top of uranium peak.
Lithologic Subunit IIB	Skeletal grainstone	152–183	153–183	Formation MicroScanner imagery shows fine-scale mottled appearance; base of subunit placed at top of uranium peak.
Lithologic Subunit IIC	Foraminifer packstone to wackestone	182–319	183–317	Formation MicroScanner imagery shows mainly fine mottling with some meter-scale diffuse bedding; base of subunit placed at top of major natural gamma peak.
Lithologic Subunit IID	Two uranium peaks	209, 243	249.5–290? 317–374	Sustained low resistivity; widened borehole.
	Chalky interval	247–277		
	Coralline grainstone	319–374		
Lithologic Subunit IIE	Two uranium peaks	319, 324	374–413	Elevated natural gamma intensity and resistivity. Elevated natural gamma intensity and resistivity. Elevated natural gamma intensity; extreme variations in resistivity; base is placed at downward increase in iron, but most logs did not reach this level.
	Uranium peak	341–350		
Lithologic Subunit IIE	Algal-dominated grainstone	374–418		
Lithologic Subunit IIF	Dark gray skeletal packstone	418–424	413–423	Increased iron concentrations; lower contact is marked by downward change to very low resistivity.

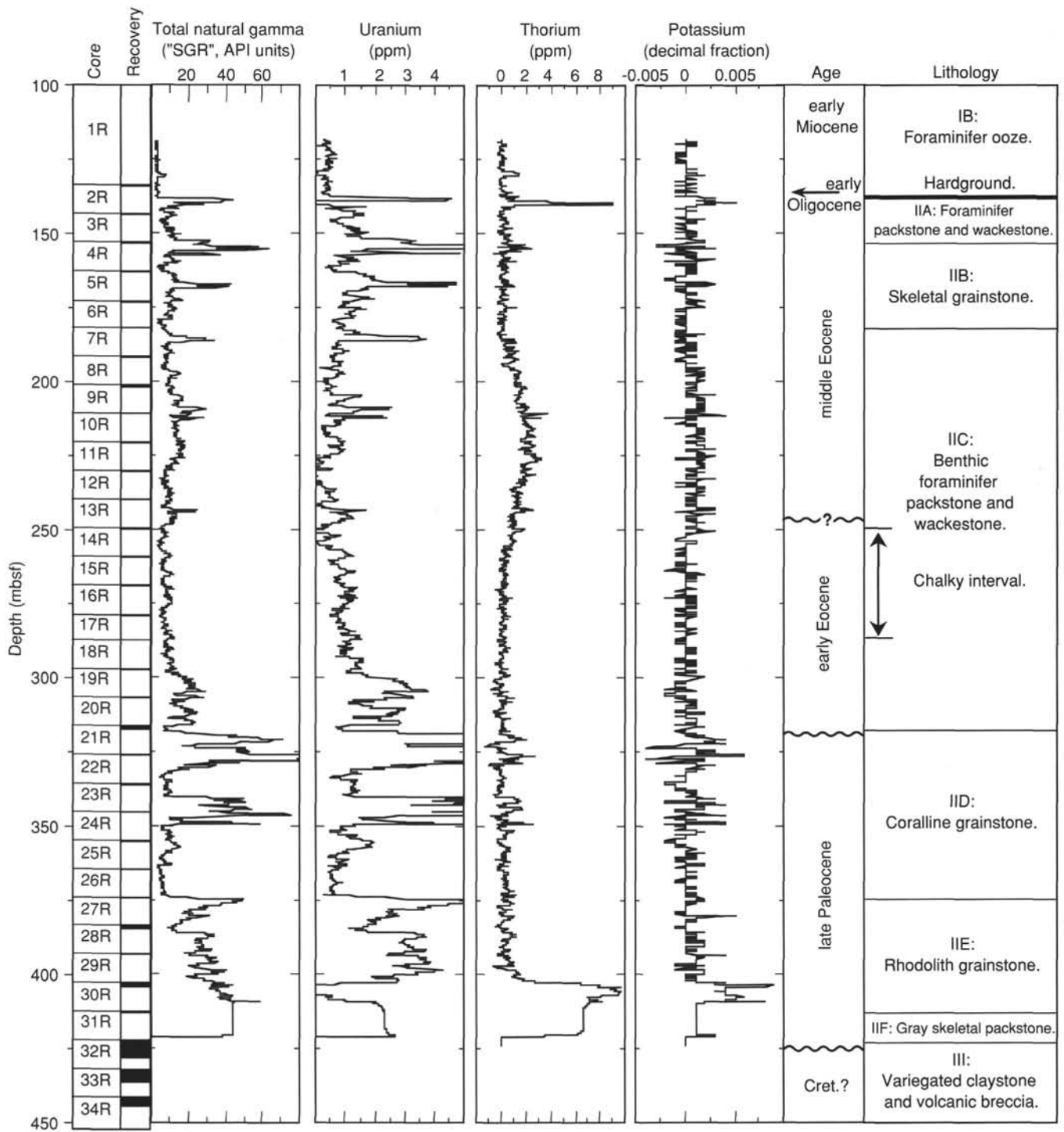


Figure 46. Radioactive element concentrations within the carbonate platform in Hole 871C. Total natural gamma, uranium, thorium, and potassium logs are from the geochemical tool-string run. Most of the natural gamma is caused by uranium, with thorium playing a minor role in some intervals. Potassium remains near the noise level of the measurements.

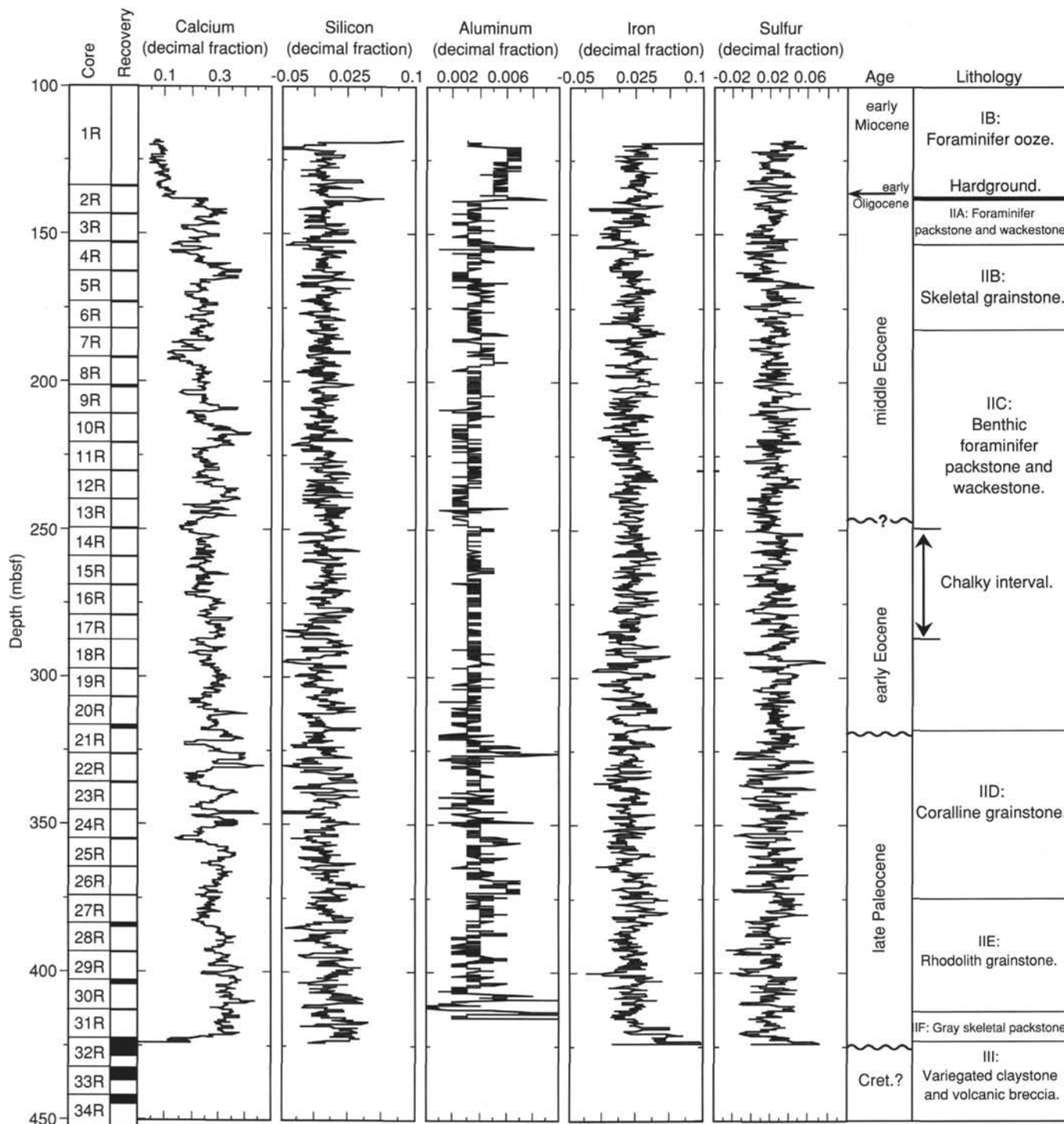


Figure 47. Relative stable elements (calcium, silicon, aluminum, iron, and sulfur) within the carbonate platform in Hole 871C. Values are given in relative proportions and have not been adjusted for porosity variations. Except for calcium, all other elements are in trace amounts within the shallow-water carbonates. At the base of the logging run, increased levels of iron and aluminum correspond to the dark gray skeletal packstone of Lithologic Subunit IIF, overlying the claystones of Lithologic Unit III.

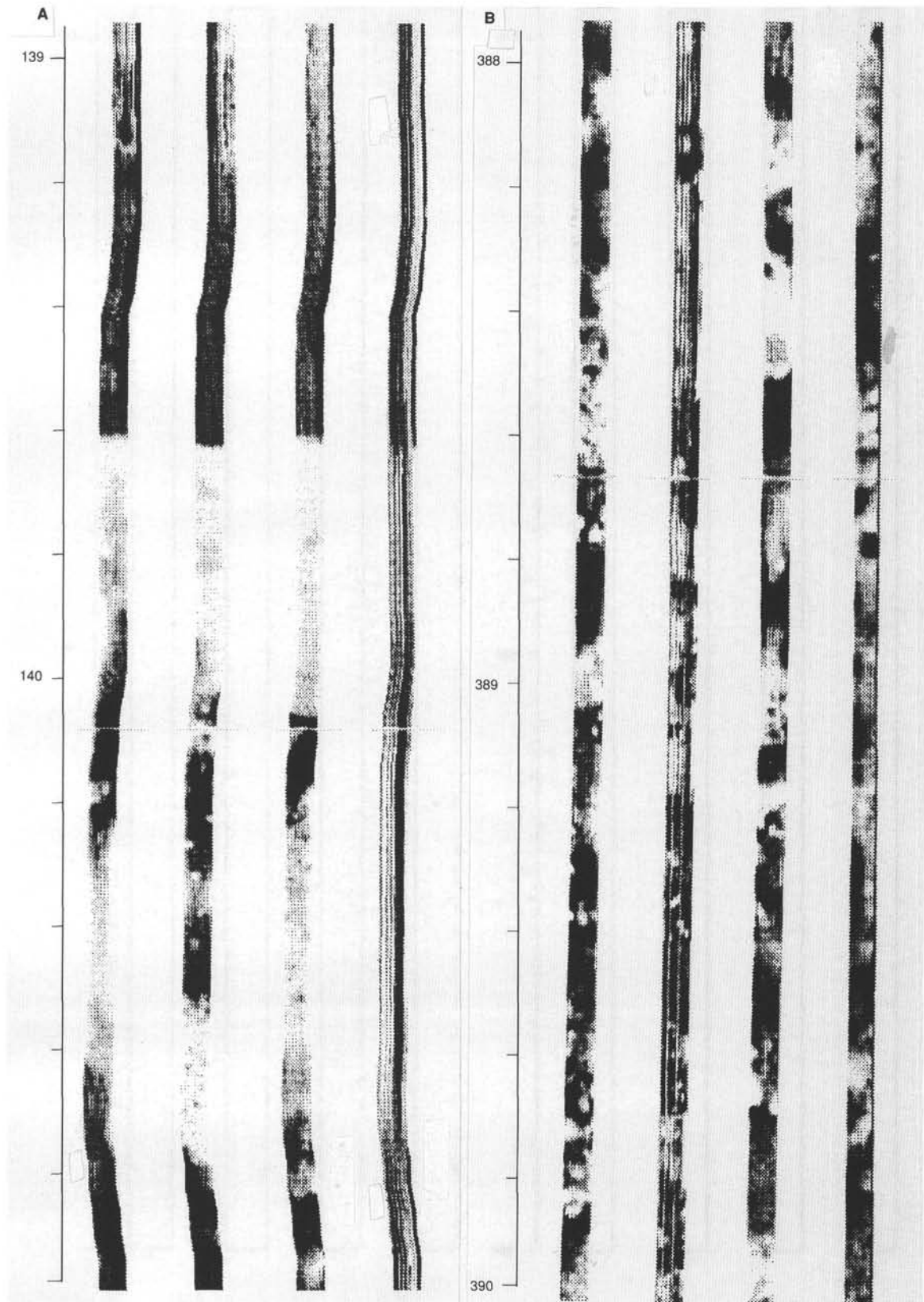


Figure 48. Selected Formation MicroScanner high-resolution resistivity imagery of the borehole in Hole 871C. **A.** Phosphatic hardground at the top of the carbonate platform corresponds to the top of a relatively high resistivity (shown as white) bed overlain by a low-resistivity (shown as black) foraminifer ooze. **B.** Typical irregular resistivity patterns within the algal-rich grainstone facies of Lithologic Subunit IIF. The sharply defined, centimeter-scale, high-resistivity (shown as white) features are probably algal oncolites (rhodoliths). The larger scale mottling is from irregular cementation.

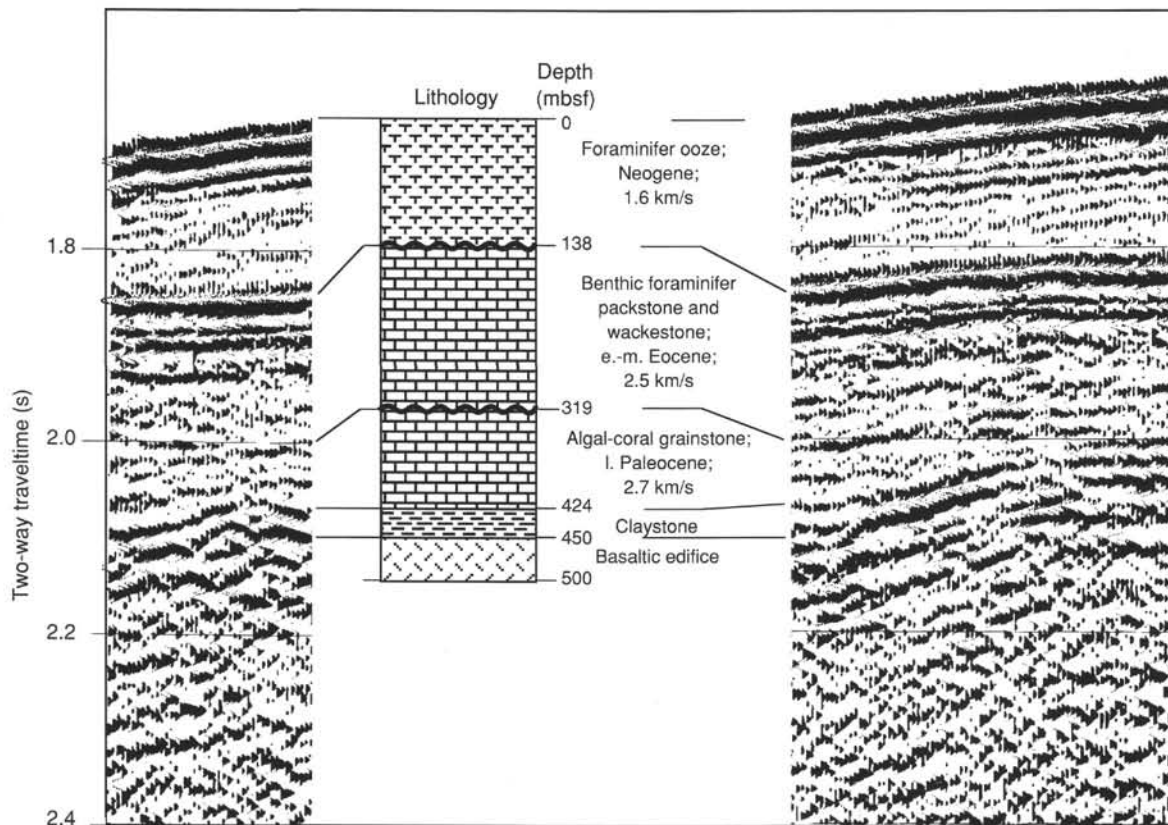
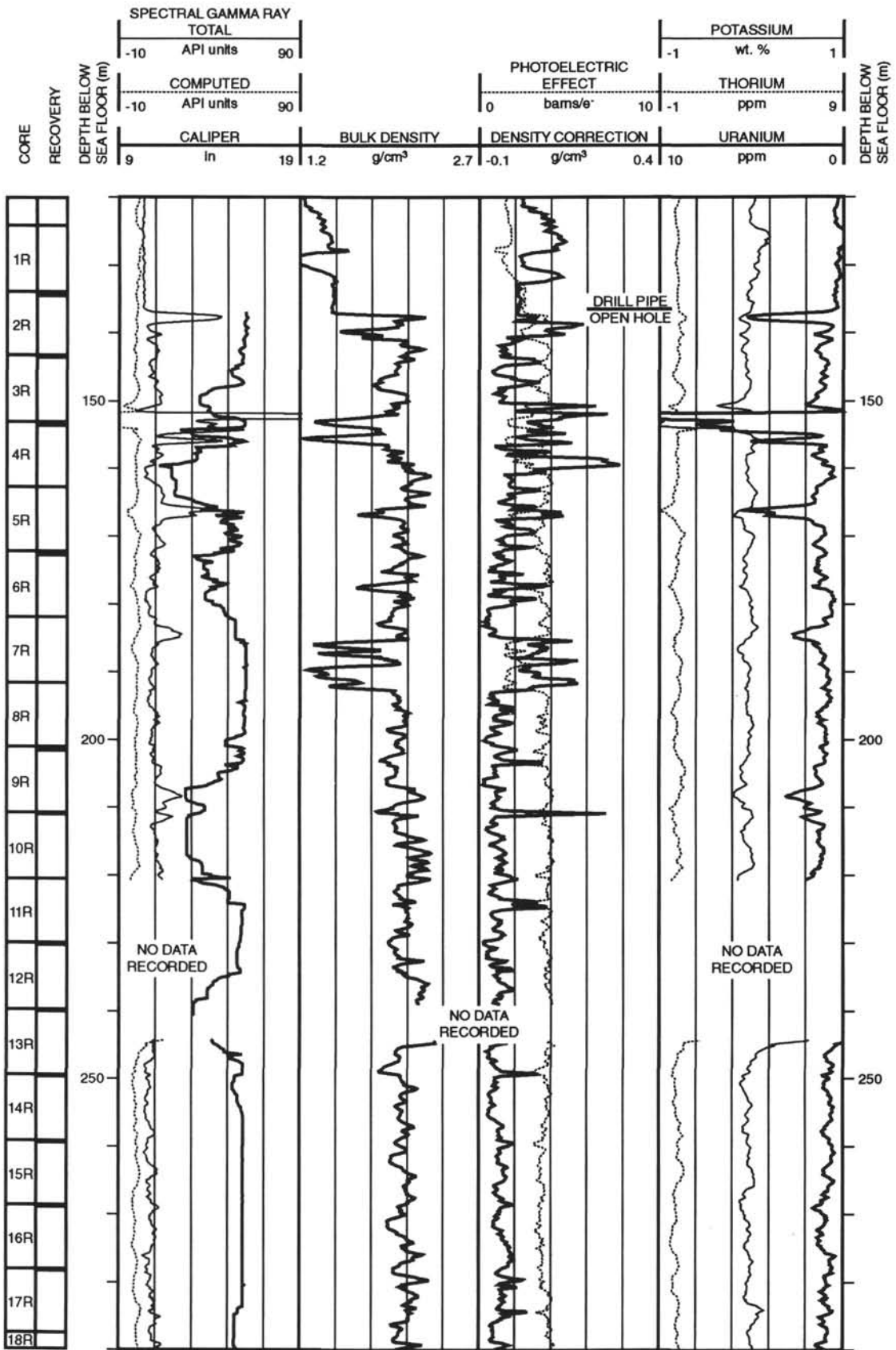
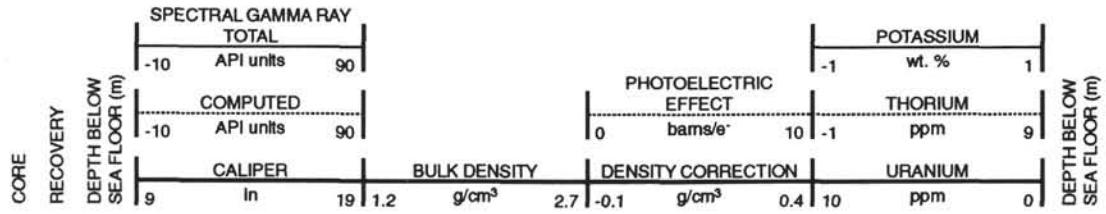


Figure 49. Lithostratigraphic correlations to the seismic stratigraphy section at Site 871. Major reflectors correspond to stratigraphic breaks in deposition or to major facies changes. Meter levels of key stratigraphic horizons are based upon the logging measurements, except for the basaltic basement interval.

Hole 871C: Density-Natural Gamma Ray Log Summary

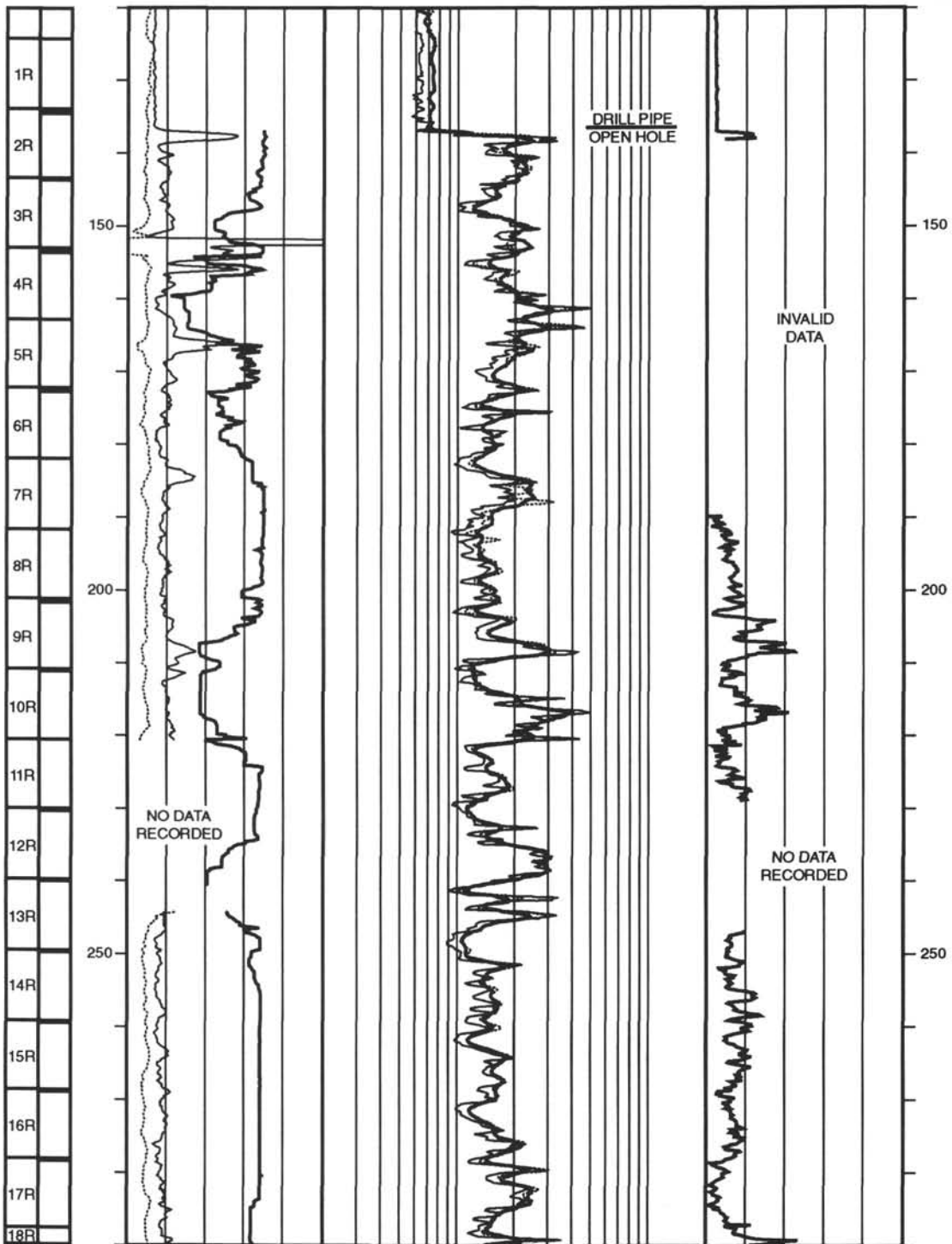


Hole 871C: Density-Natural Gamma Ray Log Summary (continued)



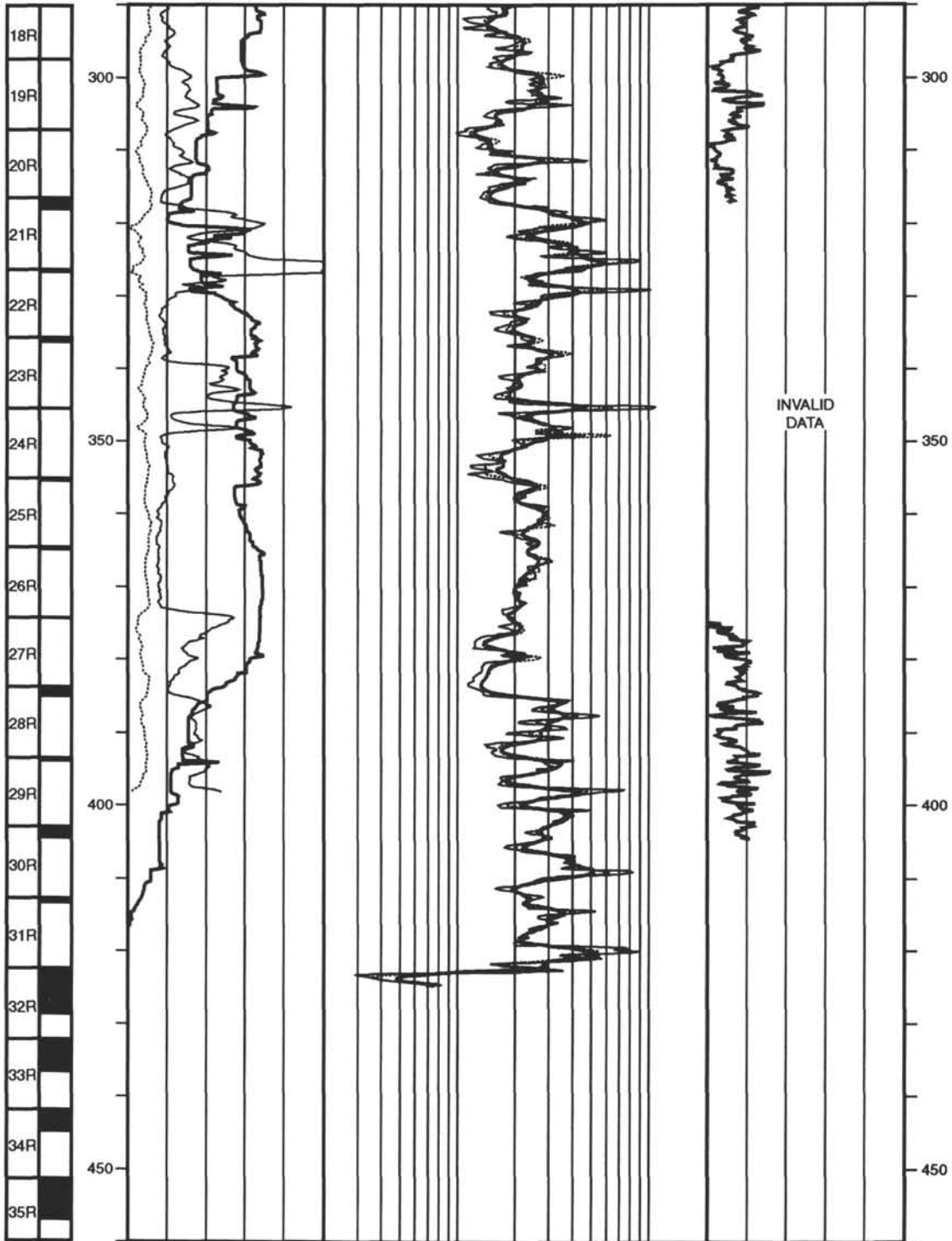
Hole 871C: Resistivity-Velocity-Natural Gamma Ray Log Summary

CORE RECOVERY	SPECTRAL GAMMA RAY TOTAL				RESISTIVITY FOCUSED				
	-10	API units	90	.2	ohm-m				20
	COMPUTED				MEDIUM				
DEPTH BELOW SEA FLOOR (m)	-10	API units	90	.2	ohm-m				20
DEPTH BELOW SEA FLOOR (m)	CALIPER				DEEP		VELOCITY		DEPTH BELOW SEA FLOOR (m)
	9	ln	19	.2	ohm-m		20	1.5 km/s	

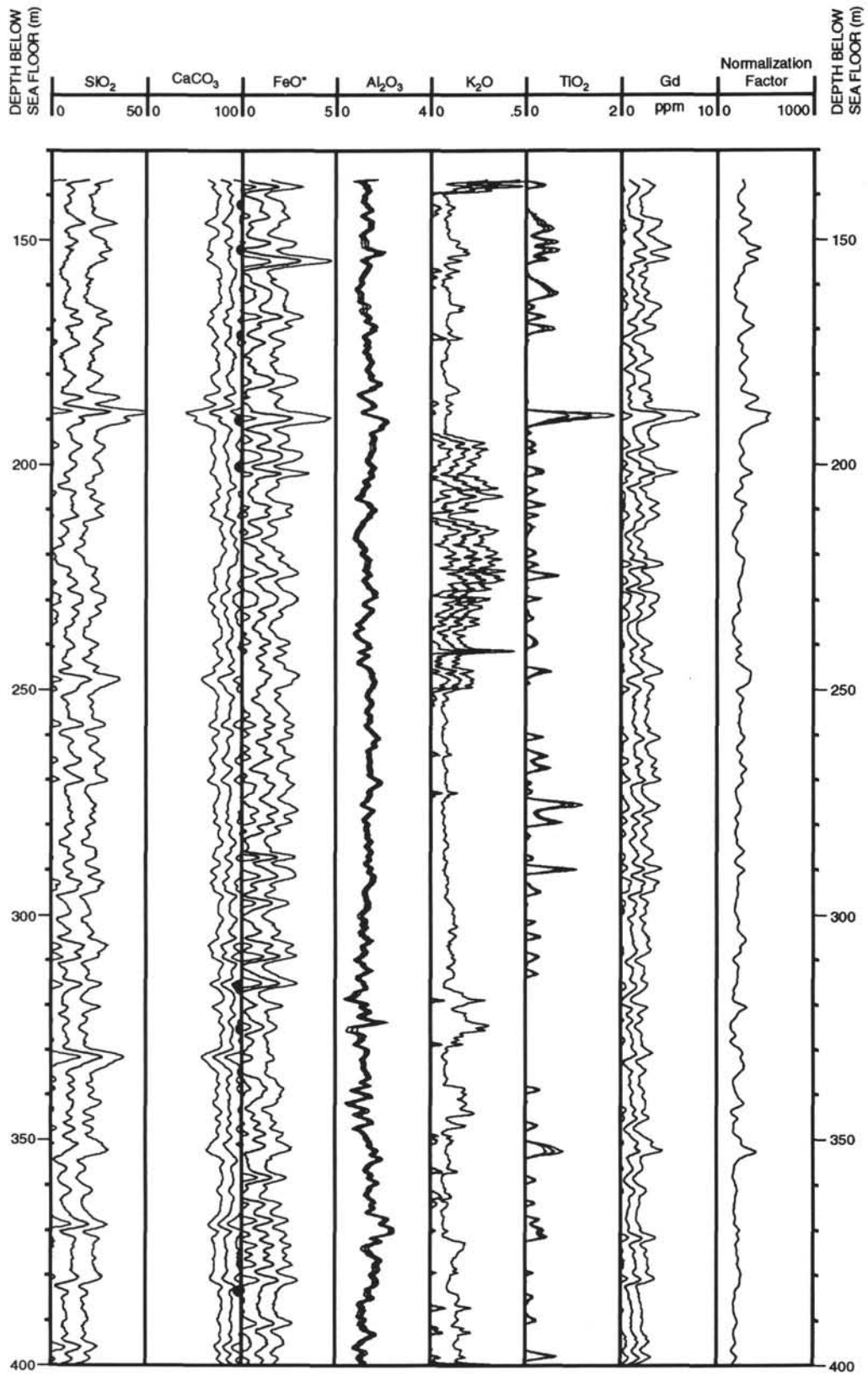


Hole 871C: Resistivity-Velocity-Natural Gamma Ray Log Summary (continued)

CORE RECOVERY	SPECTRAL GAMMA RAY				RESISTIVITY				DEPTH BELOW SEA FLOOR (m)	
	TOTAL				FOCUSED					
	-10	API units	90	.2	ohm-m	20				
	COMPUTED				MEDIUM					
	-10	API units	90	.2	ohm-m	20				
	CALIPER				DEEP				VELOCITY	
	9	in	19	.2	ohm-m	20	1.5	km/s	6.5	



Hole 871C: Geochemical Log Summary



Hole 871C: Geochemical Log Summary

